2013

Characterization of Stimulation-Induced Volume Changes in the Ca1 Region of Rat Hippocampus Slices

Amanda Brooke Gutwein
Wright State University

CHARACTERIZATION OF STIMULATION-INDUCED VOLUME CHANGES IN THE CA1 REGION OF RAT HIPPOCAMPUS SLICES

A thesis submitted in partial fulfillment of the
requirements for the degree of
Master of Science

By

AMANDA BROOKE GUTWEIN
B.S., University of Dayton, 2010

2013
Wright State University

WRIGHT STATE UNIVERSITY

GRADUATE SCHOOL

May 20, 2013

I HERBY RECOMMEND THAT THE THESIS PREPARED UNDER MY SUPERVISION BY Amanda Brooke Gutwein ENTITLED Characterization of Stimulation-induced Volume Changes in the Ca1 Region of Rat Hippocampus Slices BE ACCEPTED IN PARTIAL FULFILLMENT OF THE REQUIREMENTS FOR THE DEGREE OF Master of Science.

_____

James Olson, Ph.D.
Thesis Director

_____

Timothy Cope, Ph.D.
Chair, Department of Neuroscience, Cell Biology, and Physiology

Committee on
Final Examination

_____

James Olson, Ph.D.

_____

David Ladle, Ph.D.

_____

Robert Putnam, Ph.D.

_____

R. William Ayres, Ph.D.
Interim Dean, Graduate School

ABSTRACT

Gutwein, Amanda Brooke. M.S., Department of Neuroscience, Cell Biology and Physiology, Wright State University, 2013. Characterization of stimulation-induced volume changes of the CA1 region within in vitro rat hippocampus slices.

Intrinsic optical signals (IOS) were used to evaluate volume regulation mechanisms during Schaffer collateral stimulation-induced volume changes in hippocampal slices. The effects of stimulation frequency, synaptic function, ionotropic glutamate receptor (iGluR) activation, glutamate uptake, and volume regulatory anion channels (VRAC) were examined with IOS. Data were analyzed using ANOVA with Dunnett's *post hoc* test ($p<0.05$ indicated significance). IOS changes were stimulation frequency dependent between 1 Hz and 10 Hz with full recovery of IOS within 5 min. Synaptic blockage reduced the rate of swelling by 81% compared to the control and the IOS did not fully recover. Recovery rate was reduced with iGluR inhibition. Inhibition of glutamate uptake reduced the rate of swelling by 70% compared to vehicle controls. During stimulation, action potentials, iGluR activation, and glutamate uptake contribute to swelling. Regulatory volume mechanisms during stimulation were glutamate-mediated via iGluRs and VRAC independent.

TABLE OF CONTENTS

LIST OF FIGURES

LIST OF TABLES

Tables Page

ACKNOWLEDGEMENT

I would like to thank Dr. Olson for guiding me throughout this first-time research experience and patiently teaching me the research skills needed for this project. This challenging transformation into a scientist has accompanied a great gain in personal growth. After many unfruitful experiments and equipment failures, I have gained a deeper appreciation for research and the discipline in takes to complete. When I felt like my planned experiments took a turn for the worse, the entire Olson lab was always a source of steady encouragement. I would like to thank all the members of the Olson Lab; it was a pleasure to get to know you. I would especially like to thank Dr. Li for his help. Dr. Li was incredibly helpful in all of my experiments. Additionally, I would like to thank Adetutu, who eagerly looked over thousands of field potential recordings. I would also like to thank Dr. Ladle and Dr. Putnam for being on my thesis committee and offer their advice. I would like to thank the NCBP faculty and my classmates who have been supportive and reassuring throughout this process. Thank you for always listening and offering your advice. Lastly, I would like to thank my family and my boyfriend Jason for their constant love and support.

I. INTRODUCTION

Regulation of cellular volume is a vital aspect of cellular homeostasis. Cells are susceptible to volume changes when there are fluctuations in intracellular and extracellular osmolarity. Cell volume is determined by the cellular content of osmotic active compounds and by the extracellular tonicity. Cell water content will change based on the osmotic active compounds present. As the intracellular content of osmotic active compounds increases, the extracellular space becomes hypotonic to the cell, and the cells take in water in an attempt to equalize the osmotic pressure. During hypoosmotic cell swelling, an acute increase in cellular volume is restored through a mechanism termed regulatory volume decrease (RVD) by the efflux of inorganic and organic osmolytes. This mechanism decreases the intracellular osmotic content thus increasing the movement of water from the intracellular compartment. Osmolyte efflux is accomplished via activation of specific transporters and volume-activated channels. Volume-regulated anion channels (VRACs) open during cell swelling and mediate RVD. VRACs are anion channels which are permeable to chloride and a variety of small organic anions such as taurine and excitatory amino acids (EAA) like glutamate (Kimelberg et al., 1990).

Previous studies have reported stimulation-induced swelling in the central nervous system; however, mechanisms of cell swelling and volume regulation during functional activity remain unclear. Many factors have been suggested to be involved in

neuronal activity induced cell swelling including fluctuations of extracellular K^+, glutamate accumulation in astrocytes, and activation of ionotropic glutamate receptor (iGluR). The proposed research is intended to identify and characterize the features of stimulation-induced volume changes of the rat hippocampus through the application of a synaptic block solution, iGluR antagonists, glutamate reuptake inhibitors, and VRAC inhibitors. In this study, we will use imaging analysis techniques to examine changes in the light transmission (intrinsic optical signal or IOS) of hippocampal slices induced by synaptic transmission. Although it is accepted that IOS can detect cellular swelling by increased light transmittance through tissue, the cellular mechanisms underlying these changes in the IOS of neuronal tissue during activity are not precisely known as yet. Synaptic activation or moderate hypo-osmotic exposure has been shown to lead to increased light transmittance, decreased reflectance, and reduced light scattering (MacVicar and Hochman, 1991; Andrew and MacVicar, 1994; Pal et al., 2013). A decrease in extracellular space (ECS) has been shown to occur during evoked activity in the cortex (Dietzel et al., 1982) in stimulated spinal cord slices(Sykova et al., 2003) and in the hippocampal slice during synaptic stimulation (Fayuk et al., 2002).

A greater understanding of the mechanisms and osmolytes responsible for stimulation-induced swelling will lead to improved treatment plans for any pathophysiological conditions resulting in edema such as epilepsy, traumatic brain injury, and excitotoxicity.

II. LITERATURE REVIEW

Fluid movement in the brain

In the central nervous system (CNS), fluid in different compartments is regulated through specialized cellular membranes. The movement of fluid between compartments of blood, cerebrospinal fluid, extracellular fluid, and intracellular fluid of neurons and glia depends on the concentrations of inorganic and organic osmolytes. There is presumably a continuous flux of water between neurons and glial cells because of cellular transport of osmolytes such as glutamate, sodium, and potassium between these cell types (Kimelberg, 2004a). Abnormal water movements between these compartments are associated with numerous pathological conditions including stroke, brain tumors, traumatic brain injury and temporal lobe epilepsy (Unterberg et al., 2004; van Vliet et al., 2007; Freeman et al., 2010; Thompson et al., 2013).

Edema

Cerebral edema is characterized by an excess of fluid accumulation in the brain. Edema is a common pathological response to various forms of neurologic insults that affect patients with almost every category of neurologic disease, including metabolic, infectious, neoplastic, cerebrovascular, and traumatic brain injury disease states (Ryu et al., 2013). Following neurological insult, alterations in osmolyte gradients drive fluid accumulation and increase brain volume. The excess fluid deforms the brain tissue that is

restricted by the meningeal layers and skull causing an increased intracranial pressure and resulting in a high rate of morbidity and mortality.

Brain edema is classified as osmotic, vasogenic, or cytotoxic (Unterberg et al., 2004). In some cases such as trauma, hypoxic-ischemic encephalopathy, or metabolic conditions, there can be a mixed pattern of cytotoxic and vasogenic edema (Ho et al., 2012). Osmotic brain edema develops due to plasma hyposmolality compared to the brain tissue resulting in fluid accumulation into neurons and glial cells. In contrast, vasogenic edema develops when there is an increased permeability of capillary endothelial cells due to a disruption in the blood-brain barrier. The break-down of tight junctions in endothelial cells allows protein-rich fluid to accumulate in the interstitial space. Traumatic brain injury, ischemia, and hypoxia can lead to cytotoxic edema and excitotoxicity (Arundine and Tymianski, 2004). Although cytotoxic edema by itself does not imply net brain swelling, the formation of cytotoxic edema will deplete the extracellular space of electrolytes such as Na^+ and Cl^- and cause a reduction in extracellular water content (Liang et al., 2007). Thus, cytotoxic edema creates new concentration gradients. During cytotoxic edema, osmotic imbalances and excess intracellular water are not restored by adenosine triphosphate (ATP) dependent or passive movement of electrolytes which are characteristic of physiological cell volume regulation.

Cell volume regulation

Regulation of cellular volume is a vital aspect of cellular homeostasis. Cells are susceptible to volume changes when there are fluctuations in intracellular or extracellular osmolarity. During normal physiological conditions, the osmolarity of extracellular fluid (ECF) in the body including that of brain tissue is maintained relatively constant between

285 and 295 mOsm/kg (Wright, 2012). Since ECF osmolality is relatively stable, most fluctuations in cellular volume are due to changes in intracellular osmolarity (Hoffmann et al., 2009). Osmotic imbalances can be produced across the plasma cell membrane due to cellular activity from transport, metabolism, and brain injury (Okada, 2004; Ho et al., 2012). Cell volume is determined by the cellular content of osmotically active compounds and by the extracellular osmolality. Thus, as the intracellular content of osmotically active compounds increases, the extracellular space becomes hypotonic to the cell interior, and water enters the cell to equalize the osmotic pressure across their plasma membranes.

Regulatory volume decrease

In response to increased cellular water content, cellular volume can be restored by the efflux of inorganic and organic osmolytes through a mechanism termed regulatory volume decrease (RVD). Mechanisms of RVD are not fully understood but involve efflux of intracellular osmotic content to increase movement of water from the intracellular compartment. For osmoeffective efflux, net anion efflux must be accompanied by K^+ efflux to maintain electroneutrality (Okada et al., 2001). Three different mechanisms are known to be involved during RVD: K^+Cl^- co-transporters (KCCs), K^+ channels, and Cl^- channels (Okada, 2004). The organic osmolytes predominantly contributing to RVD in the brain are amino acids such as aspartate, glutamate, and taurine (Pasantes-Morales, 1996). Mechanisms of RVD are summarized in Figure 1.

Volume-regulated anion channels

Volume-regulated anion channels (VRACs or I_{Clvol}) are ubiquitously present in mammalian cells and are required for the regulation of electrical activity, cell volume,

intracellular pH, immunological responses, cell proliferation and differentiation (Duan et al., 1997). The molecular identity of VRAC remains elusive despite extensive research and several candidates (Abdullaev et al., 2006; Okada et al., 2009). VRACs are typically activated during swelling and provide a pathway for efflux of intracellular anions, with the permeability sequence of $SCN^->I^->NO_3^->Br^->Cl^->F^->$gluconate (Kimelberg et al., 2004). During cellular swelling, RVD mechanisms involve VRACs to mediate an efflux of osmolytes but may also show limited activity in non-swollen cells (Mongin and Kimelberg, 2005). VRACs have a relatively large pore diameter of approximately 1.1 nm that permits the efflux of small organic osmolytes. VRACs have been shown to release excitatory amino acids such as aspartate, glutamate, and taurine during increased extracellular K^+, hypoosmotic conditions, oxidative stress, excitotoxic stimulation, and ischemia (Rutledge et al., 1998; Kreisman and Olson, 2003; Kimelberg, 2004b; Kimelberg et al., 2004; Abdullaev et al., 2006; Inoue and Okada, 2007; Tucker and Olson, 2010; Zhang et al., 2011). Inhibition of VRACs has been shown to reduce water permeability of cellular membranes suggesting that VRACs might also be water permeable (Nilius, 2004).

Figure 1: Mechanisms of regulatory volume decrease. (Left) Cell equalizes the osmotic pressure through an influx of water. (Right) Cell undergoes regulatory volume decrease (RVD) via several efflux pathways. Solid lines indicate the cellular membrane prior to swelling (Left) or RVD (Right). Dotted lines indicate the changes in membrane volume as a result of swelling or RVD. Abbreviations: K^+Cl^- Co-transporter (KCC), Cl^-/HCO^-_3 antiporter or anion exchanger (AE), Ca^{+2} dependent Cl^- current (I_{ClCa}), Ca^{+2} dependent K_+ current (I_{KCa}), volume activated Cl^- current (I_{Clvol}), volume activated K^+ current (I_{Kvol}) From (Hoffmann et al., 2009)

Figure 1:

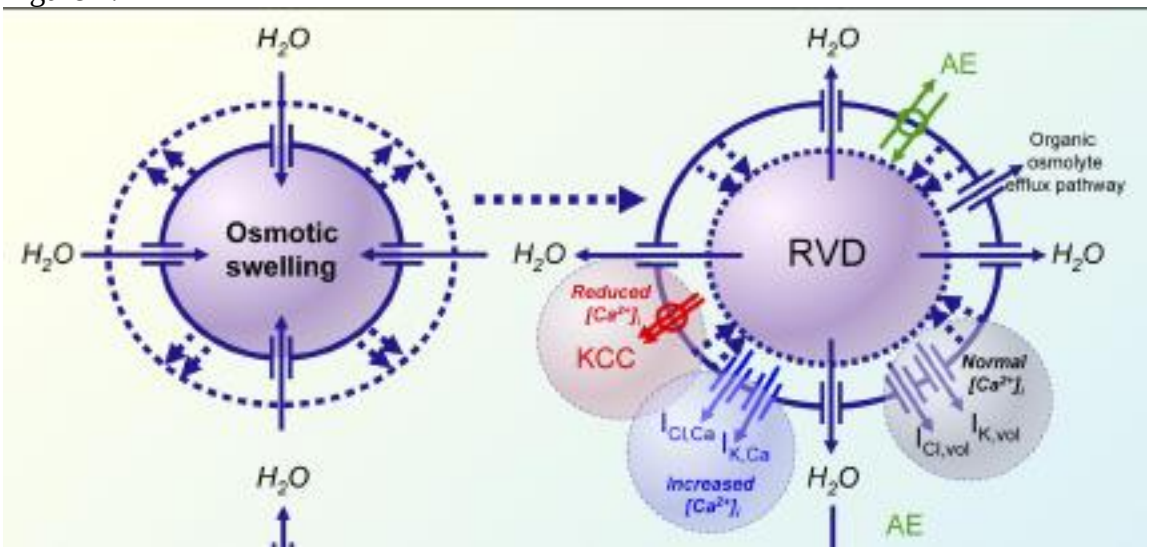
H_2O
Osmotic swelling
H_2O
H_2O
H_2O
AE
Organic osmolyte efflux pathway
RVD
H_2O
H_2O
Reduced $[Ca^{2+}]_i$
KCC
$I_{Cl,Ca}$
$I_{K,Ca}$
Increased $[Ca^{2+}]_i$
Normal $[Ca^{2+}]_i$
$I_{Cl,vol}$
$I_{K,vol}$
H_2O
AE

Hippocampus

The hippocampus, a part of the limbic system, is a major component of the mammalian brain involved in learning and memory. The hippocampus, sometimes referred to as the hippocampal formation, is a paired structure located in the medial temporal lobe of the cerebral cortex. In the human brain, the hippocampus appears as a seahorse-shaped structure that extends into the floor of the lateral ventricle and becomes continuous with the fornix posterior to the splenium of the corpus callosum. Extensive research has established microanatomy and circuitry pathways of the hippocampus. Since different cell types within the hippocampus are organized into layers, the hippocampus serves as an excellent model for studying neurophysiology.

Cognitive deficits involving the hippocampus are often persistent and severely debilitating. Individuals with damage to the hippocampus exhibit an inability to form or retain new memories. Research has connected the hippocampus to multiple diseases including vascular disease, temporal lobe epilepsy, cognitive aging, post-traumatic stress disorder, transient global amnesia, schizophrenia, and depressive and anxiety disorders (Small et al., 2011). Even within the hippocampus, there exists regional differences in vulnerability to metabolic diseases and stressors that increase with age (Jackson and Foster, 2009). In addition, due to the physiology of the hippocampus, there is a regional vulnerability for ischemic injury and cytotoxic edema. Further understanding of the mechanisms of cell volume regulation in the hippocampus will be vital for addressing the pathophysiological conditions associated with this structure and will have implications for damage in the rest of the central nervous system (CNS).

Structure of the hippocampus

The hippocampus appears as two interlocking C-shaped laminar structures and typically refers to the dentate gyrus (DG), the hippocampus proper, and the subicular cortex. Frequently, the extorhinal cortex (EC) is included as part of the hippocampal formation. The region within the hippocampus proper is subdivided into CA1, CA2 and CA3 (Amaral and Witter, 1989). In figure 2, regions of the hippocampal formation and the primiary synaptic connections between these regions are shown in a schematic drawing. CA1 extends from the dorso-medial subiculum to CA2. CA2 is considered a small region between CA1 and CA3. CA3 comprises the ventro-medial portion of the hippocampus. The terminal portion of CA3, as it courses into the dentate hilus, is sometimes referred to as CA4. Since there is no clear histological features distinguishing CA3 from CA4, many authors consider CA3 and CA4 regions together as CA3 (DeFelipe et al., 2007).

Basic synaptic pathways in the hippocampus

The lamellar model considers the hippocampal cortex to be organized into parallel lamellae forming a tri-synaptic circuit lying within a transverse plane of the hippocampus (Andersen et al., 1971). Synaptic transmission flows mainly unidirectionally in the hippocampus proper by three principal pathways: perforant pathway (PP), mossy fiber pathway, and the Schaffer collateral pathway (SC).

The major input to the hippocampus originates from EC layer II/III neurons through the PP and directly targets neurons in the CA1, CA2 ,CA3, DG, and subiculum (Canto et al., 2008). The DG is unique compared to the hippocampus proper because it has two glutamatergic principal cells: granule cells and hilar mossy cells (Scharfman and

Myers, 2012). Hilar mossy cells can either excite or inhibit granule cells, depending on whether their direct excitatory projections to granule cells or their projections to local inhibitory interneurons dominate (Jinde et al., 2013). Granule cells, the major principal cell type in the DG, are quiescent and send projections exclusively to the CA3 region via mossy fibers (Krautwald and Angenstein, 2012). In contrast, mossy cells exhibit spontaneous activity (Duffy et al., 2013) and receive back-projections from CA3 pyramidal neurons (Jinde et al., 2013). The CA3 pyramidal neurons send axons to CA1 pyramidal cells through the SC and to the CA1 cells in the contralateral hippocampus. The CA1 and the subiculum receive direct input from EC layer III neurons through the temporoammonic pathway (TA). CA1 pyramidal cells mainly target the adjacent subiculum and the entorhinal cortex in addition to various cortical areas (Cenquizca and Swanson, 2007). The CA1 and subiculum are the major output structures of the hippocampus given that their projections terminate in a variety of subcortical and cortical areas including the entorhinal cortex (Witter, 2006).

Figure 2: Anatomy of the rodent hippocampus and neural network.

a) A transverse slice from the rodent brain is enlarged to depict the regions of the hippocampus and basic circuitry. b) Schematic of the excitatory trisynaptic pathway is depicted by solid black arrows. Abbreviations: EC, entorhinal cortex; DG, dentate gyrus; PP, perforant pathway; LPP, lateral perforant pathway; MPP, medial perforant pathway; CA, Cornu Ammonis; TA, temporoammonic pathway. From (Deng et al., 2010)

Figure 2:

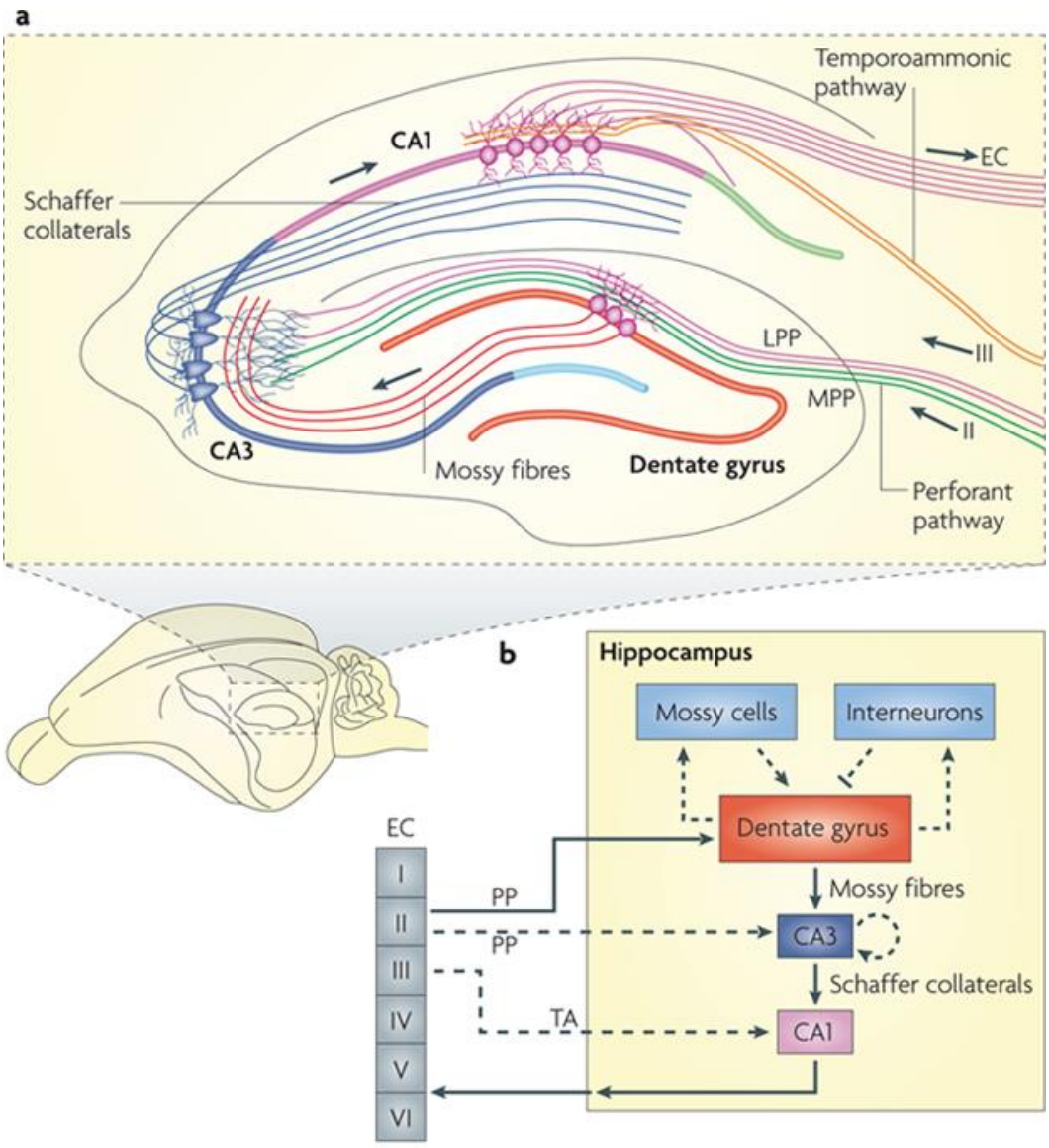
a
Temporoammonic pathway
CA1
EC
Schaffer collaterals
LPP
III
MPP
II
CA3
Mossy fibres
Dentate gyrus
Perforant pathway
b
Hippocampus
Mossy cells
Interneurons
Dentate gyrus
EC
I
II
III
IV
V
VI
PP
PP
Mossy fibres
CA3
Schaffer collaterals
TA
CA1

Layers of the hippocampus

The axons, cell bodies, and dendrites of pyramidal cells, the principal excitatory neurons of the hippocampus, are arranged through seven well-defined layers: alveus, stratum oriens, stratum pyramidale, stratum lucidum, stratum radiatum, stratum lacunosum, and stratum moleculare. Hippocampal pyramidal neurons, frequently regarded as a homogeneous cell population, (Szilagyi et al., 2011) form the stratum pyramidale with the cell bodies of various interneurons.

In the rodent, CA1 pyramidal neurons form a compact layer consisting of 5 to 8 superimposed rows of pyramidal neurons (Mizuseki et al., 2012). The ventricular portion, or deepest layer of the hippocampus, known as the alveus, consists of the myelinated axons from pyramidal cells (DeFelipe et al., 2007). Axons in the alveus bifurcate with branches extending rostrally through the fornix system and caudally toward the retrohippocampal region of the hippocampus where they contribute to the intrahippocampal circuit (Cenquizca and Swanson, 2007).

Stratum oriens (str. oriens) is superficial to the alveus consisting mainly of the basal dendrites from the pyramidal cells and several classes of interneurons. Oriens lacunosum-moleculare (O-LM) cells, a major class of GABAergic interneurons, have their horizontal dendrites and somata in the str. oriens (Szilagyi et al., 2011) and inhibit the distal apical dendrites of pyramidal cells (Leao et al., 2012).

The stratum lucidum (str. luc.) is only present in the CA3 region and contains mossy fibers from dentate gyrus granule cells. The stratum radiatum (str. rad.) contains apical dendrites from pyramidal cells and several types of interneurons. Interesting,

astrocytic processes in stratum radiatum of area CA1 represent only ~5% of the neuropil contrasting with ~27% in cerebellar cortex (Ventura and Harris, 1999).

The SC fibers, which are the axons from the CA3 pyramidal neurons innervating predominantly dendritic spines of CA1 pyramidal cells, run through the str. rad. and the stratum lacunosum (str. lac.). Interneuron cell bodies of the Schaffer collateral associated cells course along the SC fibers in the str. rad. up to the border of the str. lac. (Szilagyi et al., 2011). The str. lac. also contains PP fibers from the superficial layers of EC. Due to the small size of the str. lac., it is often grouped together with stratum moleculare (str. mol.) into a single stratum called stratum lacunosum-moleculare (str.lac-mol) which has an approximate thickness of 150 μm (Kajiwara et al., 2008). The str.lac-mol contains axons of the TA pathway from layer III EC neurons which synapse with the distal apical dendrites of CA1 pyramidal cells (van Groen et al., 2002; Cai et al., 2013). Str. mol. is the most superficial stratum in the hippocampus and consists of PP fibers which form synapses onto the distal portion of the apical dendrites of CA3 pyramidal cells.

Figure 3: Labeled regions and layers of rodent hippocampus from a ^{3}H-thymidine autoradiogram of a rodent hippocampus slice. The picture shows stratum lacunosum and stratum moleculare together as stratum lacunosum-moleculare. CA2 region is not labeled. Taken from the website of braindevelopmentmaps.org (Altman and Bayer, 2012)

Figure 3:

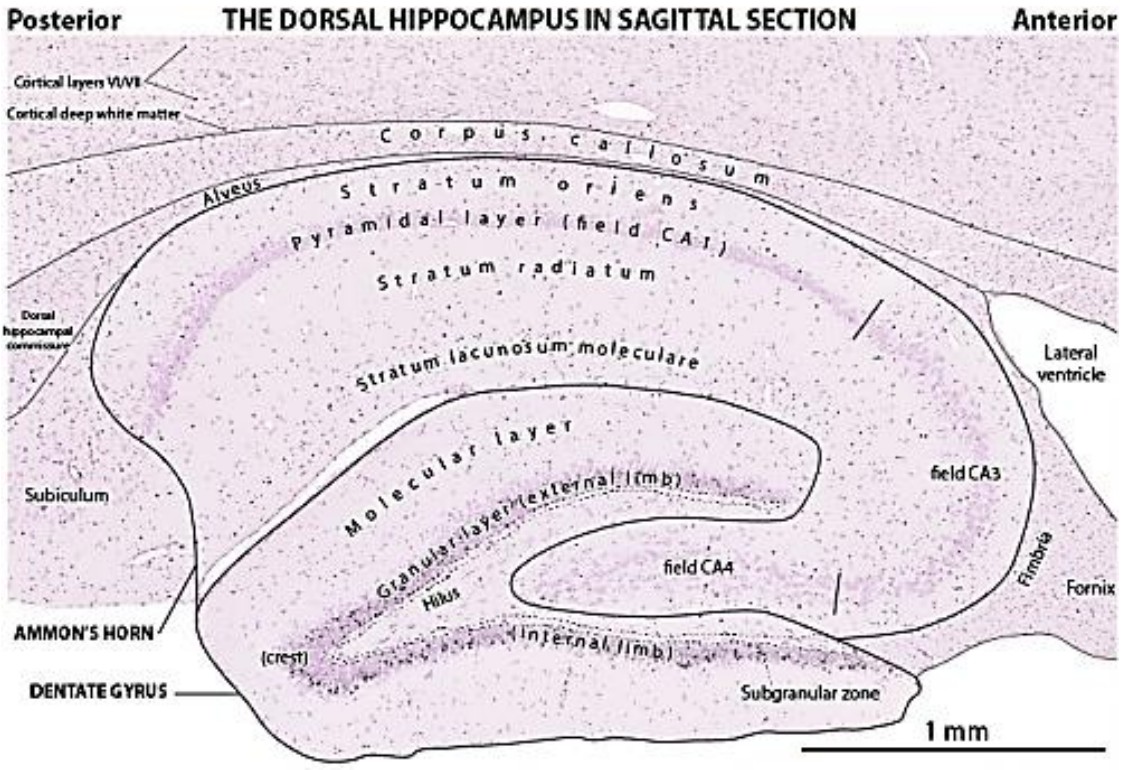
Posterior
THE DORSAL HIPPOCAMPUS IN SAGITTAL SECTION
Anterior
Cortical layers VI/VII
Cortical deep white matter
Corpus callosum
Alveus
Stratum oriens
Pyramidal layer (field CA1)
Stratum radiatum
Dorsal hippocampal commissure
Stratum lacunosum moleculare
Lateral ventricle
Molecular layer
Subiculum
Granular layer (external limb)
field CA3
field CA4
Hilus
Fimbria
Fornix
AMMON'S HORN
(crest)
(internal limb)
DENTATE GYRUS
Subgranular zone
1 mm

Schaffer collateral synaptic physiology

Schaffer collateral pathway action potentials

The SC pathway was utilized in these studies to elicit monosynaptic stimulation of pyramidal cells in the CA1 region. Synaptic transmission of the SC pathway is controlled by the ionic gradient across the axolemma that supports action potentials which travel towards the nerve terminal. At rest, the cytoplasm of neurons has a low concentration of Na^+ and Cl^- and a high concentration of K^+ relative to the extracellular fluid. In adult pyramidal neurons, intracellular Cl^- is estimated to be 4 mM (Tyzio et al., 2008). Several specialized leak channels and the Na^+/K^+ ATPase, which pumps 3 Na^+ out of the cell in exchange for 2 K^+ into the cell, maintain this concentration gradient of ions. Due to the constant pumping activity of the Na^+/K^+ ATPase, cells maintain a high intracellular K^+ concentration.

During synaptic activity of the SC pathway, the CA3 pyramidal neuron membrane potential first becomes depolarized due to voltage-gated Na^+ channels that mediate an influx of Na^+ ions into the cell body. Once the membrane potential reaches a threshold voltage, an action potential can be elicited. The large depolarization peak of the action potential causes voltage-gated Na^+ channels to inactivate such that Na^+ influx stops before the cells reach the equilibrium potential for Na^+. Then a rapid efflux of K^+ ions through voltage-gated K^+ channels causes the membrane potential to repolarize towards resting membrane potential. The membrane potential continues towards the equilibrium of K^+ ions. An afterhyperpolarization of the membrane occurs where the membrane potential is transiently more negative than the resting membrane due to slow inactivation of voltage-gated K^+ channels. Once the voltage-gated K^+ channels close, the resting

membrane potential is reestablished through the specialized leak channels and Na^{+}/K^{+} ATPase.

The action potential of the CA3 pyramidal neuron propagates towards the nerve terminal through an axon in the str. rad. and str. lac. When action potentials arrive at the presynaptic nerve terminal, Ca^{2+} influx is mediated by voltage-gated Ca^{2+} channels. Presynaptic Ca^{+2} influxes contribute to approximately 75% of stimulus-induced intracellular Ca^{+2} transients in the stratum radiatum (Liotta et al., 2012). Each presynaptic nerve terminal contains hundreds of synaptic vesicles that are filled with neurotransmitters (Sudhof and Rizo, 2011). Various specialized proteins assemble to release synaptic vesicles in the presence of elevated intracellular Ca^{+2}. The synaptic vesicles fuse with the presynaptic membrane and release neurotransmitters into the specialized extracellular space of the synaptic cleft to bind on postsynaptic membrane receptors of the CA1 pyramidal cells. Postsynaptic activation and generated action potentials contribute to approximately 50% of the stimulus-induced ion fluxes in the stratum radiatum during SC activity (Liotta et al., 2012).

Glutamatergic synapse

Glutamate, a small amino acid, is the primary excitatory neurotransmitter in the CNS including the hippocampal pyramidal cells. When in excess, glutamate is considered a powerful neurotoxin. Although glutamate serves multiple roles in the central nervous system, this review will concentrate on glutamate as a neurotransmitter in the Schaffer Collateral pathway of the hippocampus and the ionotropic glutamate receptors involved in glutamatergic signaling. In the nerve terminal of pyramidal cells, glutamate is stored in small spherical synaptic vesicles for eventual release as a neurotransmitter. Upon

stimulation of the nerve terminal, synaptic vesicles fuse with the presynaptic cell membrane, releasing their content into the synaptic cleft. Glutamate diffuses across the synaptic cleft between the nerve terminal and dendritic spine of the CA1 pyramidal cell. Once in the synaptic cleft, glutamate binds to glutamate-specific receptors (GluRs) present on neurons and glia. Activation of GluRs alters membrane permeability primarily to cations and depolarizes the post-synaptic membrane of the CA1 pyramidal cell. The process is terminated as glutamate is transported via specific glutamate transporters (GluTs) back into the pre-synaptic neuron and into surrounding glial cells. Glutamate returning into the pre-synaptic neuron is packaged directly into synaptic vesicles by vesicular glutamate transporters (VGluTs). However, glutamate transported into glial cells rapidly enters the glutamate-glutamine cycle. Glial cells convert the accumulated glutamate to glutamine for transfer into neurons. Then glutamine is converted back to glutamate and re-packaged into vesicles. Glutamate re-uptake into glial cells is vital for maintaining a low extracellular concentration of this excitatory neurotransmitter, thus preventing excessive glutamate excitation and excitotoxicity.

Glutamate receptors

Glutamate triggers rapid changes in membrane conductance through activation of glutamate receptors. There are two general classes of GluRs present on neurons and glia: ionotropic glutamate receptors (iGluRs) and metabotropic glutamate receptors (mGluRs). iGluRs are glutamate-gated cation channels that have traditionally been classified into three subtypes based upon pharmacological and electrophysiological data: NMDA (N-methyl-D-aspartate) receptors (NMDARs), AMPA (α-amino-3-hydroxy-5-methyl-4-isoxazolepropionic acid) receptors (AMPARs) , and kainate receptors (KARs)

(Dingledine et al., 1999). The mGluRs are G-protein coupled receptors that exert a variety of modulatory effects through their recruitment of second messenger systems (Pinheiro and Mulle, 2008). In this study, the focus on glutamate receptors will be limited to the ionotropic glutamate receptors and their roles in the glutamatergic synapse in the hippocampus.

AMPARs

The AMPARs consist of four subunits, GluA1-GluA4, (Hollmann and Heinemann, 1994; Collingridge et al., 2009) that assemble into a tetrameric complex to form a functional ion channel that is permeable to Na^+ and K^+ ions (Mano and Teichberg, 1998). Although most AMPARs are impermeable to Ca^{+2}, recent research has revealed the presence of calcium-permeable AMPARs (CP-AMPARs) in hippocampal neurons and astrocytes (Sans et al., 2003; Verkhratsky and Kirchhoff, 2007). Certain types of neural activity such as paired-pulse stimulation reveal CP-AMPARs present at perisynaptic sites of the CA1 synapses from Schaffer collaterals (He et al., 2009). But under physiological conditions, CA1 pyramidal cells abundantly express GluA2-containing Ca^{2+} -impermeable AMPARs (Liu and Zukin, 2007). In neurons, AMPARs are located predominantly on the post-synaptic membrane but are also found at extra-synaptic sites and occasionally on the pre-synaptic membranes (Sprengel, 2006). Fluorescent *in situ* hybridization and immunocytochemistry studies have localized AMPAR subunits in the somata and dendrites of CA3 and CA1 pyramidal cells, especially in the apical dendrites of pyramidal cells (Cox and Racca, 2013). Glutamate activated neuronal AMPARs allow an influx of cations which depolarize the membrane and generate excitatory postsynaptic potentials (EPSPs). Since AMPAR activation

requires only the presence of glutamate, AMPARs can mediate fast excitatory synaptic transmission in the hippocampus (Lau and Tymianski, 2010).

KARs

The KAR is a tetrameric iGluR that is composed of diverse combinations of five subunit proteins: GluK1, GluK2, GluK3, GluK4 and GluK5 (Collingridge et al., 2009; Copits and Swanson, 2012). Until recently, KARs were often referred together with AMPARs because of similar biophysical properties and the limited ability to selectively target KARs pharmacologically (Jane et al., 2009; Copits and Swanson, 2012). KARs are glutamate-gated channels that are permeable to cations and display rapid activation and desensitization characteristics (Pinheiro and Mulle, 2006). KARs are ubiquitously distributed throughout the brain and act predominantly as modulators of synaptic transmission and neuronal excitability (Contractor et al., 2011). Numerous studies have demonstrated the presence of functional KARs in various neuronal populations on presynaptic and postsynaptic membranes (Pinheiro and Mulle, 2006). In the hippocampus, KARs have been shown to modulate inhibitory synaptic transmission in the CA1 region and require high-frequency stimulation in CA3 pyramidal neurons (Swanson and Heinemann, 1998). KARs are most likely localized at presynaptic GABAergic synapses to modulate GABA release from interneurons (Rodriguez-Moreno et al., 1997). Glial KARs also have been localized diffusely with AMPARs on the somata of oligodendrocytes (Salter and Fern, 2005).

NMDARs

NMDARs are heteromeric complexes composed of different subunits from a collection of three subtypes: GluN1, GluN2, and GluN3 (Paoletti and Neyton, 2007;

Collingridge et al., 2009). NMDARs have binding sites for glutamate, polyamines, Mg^{+2}, and glycine (Wollmuth et al., 1998b, a; Ghasemi and Dehpour, 2011). Similar to the manner in which Mg^{2+} interacts with residues that form the narrow constriction in the NMDA channel pore, numerous polyamines have been identified that modulate NMDARs (Berger et al., 2013). The activation of NMDARs requires binding of glutamate in addition to glycine or D-serine. In neurons at resting membrane potential, NMDARs which bind glutamate remain in a low conductance state because the channel pore is blocked by Mg^{2+} ions. Under these basal conditions, an EPSP resulting from a glutamatergic synapse will be mediated entirely by AMPA receptors. However, membrane depolarization due to AMPAR activation can expel the Mg^{2+} from the NMDA channel. With a depolarized membrane and a co-agonist (glycine or d-serine), the glutamatergic impulses can activate NMDARs to allow the influx of monovalent cations, including Na^{+} and divalent cations, most notably Ca^{2+} (Kalia et al., 2008). Ca^{+2} ions then can act as an important second messenger to activate intracellular signaling cascades. NMDARs have been found to be co-localized with AMPARs in the postsynaptic density of the vast majority of glutamatergic synapses in the brain (Pinheiro and Mulle, 2006).

Once considered exclusively neuronal, NMDARs have now been demonstrated to be expressed in glial cells. In astrocytes and oligodendrocytes, NMDARs are expressed on the distal processes, a distribution which is unlike other iGluRs (Conti et al., 1996; Salter and Fern, 2005). Glial NMDARs have been found to be approximately 25 times more sensitive to glutamate compared to AMPA receptors (Lalo et al., 2006). Together, the location and sensitivity to glutamate suggest that NMDRs might contribute to monitoring glutamate levels in the extracellular space. Glial NMDARs have been found

to be either completely insensitive or weakly sensitive to extracellular Mg^{2+} (Lalo et al., 2006). As a result, glial NMDARs are functional at resting membrane potentials and allow the influx of Na^{+} and Ca^{2+} ions into the glia. Although the role for NMDARs in generating astroglial Ca^{2+} signals is generally neglected, synaptic stimulation of NMDARs has been shown to contribute up to 50% of intracellular Ca^{2+} in cortical astrocytes (Palygin et al., 2010; Lalo et al., 2011). As in neurons, increased intracellular Ca^{+2} ions can act as an important second messenger to activate specialized proteins and intracellular signaling cascades. In cultured astrocytes, Ca^{+2} influx is required to obtain glutamate-induced volume increases (Hansson et al., 1994).

Glutamate Transporters (GluTs)

GluTs, known as excitatory amino acid transporters (EAATs), are abundant in neuronal and glial membranes and bind glutamate rapidly. The exact stoichiometry of GluT among the different isoforms of GluTs is still debated but it is considered that the uptake of 1 glutamate molecule is thermodynamically coupled with the influx of 3 Na^{+}, 1 H^{+}, and the efflux of 1 K^{+} (Lopez-Bayghen and Ortega, 2011; Stone et al., 2012). Thus, GluTs use secondary active transport to maintain a 10^{6}-fold glutamate concentration gradient across the cell membrane (Gameiro et al., 2011). During ATP reduction and altered osmotic states, glutamate transport can be reversed (Takahashi et al., 1997). The rapid kinetics of GluT serves several functions at the glutamatergic synapse. The uptake of glutamate preserves the electrical signal by maintaining a low non-toxic extracellular glutamate concentration, typically less than 1 µM (Simard and Nedergaard, 2004). GluTs can modulate the time and extent of glutamate receptor activation. Uptake of glutamate also limits the spillover of glutamate into neighboring synapses and

extrasynaptic areas. Because of the rapid accumulation of glutamate from the extracellular space by GluT, this process is the primary mechanism for the inactivation of synaptically released glutamate (Rothstein et al., 1996). For astrocytes, glutamate uptake can be mediated either by Na^+-independent or Na^+-dependent mechanisms. The Na^+-independent uptake represents only a small proportion of total astrocyte glutamate uptake and is typically done via chloride dependent glutamate/cysteine antiporters (Anderson and Swanson, 2000). Na^+-dependent glutamate uptake governs the majority of Na^+ influx into astrocytes *in situ* (Langer and Rose, 2009) GluTs in astrocytes are considered the most important for maintaining normal glutamate concentrations and providing a pathway for glutamate metabolism. Astrocytic GLuTs clear approximately 80% of glutamate released during synaptic transmission (Verkhratsky and Kirchhoff, 2007). The task of glutamate clearance in the CNS is spread among six different GluTs, encoded by five distinct genes: EAAT1, EAAT2, EAAT3, EAAT4, and EAAT5 (Huang and Bergles, 2004). The subtypes EAAT1 and EAAT2 are mostly expressed in glial cells, whereas EAATs 3–5 are neuronal (Gameiro et al., 2011). In the hippocampus, EAAT1, EAAT2, and EAAT3 (Stone et al., 2012) are expressed and of those EAAT2 is considered the most prominent (Danbolt, 2001). The rat homologs of EAAT1, EAAT2, and EAAT3 are GLAST, GLT-1, and EAAC1 respectively. In the hippocampus, GLAST and GLT-1 are expressed as glial glutamate transporters in astrocytes, while EAAC1 is expressed as a neuronal glutamate transporter (Tsukada et al., 2005). Glial processes contain high levels of GLT as well as GLAST (Lehre and Danbolt, 1998). The concentration of GluTs in the stratum radiatum of hippocampus CA1 is approximately 15,000 per μm^3 tissue with GLT concentration as high as 12,000 per μm^3 (Lehre and

Danbolt, 1998). GLT and GLAST clear the majority of extracellular glutamate while EAAC1 is estimated to account for the remaining 40% of glutamate uptake (Rothstein et al., 1996).

Figure: 4 Summary of glutamatergic synaptic activity. The illustration shows the basic aspects of the Schaffer collateral glutamatergic synapse. Glutamate (Glu) from the presynaptic neuron (purple) is released into the extracellular space. Glutamate then can bind to NMDARs, AMPARs, KARs and mGluRs. (Note that, although not shown here, iGluRs also are located on presynaptic neuronal and on glial membranes). Glutamate is cleared from the extracellular space by EAATs present in astrocytes (blue) and neurons (purple). Glutamate is recycled and packaged into synaptic vesicles via VGluTs. From (Swanson et al., 2005)

Figure 4:

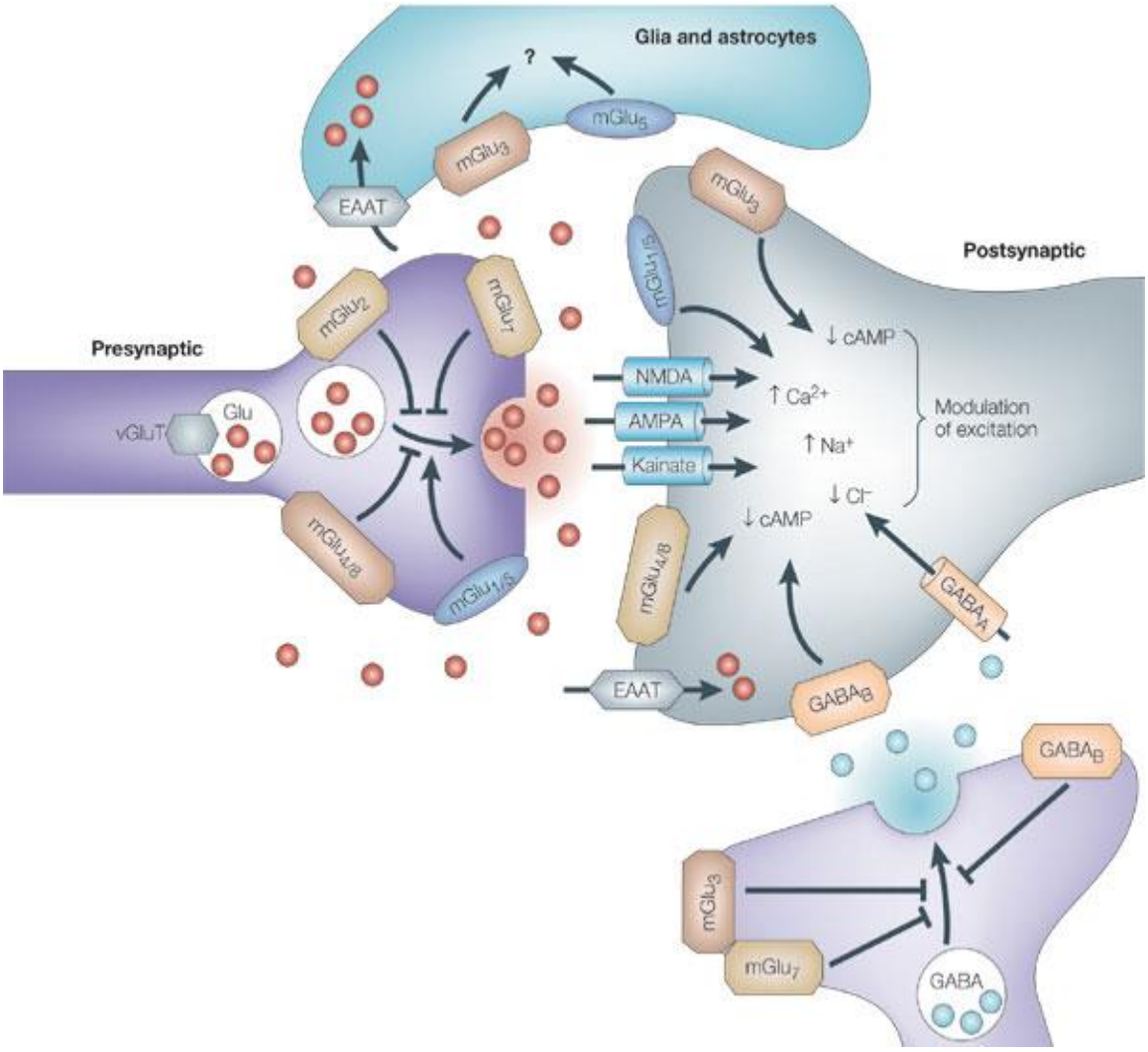
Glia and astrocytes
?
mGlu5
mGlu3
EAAT
mGlu3
mGlu1/5
Postsynaptic
mGlu2
mGlu7
Presynaptic
↓ cAMP
NMDA
↑ Ca2+
Modulation
of excitation
AMPA
↑ Na+
Kainate
↓ Cl-
Glu
vGluT
↓ cAMP
mGlu4/8
mGlu1/5
mGlu4/8
GABAA
EAAT
GABAB
GABAB
mGlu3
mGlu7
GABA

Glutamate-glutamine cycle

The uptake of glutamate by glial cells serves as the major pathway by which glutamate is recycled back to neuronal synaptic boutons. Glutamate released during neurotransmission is taken up primarily by neighboring astrocytes through GluTs. Glutamate then is amidated to glutamine by the ATP-dependent, glia-specific enzyme glutamine synthetase (Danbolt, 1994; Albrecht et al., 2010) . Glutamine also can be converted into alpha-ketoglutarate by glutamate dehydrogenase or aspartate aminotransferase for subsequent oxidative metabolism in the TCA cycle (Stobart and Anderson, 2013). Efflux of glutamine from astrocytes into the extracellular fluid occurs via system N transporters while system A transporters (SAT) actively transport glutamine into neurons (Chaudhry et al., 2002). Imported glutamine is converted back into glutamate in the neuron through deamination by mitochondrial phosphate activated glutaminase (Kvamme et al., 2000). Neuronal glutamate is transported into synaptic vesicles via vesicular glutamate transporters (VGluTs) which are located in the membrane of synaptic vesicles. VGluTs are supplied with energy through a Mg^{+2}-dependent ATPase in the vesicular membrane which pumps H^{+} ions into the vesicles (Danbolt, 2001). Without Mg^{+2} and ATP to fuel the proton pump, glutamate leaks out of the vesicles down the concentration gradient by reversal of VGluT (Danbolt, 1994).

Figure 5: Glutamate-glutamine cycle. This basic schematic of the glutamate-glutamine cycle between astrocytes and neurons is shown here. This schematic does not show system N transporters, system A transporters, and vesicular glutamate transports. Abbreviates: glutamate (Glu), excitatory amino acid transports (EAATs), glutamine (Gln), glutamine synthase (GS), alpha-ketoglutarate (α-KG), glutamate dehydrogenase (GDH), aspartate aminotransferase (AAT), phosphate-activated glutaminase (PAG), tricarboxylic acid cycle (TCA). From (Stobart and Anderson, 2013).

Figure 5:

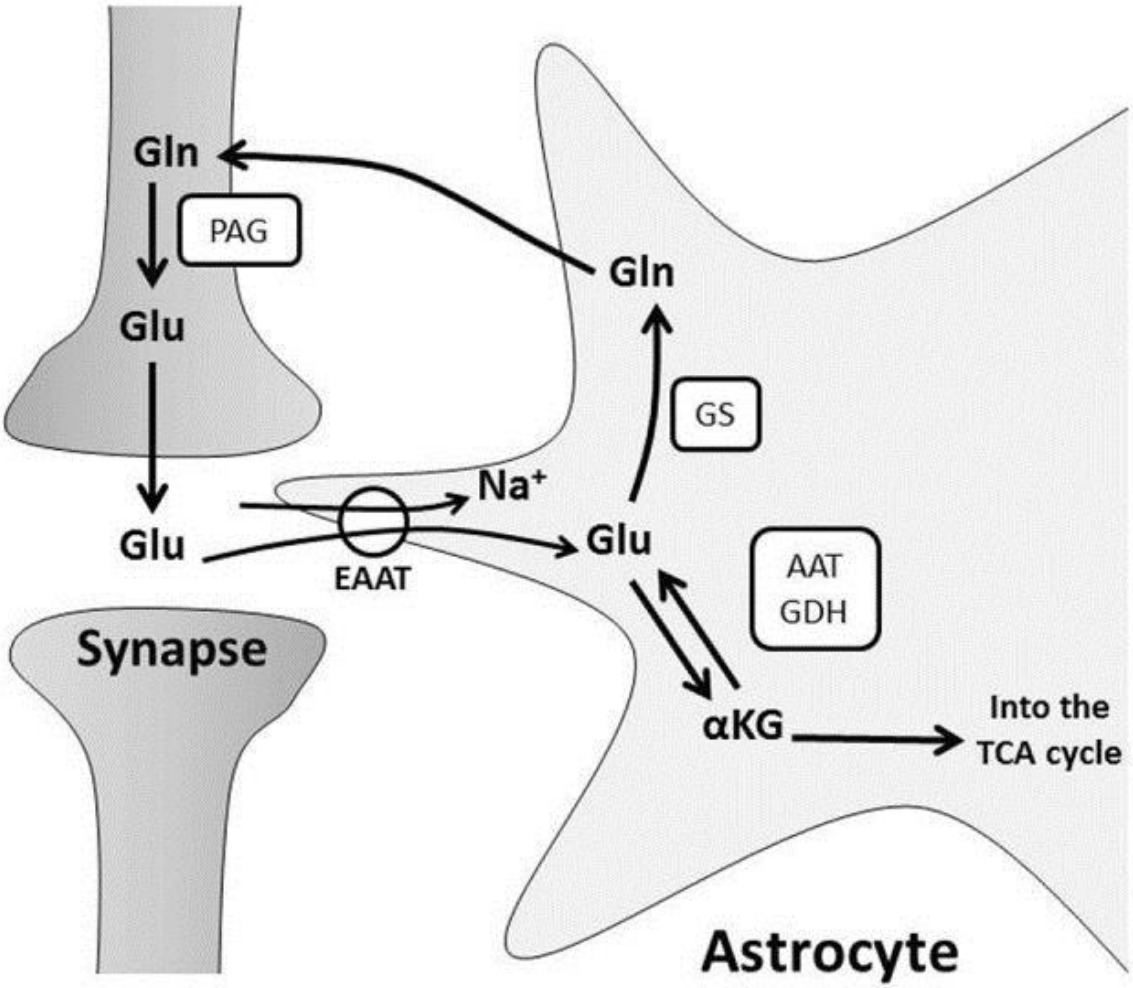
Gln
PAG
Glu
Glu
Synapse
Gln
GS
Na+
EAAT
Glu
AAT
GDH
αKG
Into the
TCA cycle
Astrocyte

Electric-activity dependent volume changes

Potassium spatial buffering of action potentials

Regulation of extracellular K^+ in the brain is essential for neuronal excitability and is recognized as a major function of astrocytes (Bay and Butt, 2012). There are narrow ranges for K^+ fluctuations and yet these fluctuations are a necessary consequence of synaptic transmission (Walz and Hertz, 1983). An elevated extracellular K^+ may induce uncontrolled hyperexcitability and abnormal synchronization of neurons. Seizure activity *in vivo* is characterized by elevations in extracellular K^+ from 3 mM to a ceiling level of 10–12 mM (Seifert et al., 2006). Conduction properties of CA1 afferents are sensitive to elevations in extracellular K^+ (Poolos et al., 1987).

During synaptic transmission, neural depolarization is halted by an efflux of K^+ through voltage-gated K^+ channels. The concentration of extracellular K^+ increases in the compact extracellular space surrounding neurons and glia following activity. Gap junctions in astrocytes constitute a syncytium for ion movement (Witte et al., 2001) and are thought to facilitate spatial buffering of extracellular K^+ during synaptic activity by redistributing K^+ to places with low extracellular K^+. However, recently, transgenic mice with gap junction deficient astrocytes revealed a large capacity for K^+ redistribution suggesting that gap junction-dependent processes only partially account for K^+ buffering in the hippocampus (Wallraff et al., 2006). At perivascular endfeet, K^+ efflux is an effective vasodilator which serves to satisfy enhanced glucose and oxygen demand during neuronal activity (Filosa et al., 2006). Gap junctions also interconnect perivascular glial endfeet which also contain various K^+ channels, aquaporin channels (AQP), and purinergic receptors (Simard et al., 2003; Assentoft et al., 2013; Stobart and

Anderson, 2013). In the hippocampus, AQP4 is expressed in CA1, where it may facilitate the rapid water fluxes that are required for maintaining K^+ homeostasis during electrical activity (Papadopoulos and Verkman, 2013). Interestingly, AQP4 expression is strongest in the CA1 str. lac-mol suggesting this sublayer is important for astrocytic K^+ and water regulation.

Studies using patch-clamp technique demonstrated expression of voltage-gated K^+ channels, Ca^{+2} activated K^+ channels, and inward rectifying potassium channels (Kir) in glial cells. However, physiological properties of Kir channels suggest that this channel is responsible for the majority of K^+ clearance from the extracellular space (Horio, 2001). Recent work suggests astrocytes exhibit co-localization of Kir4.1 with AQP4 (MacAulay and Zeuthen, 2010). Thus, volume regulation in glia may require cooperation of AQP4 and Kir4.1 activities (Seifert et al., 2006). Kir and Na^+/K^+ ATPase have been found important for K^+ clearance during synaptic activity (Bay and Butt, 2012). However, recent data from other studies have stressed the importance of brain Na^+/K^+ ATPase rather than glial channel-mediated removal for clearing extracellular K^+ (Meeks and Mennerick, 2007). Finally, during stimulation, astrocytes experience an influx of Ca^{+2} which has been found to stimulate Na^+/K^+ ATPase thus decreasing extracellular K^+ (Wang et al., 2012). From these studies, Na^+/K^+ ATPase is thought to be responsible for K^+ clearance during stimulation while glial Kir4.1 is primarily responsible for maintaining steady-state extracellular K^+ by releasing K^+ back into the extracellular space to off-set active K+ uptake via Na^+/K^+ ATPase.

Although glial swelling during neuronal activity is well known, the exact mechanisms underlying this swelling are unclear (MacAulay and Zeuthen, 2010). It is

thought that astrocytes experience a water influx to balance the osmotic pressure due to the increase in astrocytic K^+, leading to swelling of the astrocyte and a decrease in the extracellular space.

Glutamate-mediated cell volume regulation

In the glutamatergic synapse, glutamate has been shown to mediate volume regulation through different pathways. Several studies have shown that glutamatergic-purinergic signaling contributes to osmotic volume regulation of retinal glial cells (Wurm et al., 2008; Wurm et al., 2010; Linnertz et al., 2011). A purinergic signaling cascade includes the release of ATP, activation of purinergic receptors on glia, and subsequent efflux of Cl^- and K^+ accompanied by water efflux as part of the regulatory volume decrease mechanism (Darby et al., 2003; Uckermann et al., 2006). It is thought that glutamate activation of mGluRs causes a release of ATP from glial cells to activate purinergic receptors (Kalisch et al., 2006; Wurm et al., 2008). In addition, glutamatergic-purinergic signaling has been found to evoke taurine efflux in the substantia nigra in response to hypoosmolarity (Morales et al., 2007; Morales et al., 2009). These findings suggest that glutamatergic-purinergic signaling also may apply to volume regulation during synaptic activity.

Glutamate activation of all three iGluRs has been found to significantly enhance taurine release (Oja and Saransaari, 2013b) while activation of mGluRs was found to have a minor role in the regulation of taurine release (Oja and Saransaari, 2013a). During oxidative stress, NMDAR activation was found to be associated with volume regulation in the hippocampus (Tucker and Olson, 2010). Interesting, activation of AMPARs in the

substantia nigra induced a dose-response increase of taurine while NMDARs showed no response (Garcia Dopico et al., 2004).

Despite the years of research, the mechanisms underlying glutamate-mediated volume regulation in neurons and glial cells during synaptic transmission remain largely unclear. In this present study, volume regulation of neurons and glia in the glutamatergic synapse will be examined. These experiments will elucidate the specific role of glutamate in cell swelling and volume regulation during stimulation.

Model of volume regulation during synaptic activity

Figure 6 illustrates the current understanding of volume regulation during stimulation. When an action potential reaches the glutamatergic pre-synaptic terminal of a nerve cell, it causes an elevation in intracellular Ca^{+2} due to the opening of voltage-dependent Ca^{+2} channels. This rise in calcium ultimately triggers the fusion of glutamate containing synaptic vesicles with the cell membrane. The release of glutamate diffuses across the narrow region of the synaptic cleft between the presynaptic membrane of the axon and the postsynaptic membrane of the target dendrite.

Glutamate binds to iGluRs on neurons and glial cells causing an influx of cations. Additionally, astrocytes rapidly clear excess K^{+} and glutamate from the extracellular space. The intracellular water influx which results from these ion movements into cells relieves osmotic pressure gradients and decreases the volume of the extracellular space. The cells which are swollen then can undergo RVD via several specialized channels including VRACs to release ions and organic osmolytes into the extracellular space. Several studies have demonstrated that glutamate-mediated volume regulation mechanisms involving iGluRs facilitate RVD.

While each of these mechanisms has been studied in isolated cell systems, there has been no attempt to examine these processes in the context of physiological neuronal activity *in situ.* Thus, the role of synaptic activity, glutamate, and VRACs in stimulation-induced swelling and recovery is unclear. In this present study I will examine the effects of stimulation, iGluR inhibition, GluT inhibition, and VRAC inhibition to elucidate the specific role of glutamate in cell volume regulation during stimulation-induced cellular swelling.

Figure 6: Mechanisms underlying stimulation-induced volume changes (A) Representation of an astrocyte (purple) and myelinated neurons (blue myelin, yellow neuron). The active synapse is highlighted in red. (B) The active synapse is enlarged to illustrate astrocytic swelling in response to synaptic activity. (Left) Inactive glutamatergic synapse and astrocytic VRACs are inactive. (Middle) During synaptic activity, K^+ and glutamate are released into the extracellular space. Glutamate binds to GluRs causing neurons and glia to experience an influx of cations (not shown). Neuronal swelling is not shown due to cations is not shown. Astrocytes experience an influx glutamate and K^+ via glutamate transports and K^+ channels respectively. A water influx via aquaporins relieves the osmotic pressure in astrocytes resulting in an increased cellular volume and decreased extracellular space. (Right) Osmotic swelling triggers VRACs to mediate the efflux of anions and excitatory amino acids. From (Mulligan and MacVicar, 2006). Reprinted with permission from AAAS.

Figure 6:

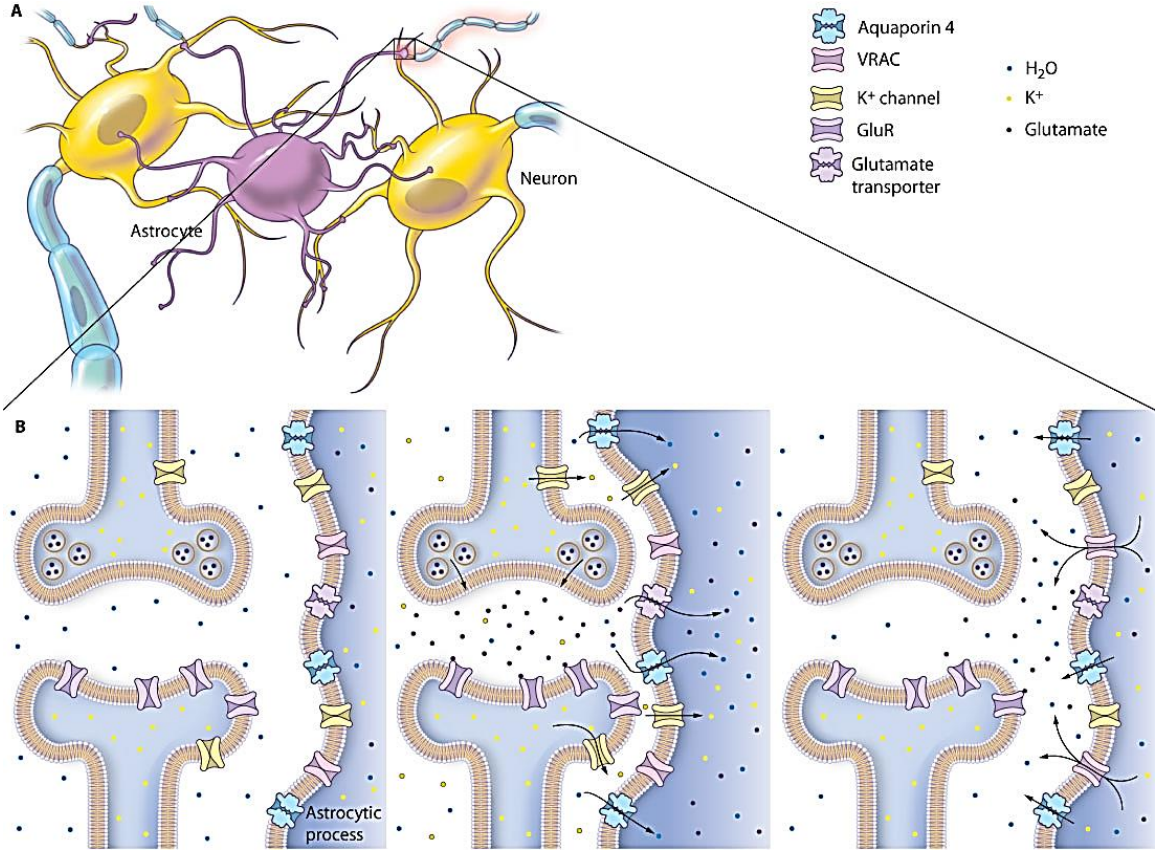
A
Astrocyte
Neuron
Aquaporin 4
VRAC
K+ channel
GluR
Glutamate transporter
H2O
K+
Glutamate
B
Astrocytic process

III: OBJECTIVE & SPECIFIC AIMS

The complex and dynamic interactions that occur at the synaptic level between neurons and glia pose a challenge for understanding volume regulation during functional brain activity. The mechanisms and osmolytes involved in cellular volume regulation during synaptic activity remain uncertain. This research is intended to characterize stimulation–induced volume changes in the hippocampus. To accomplish this task, the interactions between neurons and glia were studied with several specific aims.

Specific aims

Examine the effects of stimulation frequency on cell volume.

The first goal of this study was to identify and characterize the effects of different stimulation frequencies on cell volume. This was accomplished using several different frequencies to orthodromically stimulate the Schaffer collateral pathway while measuring cellular volume simultaneously. A frequency with a measurable change in IOS that offered the most consistent results was selected for the remainder of this project.

Investigate the effects of synaptic block on cell volume.

The second goal of this study was to determine if pre-synaptic activity contributed to stimulation-induced swelling. The synaptic transmission was blocked with

a pharmacological agent and field potential records were used to confirm that synaptic transmission was blocked.

Distinguish the effects of iGluR inhibition on cell volume.

The third goal of this study was to determine the involvement of ionotropic glutamate receptors in volume regulation during stimulation. Pharmacological agents were used during stimulation to inhibit iGluRs present on neurons and glia while observing the changes in cellular volume. The effects of AMPA inhibition and NMDA inhibition were studied separately, as well as together, to observe the effects of total iGluR inhibition. The field potential recordings were used to confirm effectiveness of AMPA inhibition by the absences of excitatory post-synaptic potentials. Field potentials during NMDA inhibition were used to confirm that excitatory post-synaptic potentials remained because neurons were being depolarized by the AMPARs. During total iGluR inhibition, the field potentials were used to confirm that excitatory post-synaptic potentials were blocked due to AMPA inhibition.

Identify the effects of glutamate reuptake inhibition on cell volume.

At the excitatory glutamatergic synapse of the Schaffer collateral pathway, the effects of glutamate reuptake were investigated by the application of a pharmacological agent to block GluTs present on neurons and glia. The field potential recordings were used to confirm that glutamate was accumulating within the synaptic cleft resulting in increased excitability. The cellular volume changes were observed during stimulation with the inhibition of GluTs.

Characterize the effects of VRAC inhibition on cell volume.

The final goal of this study was to determine the involvement of VRAC during stimulation-induced swelling. Given that VRACs activate during cell swelling, the involvement of VRACs was expected to be evident. The inhibition of VRACs was achieved with several different drugs to characterize the changes in IOS.

Significance

These studies will further our understanding of volume regulation that occurs during functional brain activity. This information will provide insight into the osmolytes that are contributing to stimulation-induced swelling and the recovery process of cellular volume. Together, the understanding of volume regulation and the osmolytes involved in volume regulation during physiological conditions will advance treatment protocols for pathophysiological conditions that potentially could lead to brain edema.

IV. MATERIALS AND METHODS

Chemicals

NaCl, dimethyl sulfoxide (DMSO), 2-aminoethanesulfonic acid (taurine), 5-nitro-2-(3-phenylpropylamino)benzoic acid (NPPB), 6-cyano-7-nitroquinoxaline-2,3-dione (CNQX), (+)-MK-801 hydrogen maleate (MK801) were obtained from Sigma-Aldrich (St. Louis, MO)**.** $MgSO_4$, $NaHCO_3$, and KCl were procured from Fisher Scientific (Fairlawn, NJ)**.** $CaCl_2 \cdot 2H_20$, $NaH_2PO_4 \cdot H_20$ and D-glucose (dextrose) were from JT Baker (Phillipsburg, NJ)**;** $NaH_2PO_4 \cdot H_20$ was also obtained from VWR (Westchester, PA); 4-[(2-butyl-6,7-dichloro-2-cyclopen-tyl-2,3-dihydro-1-oxo-1H-inden-5-yl)oxy]butanoic acid **(**DCPIB) and (3S)-3-[[3-[[4-(trifluoromethyl)ben-zoyl]amino]phenyl]methoxy]-L-aspartic acid (TFB-TBOA) were acquired from Tocris Biosciences (Ellisville, MO); 2-[3-(trifluoromethyl)anilino]nicot-inic acid (niflumic acid) was procured from ICN Biomedicals (Aurora, OH); 95% ethyl alcohol (ethanol) was from AAPER (Shelbyville, KY).

Animals

All experiments performed were approved by the Laboratory Animal Care and Use Committee (LACUC) at Wright State University. Fifty-five adult Sprague-Dawley rats of either sex 237±83g (mean ± standard deviation) were housed in a controlled

environment at the Laboratory Animal Care facility at Wright State University. The room temperature was maintained at 74˚F. Rats were housed in full-spectrum fluorescent lights on a 12:12 light:dark cycle. All rats were provided standard tap water and standard feed ofTeklad 8640 Rodent diet (Harlan Laboratories, Madison, WI) ad libitum. The contact bedding used for all experiments was either corn cob (0.6 cm), (The Andersons Inc., Maumee, OH) or aspen chip (Sani Chip, Harlan Laboratories). Rats were transported individually to the laboratory in cages with bedding, food and water. Cages were designed to minimize potential exposure of the animals to disease and personnel to animal allergens on the day of the experiments.

Slice preparation

Once the animal arrived to the laboratory, its weight was recorded and it was anaesthetized for perfusion. Transverse 400 µm thick hippocampus slices were prepared using methods similar to those previously described (Tucker and Olson, 2010; Lein et al., 2011). Animals were anaesthetized to apnea using isoflurane and then perfused via the left cardiac ventricle with ice-cold isotonic artificial cerebrospinal fluid (aCSF) that had been equilibrated with 95% O_2 plus 5% CO_2. Isotonic aCSF consisted of (in mM): 124 NaCl, 3.5 KCl, 2 $CaCl_2$, 1 $MgSO_4$, 1 Na_2HPO_4, 26 Na_2HCO_3, and 10 glucose. Animals then were decapitated and the brain placed into a frozen slurry of aCSF for at least 5 min. Transverse hippocampal tissue slices then were prepared from the middle third of each hippocampus. Figure 7 illustrates the relative position of such a transverse slice within the rat brain (Amaral and Witter, 1989). Slices were cut in a plane that preserved Schaffer collateral connections (Teyler, 1980) and then were transferred to a preincubation chamber where they remained for at least 60 min at room temperature in aCSF

equilibrated with 95% O_2 plus 5% CO_2. For most slices, 1 mM taurine was added to the aCSF to maintain normal tissue taurine content (Kreisman and Olson, 2003). After the slice preparation and a 60 min preincubation period, slices were transferred individually to the recording stage of a Haas-type interface chamber and perfused with aCSF equilibrated with 95% O_2 plus 5% CO_2 at 35°C. For slices exposed to 1 mM taurine during room temperature incubation, the same taurine concentration was present during the first 30 min of perfusion on the recording stage.

Figure 7: Lateral view of hippocampal formation in the rodent brain. The parietal and temporal neo-cortex are removed to expose the position of the hippocampal formation. The transverse axis (Trans) is shown perpendicular to the long septotemporal axis of the hippocampus. A transverse slice is depicted from the middle of the left hippocampus and enlarged at the top left to show the intrinsic synaptic connections. Abbreviations: CA1, Cornu Ammonis 1;CA3, Cornu Ammonis 3;DG, dentate gyrus; mf, mossy fibers; pp, perforant path; S, subiculum; Se, septal; sc, Schaffer collaterals; T, temporal.

Figure 7:

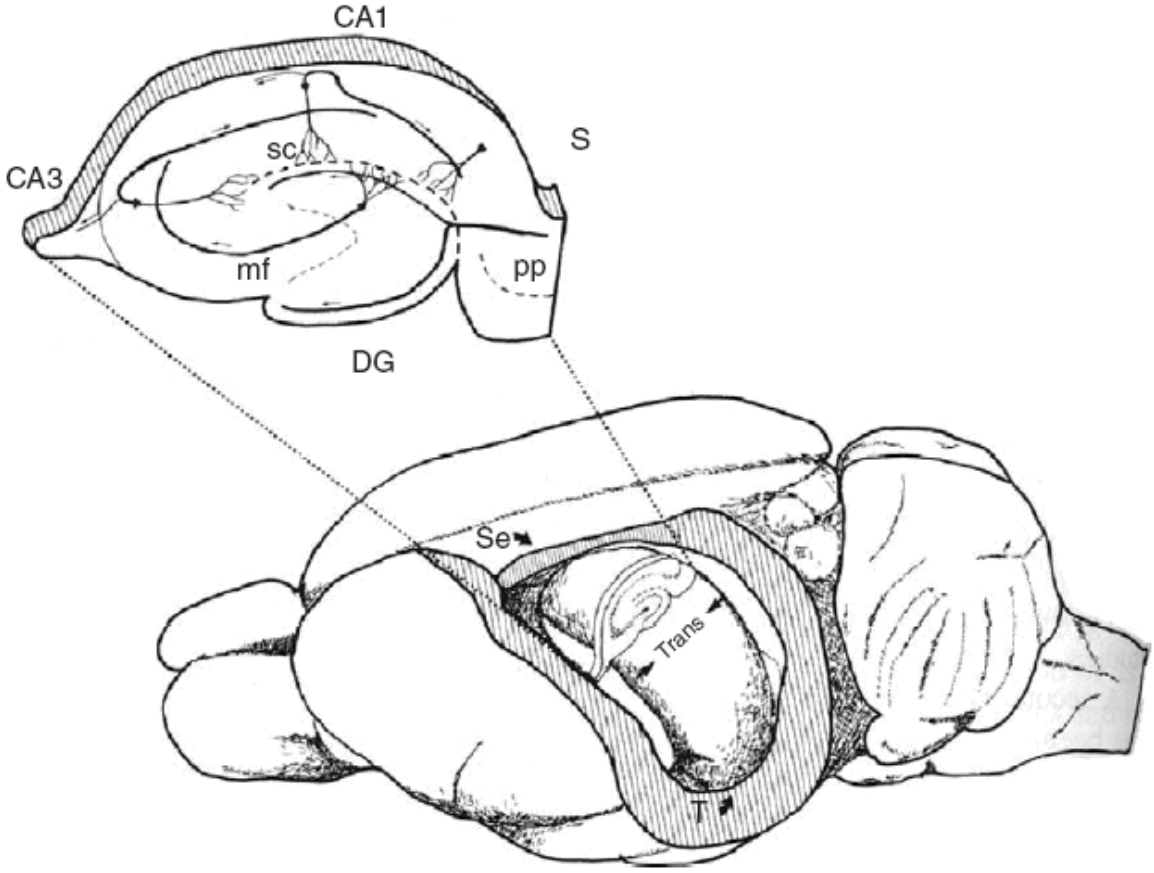

Electrophysiology

Electrical stimulation

All experiments were conducted inside a Faraday cage to prevent electrostatic and electromagnetic inference. pClamp 6 software (Axon Instruments, Union City, CA) was used for stimulation control in combination with a single channel stimulator (S-900, Dagan Corporation, Minneapolis, MN) and stimulus isolation unit (S-910, Dagan Corporation, Minneapolis, MN). A stimulation pulse of 200 μsec length was delivered at 30 sec intervals to a bipolar electrode made of 178 μm diameter Teflon-coated stainless steel wires. The stimulating electrodes were placed in the stratum radiatum of the CA3 region to orthodromically stimulate the Schaffer collateral pathway (Figure 8). These electrodes were placed prior to positioning the glass recording electrode to prevent damage to the recording electrode by movement of the slice. Low frequency stimulation, considered a pulse frequency rate of once every 30 sec, was delivered to slice prior to high frequency stimulation trains. During high frequency stimulation, slices received a train of pulses at 1, 3, 5, or 10 Hz for 5 minutes. After the stimulation train, low frequency stimulation resumed. If slices were given more than one high frequency stimulation train, the trains were separated by 5 min. pClamp 6 software was used for data acquisition and analysis.

Field potential recording

Population field potentials from pyramidal neurons were recorded with a glass microelectrode (WPI inc, Sarasota, FL) filled with aCSF (~50 MΩ) and positioned in either the pyramidal cell layer or stratum radiatum of CA1 (Figure 2). Voltages were

measured with a high input impedance dual differential electrometer (FD223, WPI Inc, Sarasota, FL). The responses to stimulation were filtered using a 2 pole 5 kHz low-pass and amplified ×10 during data acquisition. The resulting waveform was displayed on an oscilloscope and digitized with pClamp software (TDS-340A, Tektronic, Beaverton, OR). By monitoring the peak-to-peak response of the population spike with the oscilloscope, the stimulus current amplitude was adjusted to give the maximum signal with the lowest stimulus strength. This typically resulted in stimulus currents between 0.2 and 0.9 mA. Baseline responses were recorded to assure slice quality and viability.

Figure 8: Image of a hippocampal slice on recording stage. Single line labeled "Recording" shows the placement of the glass microelectrode within the in the pyramidal cell layer of CA1. The two lines labeled "Stimulation" point to the bipolar stimulating electrodes placed in the stratum radiatum of the CA3. The subiculum, dentate gyrus, and entorhinal cortex are labeled for orientation.

.

Figure 8:

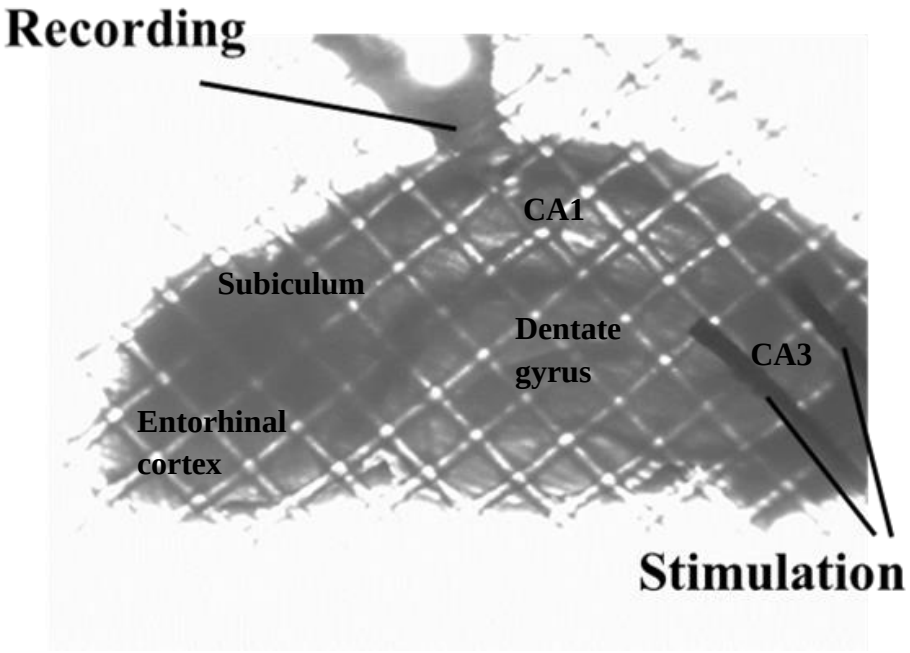
Recording
CA1
Subiculum
Dentate
gyrus
CA3
Entorhinal
cortex
Stimulation

Imaging

Slices were transluminated from below with white light from a DC-regulated illuminator (PL-900 Dolan-Jenner, Boxborough, MA) and viewed with an upright stereo microscope (SMZ 800, Nikon, Melville, NY). Slice images were acquired at 10-sec intervals using a charge-coupled device (CCD) fixed gain camera with 640 x 480 pixel spatial resolution and 8-bit intensity resolution (maximum of 255 units). Images were captured and a region of interest (ROI) in the stratum radiatum of CA1 between the stimulation and recording electrodes was selected using ImageJ software. The average pixel intensity within the ROI was calculated to indicate the magnitude of light transmission through the slice. The intensity of the illuminating light source was adjusted to give an average intensity in the ROI of approximately 120 units at the start of recordings. Baseline images were taken prior to drug treatment. All experiments were performed in a darkened room to prevent reflected light from other sources from interfering with the transmitted light signal.

Drug application

For some experiments, isotonic aCSF was modified to block synaptic activity in the slices by reducing the concentration of $CaCl_2$ to 0.2 mM and increasing the concentration of $MgSO_4$ to 11.4 mM. Depending on the drug used. isotonic aCSF, DMSO, or 95% ethanol were used as vehicles for stock solutions. For AMPAR inhibition, slices were perfused with 25 µM CNQX for 20 min prior to beginning the stimulation train. We found this was sufficient time to completely block population field potentials. Slices exposed to NMDAR inhibitors were perfused 15 min with 10 µM MK801 prior to the stimulation train. Effects of complete iGluR inhibition was

investigated by perfusing slices with a combination of both 25 µM CNQX and 10 µM MK801 for 20 min prior to beginning the stimulation train. Slices used to study glutamate uptake inhibition were perfused with 1 µM TBF-TBOA for 20 min prior to beginning the stimulation train. Slices exposed to the VRAC inhibitors, 20 µM DCPIB, 100 µM niflumic acid, or 100 µM NPPB were perfused with for 15 min prior to the start of the stimulation train. When used, drugs also were present throughout the stimulation train and during the subsequent 15 min recovery period.

Experimental design

Figure 9 illustrates the typical experimental design for taurine-loaded slices treated with a drug. During time of taurine perfusion on the recording stage stimulating and recording electrodes were placed in the slice. Stimulation and image recording began during the taurine perfusion period. Immediately following perfusion with taurine, slices were exposed to a drug treatment for 15-20 min before the start of a high frequency stimulation train. Image and electrophysiological data collected during the experiments were archived on a network server and transferred at the end of the day to a personal computer for analysis.

Figure 9: Schematic of experiment timeline. The experimental design of a typical taurine-loaded slice involved changes in stimulation and perfusion. When a drug was not used, isotonic aCSF replaced the period of drug perfusion. Stimulation frequencies during the experiment are shown in boxes above the arrow. Changes in the composition of the perfusion solution that occurred during an experiment are shown inside the arrow. The approximate time period of each event is shown within its corresponding box.

Figure 9:

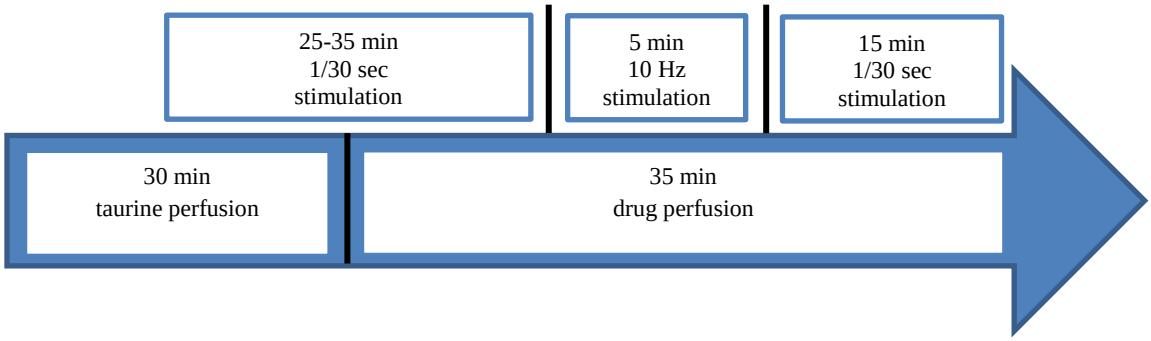
25-35 min
1/30 sec
stimulation
5 min
10 Hz
stimulation
15 min
1/30 sec
stimulation
30 min
taurine perfusion
35 min
drug perfusion

Field potential analysis

A Gaussian low pass filter with a cut off of 5 kHz was applied to the electrophysiological signals prior to digital acquisition by pClamp software. To examine drug effects on the stimulation-induced field potentials, the magnitude of the population spike was calculated by measuring the peak-to-peak amplitude at the population spike signal. The mean amplitude was calculated by averaging results from 5 sequential records over a 2.5 min time interval. These mean amplitudes were calculated at several time periods throughout the experiment: prior to drug treatment, at the end of drug loading, at the end of high frequency stimulation, and at the end of the experiment.

Image analysis

The average intensity of the ROI in the hippocampal slice acquired during the minute prior to the beginning of high frequency stimulation train was averaged to use as a baseline to normalize measurements from each of the following ROI values (Figure 10). The resulting normalized values thus describe the fractional change in light transmittance of the slice over time. The change in light transmittance within the selected ROI was graphed to characterize changes that occurred during high frequency synaptic activity and pharmacological treatments. NIH Image software was used to normalize each hippocampus slice image on a pixel-by-pixel basis to the average of seven images acquired during the minute prior to high frequency stimulation. A pseudocolor intensity scale was applied to these normalized images to display regional changes in light transmittance (Figure 11).

Intrinsic optical signal (IOS) analysis

In order to gain insight into how brain activity effects the movement of water between intracellular and extracellular compartments, we used the change in light absorption to provide an indirect measure of volume changes. Intrinsic optical signals (IOSs) refer to changes in optical properties of an unstained biological tissue measured as a change of either light transmittance or reflectance. Previous studies have shown that cellular swelling is associated with decreased light scattering, decreased reflectance, and increased light transmittance through biological tissue samples (MacVicar and Hochman, 1991; Andrew and MacVicar, 1994; Andrew et al., 1996; Aitken et al., 1999; Andrew et al., 1999; Muller and Somjen, 1999; Bahar et al., 2000; Fayuk et al., 2002; Tucker and Olson, 2010; Pal et al., 2013). In these studies, light transmission of the ROI was used to determine the IOS. IOS has been used to indirectly measure brain tissue volume changes in brain tissue slices

To characterize IOSs during high frequency stimulation, several measurements were taken during the time course of an experiment. These include: on-set slope, maximum IOS, time point of the maximum IOS, off-set slope, and the value measured 15 min after the high frequency stimulation train was terminated (Figure 10). For slices exposed to the same treatment, measurements of each parameter were averaged and the standard error of the mean (SEM) was calculated.

Figure 10: Schematic of measured IOS Parameters. A) Baseline region used to normalize light transmission signals. B) Region of IOS highlighted with a blue bar to show the linear approximation used to calculate the on-set slope. C) Region of IOS recorded for the maximum change in IOS. D) Region where the time at maximum IOS was recorded. E) Region of IOS highlighted with a blue bar to show the linear approximation used to calculate the off-set slope. F) Region where IOS recovery was measured 15 min after the high frequency stimulation train was terminated.

Figure 10:

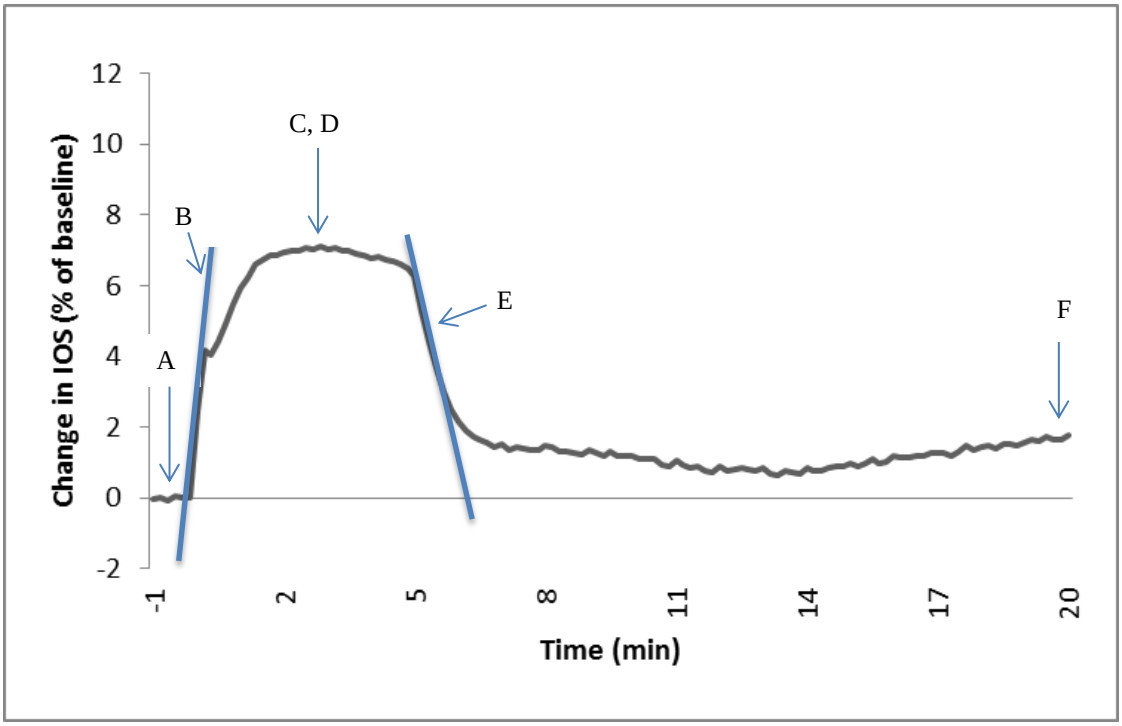
Change in IOS (% of baseline)
12
10
8
6
4
2
0
-2
A
B
C, D
E
F
-1
2
5
8
11
14
17
20
Time (min)

Figure 11: Colorized hippocampus slice image. The pseudocolor intensity scale represents percent change in IOS from baseline (black regions indicate no change in IOS). A) Baseline slice image before initiation of high frequency stimulation indicates no change in IOS. B) Slice during high frequency stimulation displays increased IOS along the SC pathway.

Figure 11:

A)

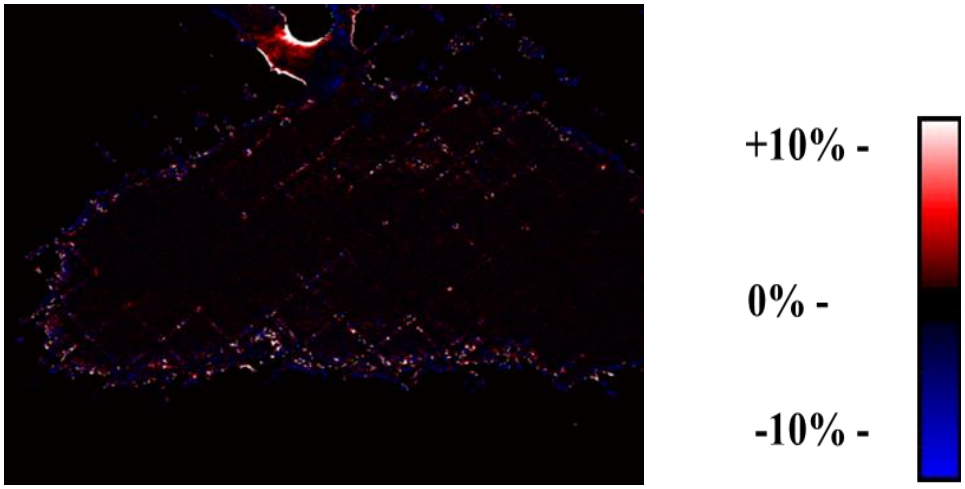

B)

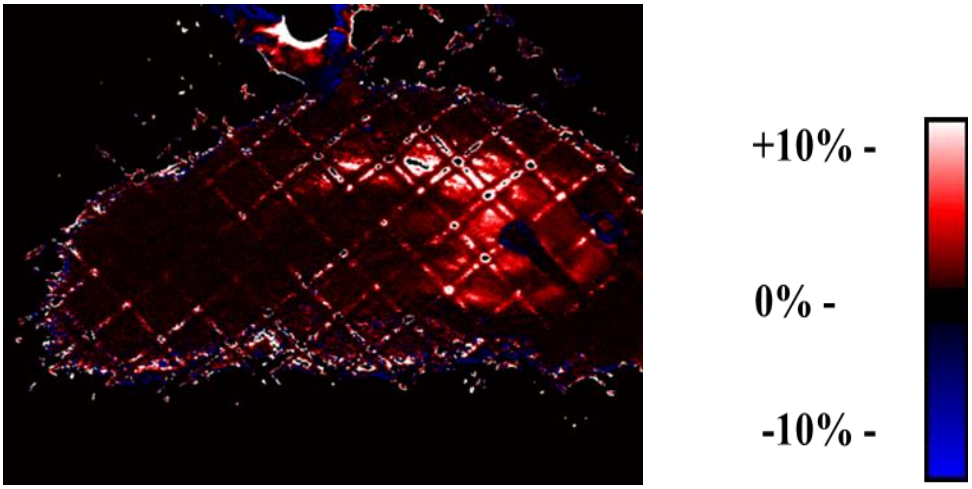

On-set slope

The on-set slope corresponds with the initial change in IOS observed at the start of high frequency stimulation. It was derived as the slope of a linear approximation calculated from 2-3 normalized IOS values. The number of values chosen to calculate on-set slope was determined as the number of points which yielded the minimum coefficient of variation across experiments. The mean on-set slope was calculated for each treatment along with the SEM of these mean values.

Maximum IOS and corresponding time

During the high frequency stimulation train, the maximum IOS and the time at which the maximum IOS point occurred was recorded. The time at which the maximum IOS point occurred is expressed relative to the beginning of the high frequency stimulation train. The mean maximum IOS and time point were calculated for each treatment along with the standard error of mean of these mean values

Off-set slope

The off-set slope measurement began immediately after the high frequency stimulation and consisted of a linear approximation of 2-6 values. The number of values chosen to calculate off-set slope was determined as the number of points which yielded the minimum coefficient of variation across experiments. The mean off-set slope was calculated for each treatment along with the SEM of these mean values.

IOS recovery

IOS was measured for each slice 15 min after the end of the high frequency stimulation train to get a measure of recovery. Slices used to study stimulation-frequency

were only given 5 min of recovery following the stimulation train. Thus IOS recovery was taken 5 min after the end of stimulation for these initial experiments. The mean IOS recovery was calculated for each treatment along with the SEM of these mean values.

Statistical analysis

Quantitative data are presented as the mean values ± SEM. Amplitude values from electrophysiological recordings and IOS values were analyzed for statistical significance using a one-way ANOVA with Dunnett's *post hoc* analysis for multiple comparisons. A two-way ANOVA without replication with Dunnett's *post hoc* analysis was used in the analysis of IOS during iGluR inhibition. For some studies, the non-parametric Mann-Whitney U test was used if data was not normally distributed. Values were considered significantly different for $p < 0.05$.

V. RESULTS

Hippocampal volume response to stimulation is frequency dependent

The Schaffer collateral pathway was stimulated at 1, 3, 5, and 10 Hz for 5 min. In slices without taurine treatment, the magnitude of changes in light transmission through the slice increased as the frequency of the stimulation train increased (Figure 12). Several parameters were taken during the time course of the experiment to characterize the effects of stimulation frequency on IOS. The on-set slope, taken from the start of high frequency stimulation was calculated for each frequency change. The on-set slope was significantly different from baseline at 10 Hz stimulation but not for lower frequencies (Figure 13). The off-set slope, taken at the end of high frequency stimulation, was significantly different from baseline at 10 Hz (Figure 13). The maximum change in IOS increased with increased stimulation; however, the maximum change in IOS from the baseline and the time at which the maximum occurred were not significant at any frequency (Table 1). The IOS measured after 5 min of recovery was not significantly different from the baseline value at any frequency.

Figure 12: Effects of stimulation frequencies on IOS. Slices were stimulated at the frequencies shown and slice images acquired every 10 sec. Values are the mean ± SEM of 5-6 slices. Some error bars for individual time points are removed for clarity.

Figure 12:

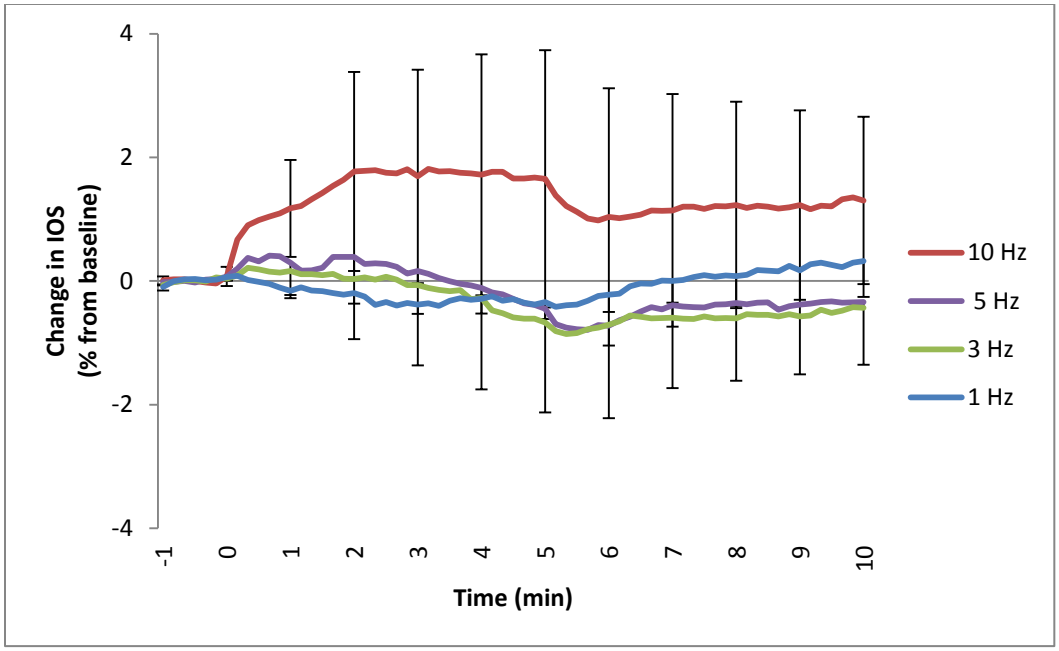
Change in IOS
(% from baseline)
4
2
0
-2
-4
-1
0
1
2
3
4
5
6
7
8
9
10
Time (min)
10 Hz
5 Hz
3 Hz
1 Hz

Figure 13: On-set slope and off-set slope measured at different stimulation frequencies. * Indicates values which are significantly different from baseline by a one-way ANOVA ($p<0.05$) and Dunnett's *post hoc* test.

Figure 13:

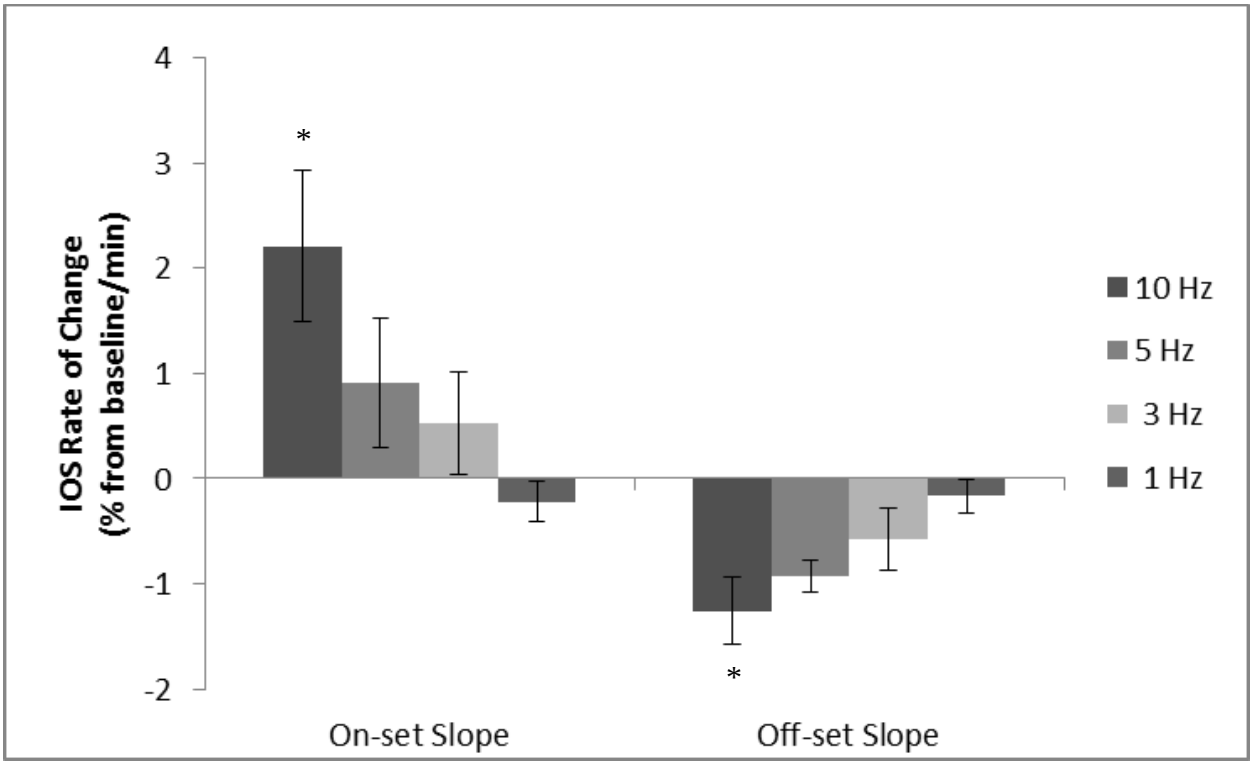
4
3
2
1
0
-1
-2
IOS Rate of Change
(% from baseline/min)
*
*
On-set Slope
Off-set Slope
10 Hz
5 Hz
3 Hz
1 Hz

Table 1: Effect of stimulation frequency on maximum IOS, time at the maximum IOS, and IOS recovery after 5 min. Values are the mean ± SEM from 5-6 hippocampal slices. No values were significantly different from baseline by a one-way ANOVA ($p<0.05$) and Dunnett's *post hoc* test.

Table 1:

Stimulation Frequency	Maximum change in IOS (% from baseline)	Time at Maximum IOS (min)	Last min of IOS (% from baseline)
1 Hz	0.23 ± 0.11	0.92 ± 0.72	0.28 ± 0.57
3 Hz	0.73 ± 0.53	1.37 ± 0.75	-0.48 ± 0.31
5 Hz	1.68 ± 1.21	1.06 ± 0.53	-0.34 ± 1.06
10 Hz	2.52 ± 1.40	1.72 ± 0.87	1.26 ± 1.29

Synaptic blockage inhibits stimulation-induced swelling

Population field potentials

A synaptic block solution (SBS) was created by modifying aCSF with low Ca^{+} and high Mg^{+} concentration. Slices were perfused with the SBS 10 min prior to high frequency stimulation and throughout the period of high frequency stimulation and recovery. Field potential recordings were used to verify that the slice was synaptically blocked. Figure 14 shows the field potential at several time periods during the course of the experiment. The mean amplitude of the population spike measured over 2.5 min prior to SBS perfusion was 2.34 ± 0.17mV. The amplitude remained significantly reduced from the baseline amplitude throughout SBS exposure. The amplitude was reduced at the end of the 10 min perfusion to 1.17 ± 0.22mV. During the last half of the high frequency stimulation, the amplitude decreased further to 1.01 ± 0.15mV. By the end of the experiment, the amplitude had increased somewhat to 1.12 ± 0.21mV but did not recover to the baseline amplitude.

Stimulation-induced changes in IOS

IOS responses to stimulation were reduced in slices perfused with SBS and remained relatively unchanged following the high frequency stimulation (Figure 15). There was a significantly reduced on-set slope in synaptically blocked slices, but the off-slope was not statistically different from that measured in control slices (Figure 16). The maximum IOS was reduced in synaptically blocked slices, but the time to reach the maximum IOS was not statistically different (Table 2). Slices exposed to SBS did not return towards the baseline following high frequency stimulation.

Figure 14: Effects of synaptic block on stimulation-induced field potentials. Individual field potentials were taken at several periods during the experiment A) Baseline field potential taken prior to SBS exposure B) Field potential after 10 min drug loading C) Field potential at the end of 10 Hz stimulation. D) Field potential 15 min after the end of the 10 Hz stimulation train. Arrows point to the composite action potential spike in the Schaffer collateral axons. The sampling interval of the individual field potential recordings was reduced by a factor of 10. The graphed field potentials were expanded to show the first 20 ms of the recording data for clarity purposes.

Figure 14:

A)

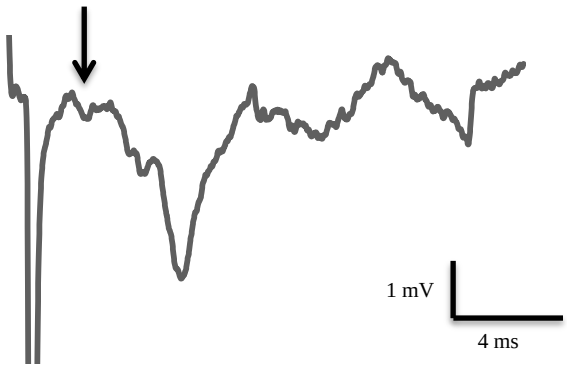

B)

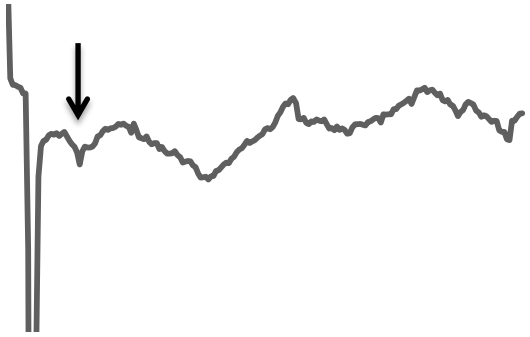

C)

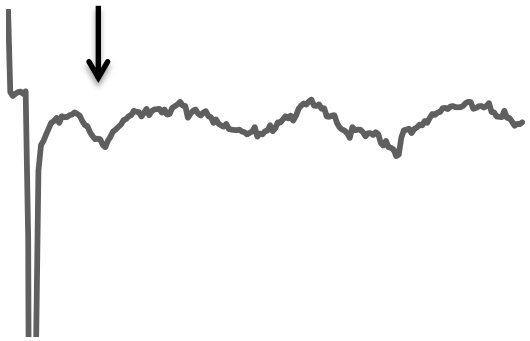

D)

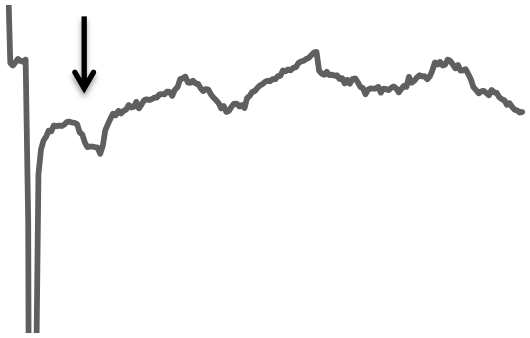

Figure 15: Effect of synaptic block on stimulation-induced changes in IOS. Values are the mean ± SEM of 5-7 slices. Some error bars for individual time points are removed for clarity.

Figure 15:

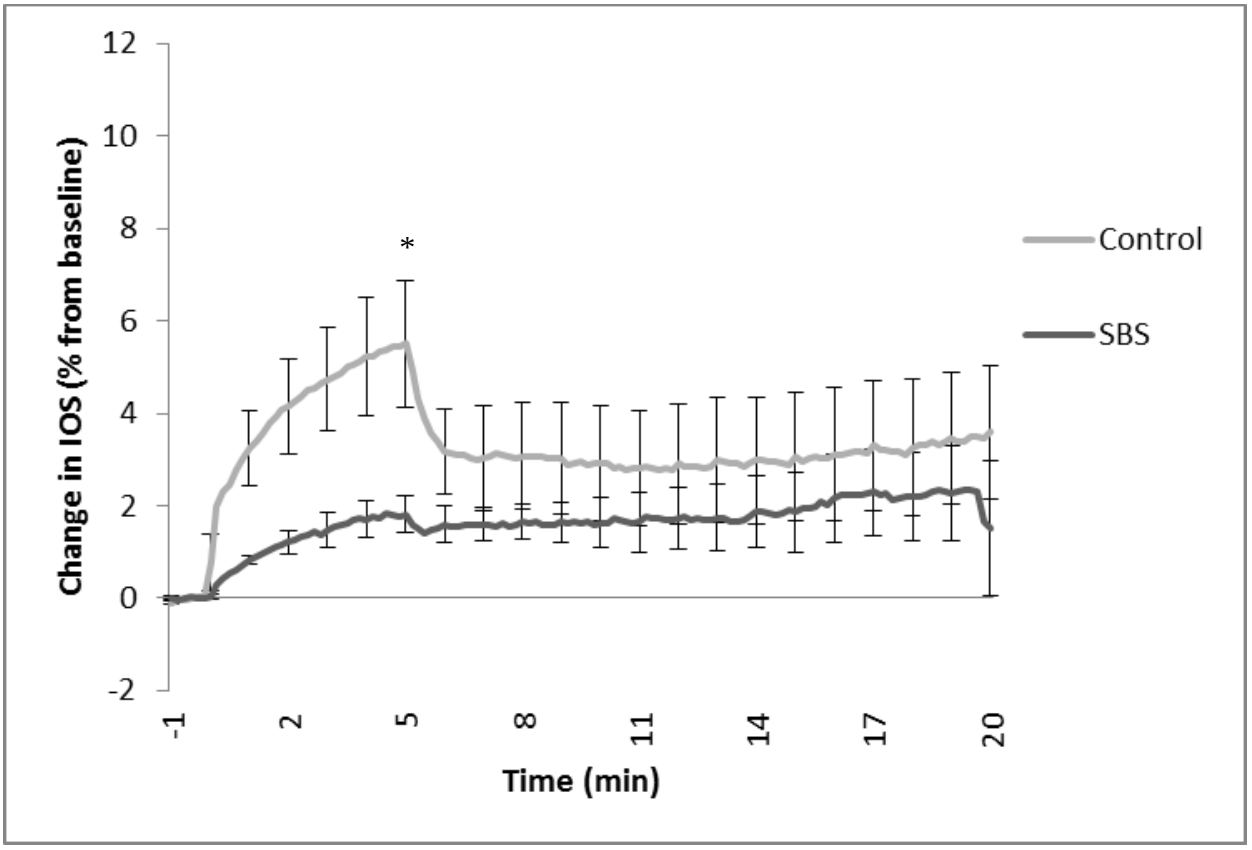
12
10
8
6
4
2
0
-2
Change in IOS (% from baseline)
*
Control
SBS
-1
2
5
8
11
14
17
20
Time (min)

Figure 16: On-set slope and off-set slope measured with perfusion with synaptic block solution. Values are the mean ± SEM of 5-7 slices. * Indicates values which are significantly different from control by a one-way ANOVA ($p<0.05$) and Dunnett's *post hoc* test.

Figure 16:

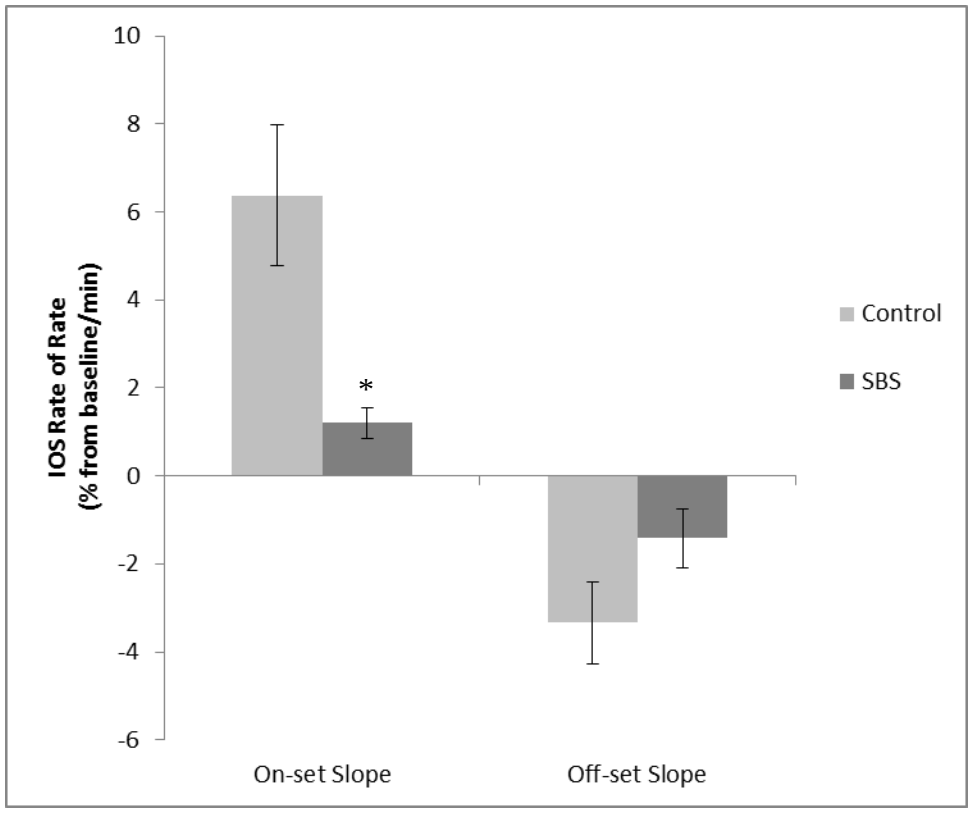
10
8
6
4
2
0
-2
-4
-6
IOS Rate of Rate
(% from baseline/min)
*
Control
SBS
On-set Slope
Off-set Slope

Table 2: Effect of SBS on maximum IOS, time at maximum IOS, and last min of IOS. Values are the mean ± SEM from 5-7 hippocampal slices. * Indicates values which are significantly different from control by a one-way ANOVA ($p<0.05$) and Dunnett's *post hoc* test or Mann-Whitney U test.

Table 2:

Group	Maximum change in IOS (% from baseline)	Time at Maximum IOS (min)	Last min of IOS (% from baseline)
Control	6.22 ± 1.61	4.69 ± 0.19	3.47 ± 1.43
SBS	1.99 ± 0.34*	3.63 ± 0.76	2.08 ± 1.16

iGluR inhibtions does not alter stimulation-induced changes in IOS

Population field potentials

Hippocampal slices were exposed to 25 µM CNQX or 10 µM MK801 to examine the role of glutamate AMPA or NMDA signaling, respectively, for stimulation-induced swelling and volume regulation. Complete inhibition of iGluRs was achieved with perfusion of both 25 µM CNQX and 10 µM MK801 in the aCSF. Control slices were exposed to aCSF containing 0.1% DMSO, the vehicle used to make stock solutions of CNQX and MK801. Field potential recordings were used to verify viability of the slice and inhibition of AMPA receptors. In the presence of CNQX, the population spike amplitude was significantly reduced in the electrophysiological recordings following 20 min of CNQX perfusion. Figure 17 shows several field potentials recorded during the course of a CNQX experiment. Perfusion with MK801 did not significantly impact the amplitude of the population spike except during the high frequency stimulation (Figure 18). In the presence of CNQX and MK801, the amplitude was significantly reduced throughout the experiment following the 20 min perfusion (Figure 19). Table 3 shows the calculated amplitudes prior to drug exposure, at the end of drug loading, at the end of the high frequency stimulation, and at the end of the experiment.

Stimulation-induced changes in IOS

The stimulation-induced IOS responses of slices perfused with CNQX were similar to that measured in slices perfused with drug vehicle (Figure 20). In contrast, slices perfused with MK801 showed a reduced IOS response (Figure 21). Perfusion with the combination of CNQX and MK801 to block all iGluRs also reduced the stimulation-induced change in IOS (Figure 22). Inhibition of iGluRs decreased the IOS rate of change

for the on-set and off-set slopes (Figure 23). The inhibition of AMPARs did not slow the rate of change as much as inhibition of NMDARs. During total iGluR inhibition, there was an additive effect on the IOS rate of change. In the presence of CNQX, the peak typically occurred later during the high frequency stimulation train. During the last min of images, the IOS was similar to controls for all drug treatments. With NMDA inhibition alone, the IOS maximum was significantly reduced. Total iGluR inhibition also tended to reduce the maximum IOS change but the value was not statistically different from controls. Table 4 summarizes effects of iGluR inhibition on the maximum IOS and when this peak occurred relative to the start of high frequency stimulation.

Figure 17: Effects of CNQX on stimulation-induced field potentials. Individual field potentials were taken at several periods during the experiment A) Baseline field potential taken prior to CNQX exposure B) Field potential after 20 min of drug loading C) Field potential at the end of 10 Hz stimulation. D) Field potential 15 min after the end of the 10 Hz stimulation train. The sampling interval of the individual field potential recordings was reduced by a factor of 10. The graphed field potentials were expanded to show the first 20 ms of the recording data for clarity purposes.

Figure 17:
A)

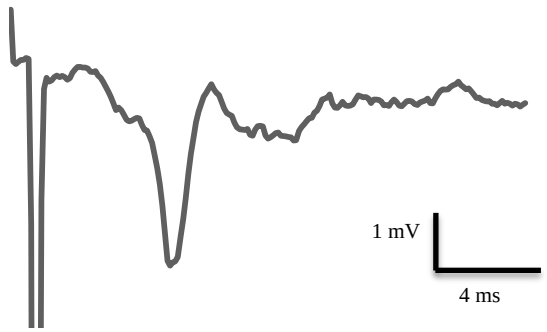

B)

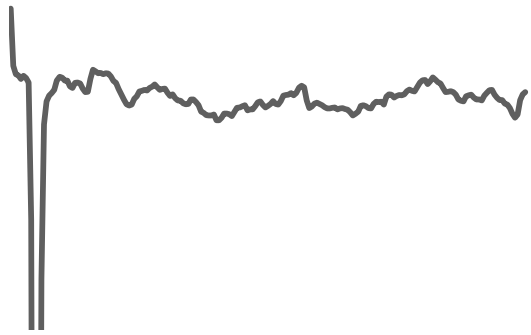

C)

D)

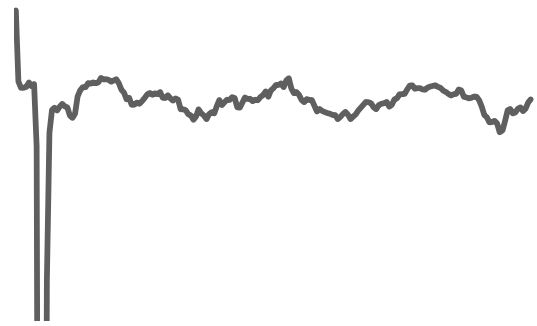

Figure 18: Effects of MK801 on stimulation-induced field potentials. Individual field potentials were taken at several periods during the experiment A) Baseline field potential taken prior to MK801 exposure B) Field potential after 15 min of drug loading C) Field potential at the end of 10 Hz stimulation. D) Field potential 15 min after the end of the 10 Hz stimulation train. The sampling interval of the individual field potential recordings was reduced by a factor of 10. The graphed field potentials were expanded to show the first 20 ms of the recording data for clarity purposes.

Figure 18:
A)

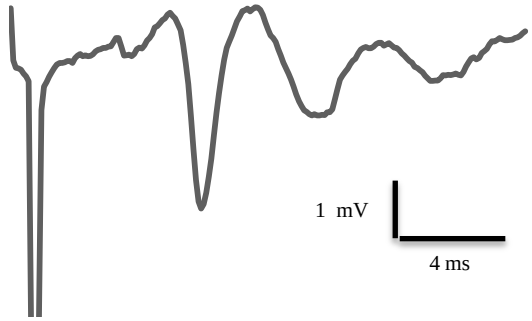

B)

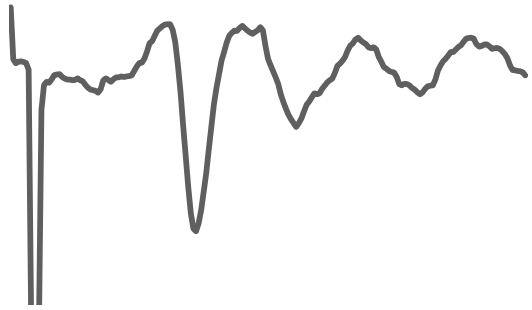

C)

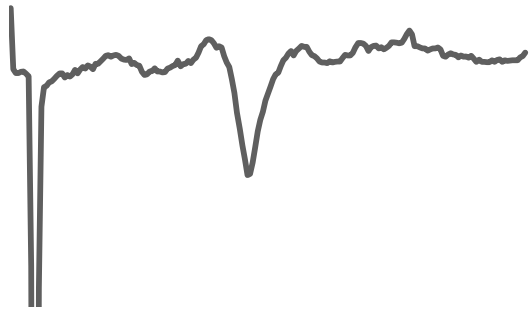

D)

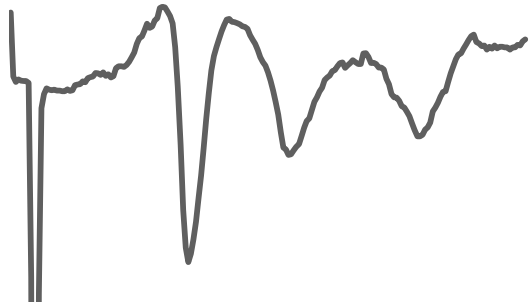

Figure 19: Effects of total iGluR inhibition on stimulation-induced field potentials. Individual field potentials were taken at several periods during the experiment A) Baseline field potential taken prior to CNQX+MK801 exposure B) Field potential after 20 min of drug loading C) Field potential at the end of 10 Hz stimulation. D) Field potential 15 min after the end of the 10 Hz stimulation train. The sampling interval of the individual field potential recordings was reduced by a factor of 10. The sampling interval of the individual field potential recordings was reduced by a factor of 10. The graphed field potentials were expanded to show the first 20 ms of the recording data for clarity purposes.

Figure 19:
A)

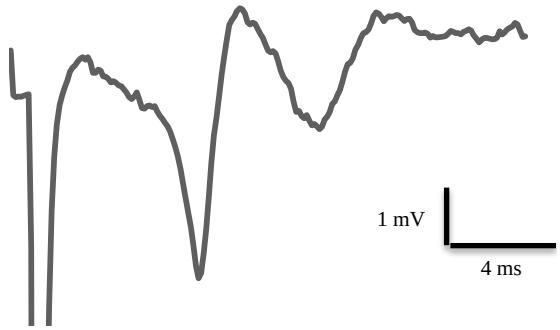

B)

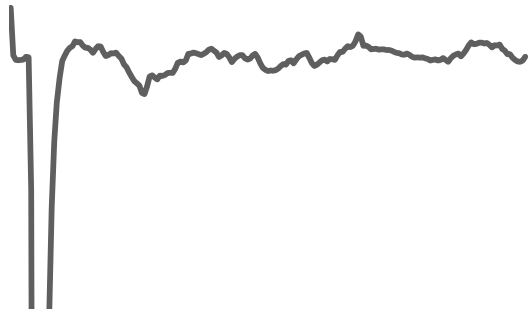

C)

D)

Table 3: Effects of iGluR inhibition on population spike amplitude. Values are the mean ± SEM from 3-6 hippocampal slices. * Indicates values which are significantly different from baseline amplitude by a one-way ANOVA ($p<0.05$) and Dunnett's *post hoc* test.

Table 3:

Group	Baseline amplitude (mV)	End of drug loading amplitude (mV)	End of 10 Hz train amplitude (mV)	End of experiment amplitude (mV)
CNQX	4.19 ± 1.40	1.02 ± 0.1 *	0.75 ± 0.07 *	1.01 ± 0.08 *
MK801	4.42 ± 0.53	4.57 ± 0.54	1.24 ± 0.12 *	4.55 ± 0.42
CNQX + MK801	4.29 ± 0.56	1.12 ± 0.05 *	0.88 ± 0.12 *	1.27 ± 0.32 *

Figure 20: Effects of CNQX on stimulation-induced changes in IOS. Values are the mean ± SEM of 4-5 independent measurements. Some error bars for individual time points are removed for clarity.

Figure 20:

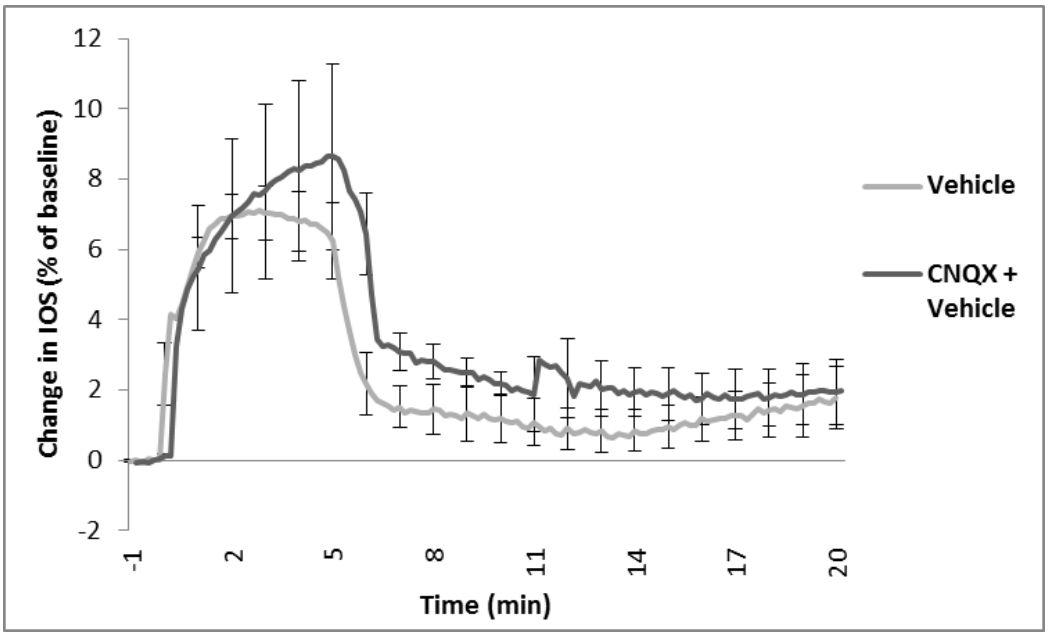
Change in IOS (% of baseline)
12
10
8
6
4
2
0
-2
-1
2
5
8
11
14
17
20
Time (min)
Vehicle
CNQX + Vehicle

Figure 21: Effects of MK801 on stimulation-induced changes in IOS. Values are the mean ± SEM of 4 independent measurements. Some error bars for individual time points are removed for clarity.

Figure 21:

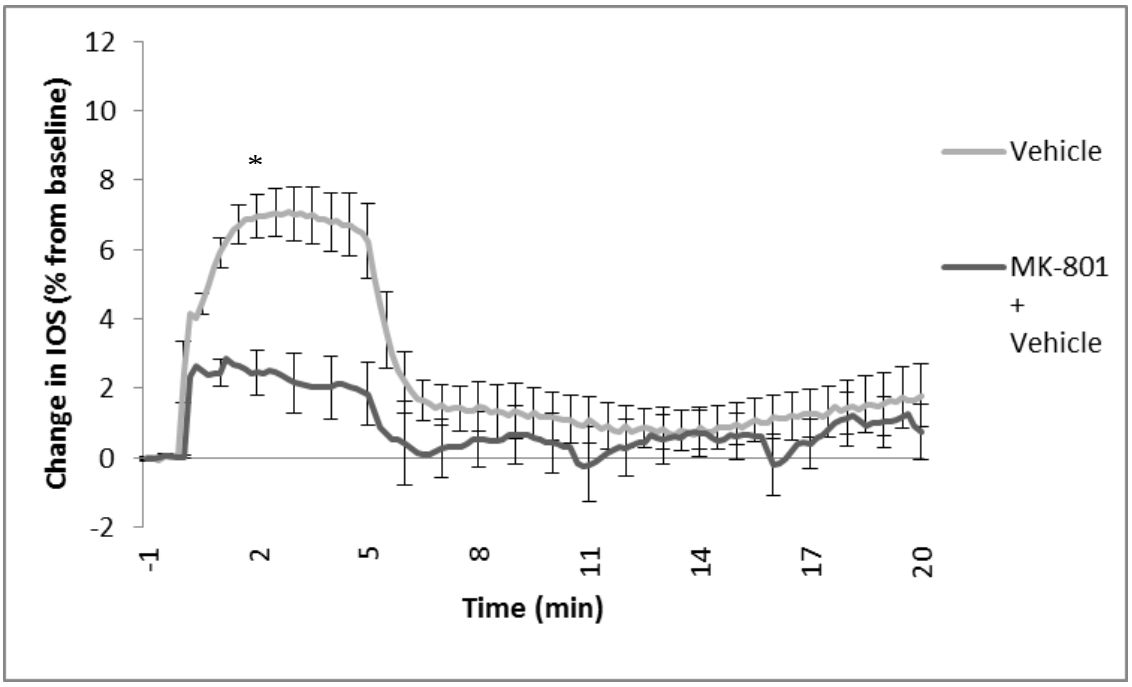
Change in IOS (% from baseline)
12
10
8
6
4
2
0
-2
*
-1
2
5
8
11
14
17
20
Time (min)
Vehicle
MK-801
+
Vehicle

Figure 22: Effects of total iGluR inhibition on stimulation-induced changes in IOS. Values are the mean ± SEM of 4 independent measurements. Some error bars for individual time points are removed for clarity.

Figure 22:

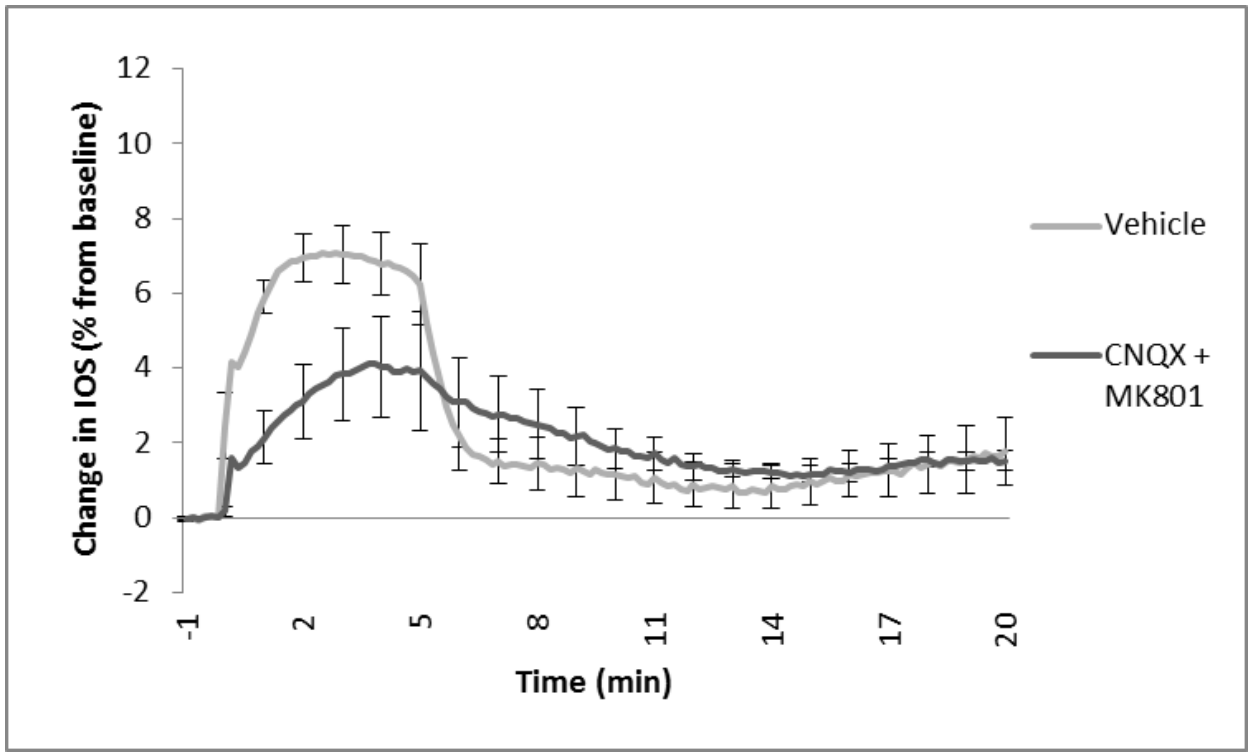
Change in IOS (% from baseline)
12
10
8
6
4
2
0
-2
-1
2
5
8
11
14
17
20
Time (min)
Vehicle
CNQX + MK801

Figure 23: Measured on-set slope and off-set slope with iGluR inhibition. * Indicates values which are significantly different from the vehicle by a two-way ANOVA ($p<0.05$) and Dunnett's *post hoc* test.

Figure 23:

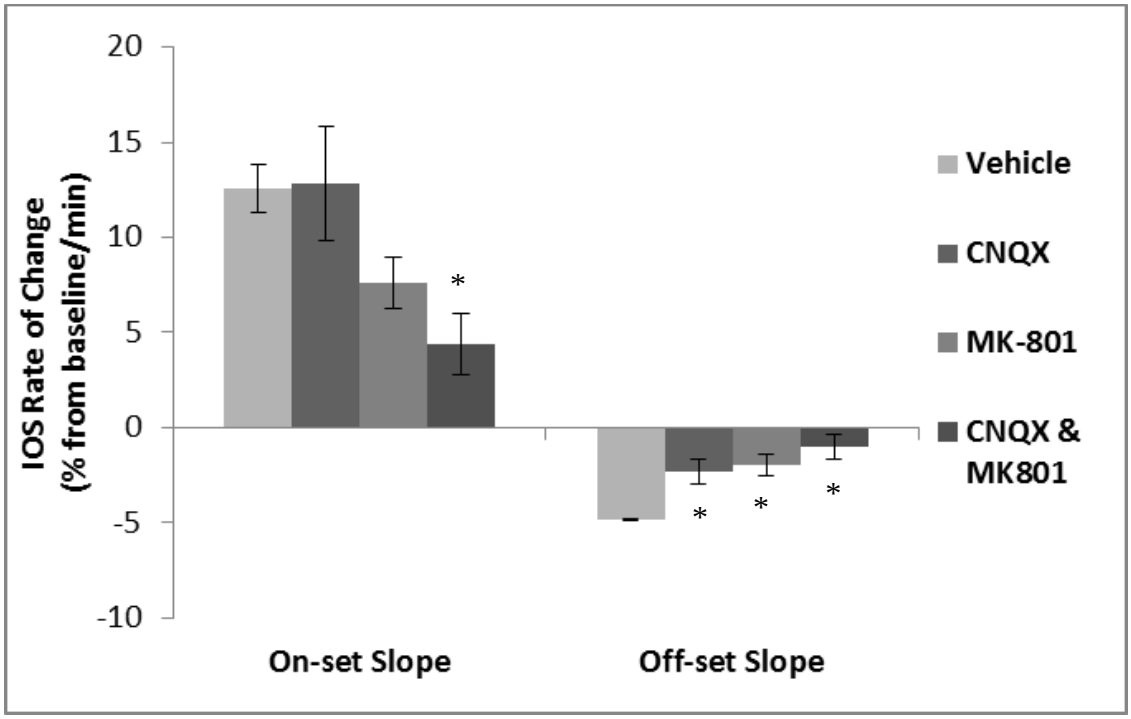
20
15
10
5
0
-5
-10
IOS Rate of Change
(% from baseline/min)
*
*
*
*
On-set Slope
Off-set Slope
Vehicle
CNQX
MK-801
CNQX &
MK801

Table 4: Effect of iGluR inhibition on maximum IOS, corresponding time at maximum IOS, and last min of IOS. Values are the mean ± SEM from 4-5 hippocampal slices. * Indicates values which are significantly different from the vehicle by a two-way ANOVA ($p<0.05$) and Dunnett's *post hoc* test.

Table 4:

Groups	Maximum IOS (% from baseline)	Time at Maximum IOS (min)	Last min of IOS (% from baseline)
Vehicle	7.34 ± 0.79	3.00 ± 0.52	1.68 ± 0.87
CNQX	8.75 ± 2.66	4.73 ± 0.30 *	1.96 ± 0.99
MK801	3.69 ± 0.82 *	1.38 ± 0.79	1.45 ± 0.88
CNQX + MK801	4.41 ± 1.35	4.58 ± 0.26	1.52 ± 0.24

Glutamate uptake inhibition prevents stimulation-induced swelling

Population field potentials

TFB-TBOA was used to inhibit glutamate uptake during high frequency stimulation. The population spike amplitude increased after 15 min of perfusion with 1μM TFB-TBOA from 2.75 ± 0.86 mV to 3.51 ± 0.62 mV. The number of repetitive population spikes with low frequency stimulation also was observed to increase during TFB-TBOA perfusion. During high frequency stimulation, the population spike amplitude was reduced to 1.89 ± 0.33 but recovered by the end of the experiment to 3.48 ± 0.61mV. Figure 24 shows several field potential taken throughout a typical TFB-TBOA experiment.

Stimulation-induced changes in IOS

TFB-TBOA perfusion reduced stimulation-induced changes in IOS (Figure 25). The on-set slope at the start of high frequency stimulation with TFB-TBOA perfusion was greatly reduced compared to that observed in control slices ($p<0.01$) (Figure 26). Although the maximum change in IOS during high frequency stimulation was reduced compared to that observed in slices with only drug vehicle, this difference was not significant. In TFB-TBOA slices, the maximum IOS appeared 1.83±0.74 min into the high frequency stimulation train which was 39% earlier than in control slices but not significant. Upon termination of the high frequency stimulation train, slices exposed to TFB-TBOA experienced a lower off-set slope at 3.00±1.58%/min compared with slices perfused with vehicle, but this difference was not statistically significant (Figure 26). The last min of IOS was not significantly different between slices perfused with TFB-TBOA and control slices.

Figure 24: Effects of TFB-TBOA on stimulation-induced field potentials. Individual field potentials were taken at several periods during the experiment. A) Baseline field potential taken prior to TFB-TBOA exposure. B) Field potential after 15 min of drug loading. C) Field potential at the end of 10 Hz stimulation. D) Field potential 15 min after the end of the 10 Hz stimulation train. The sampling interval of the individual field potential recordings was reduced by a factor of 10. The graphed field potentials were expanded to show the first 20 ms of the recording data for clarity purposes.

Figure 24:

A)

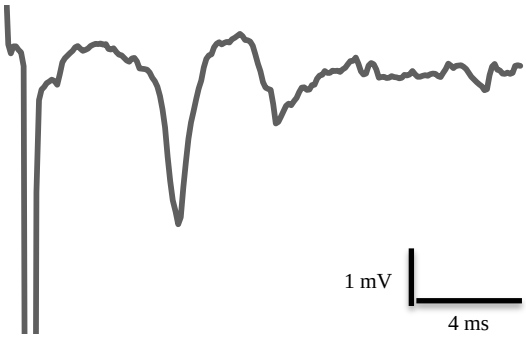

B)

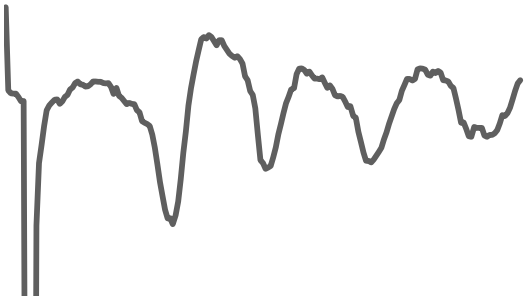

C)

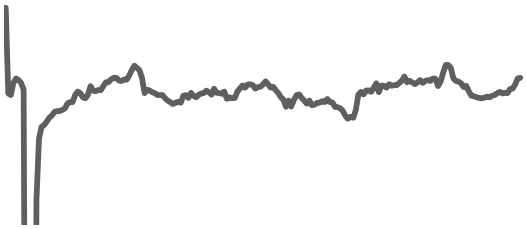

D)

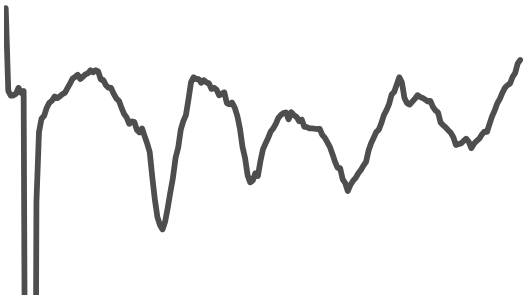

Figure 25: Effects of TFB-TBOA on stimulation-induced changes in IOS. Control slices were exposed to aCSF with DMSO, the vehicle for TFB-TBOA. Values are the mean ± SEM of 4 independent measurements. Some error bars for individual time points are removed for clarity.

Figure 25:

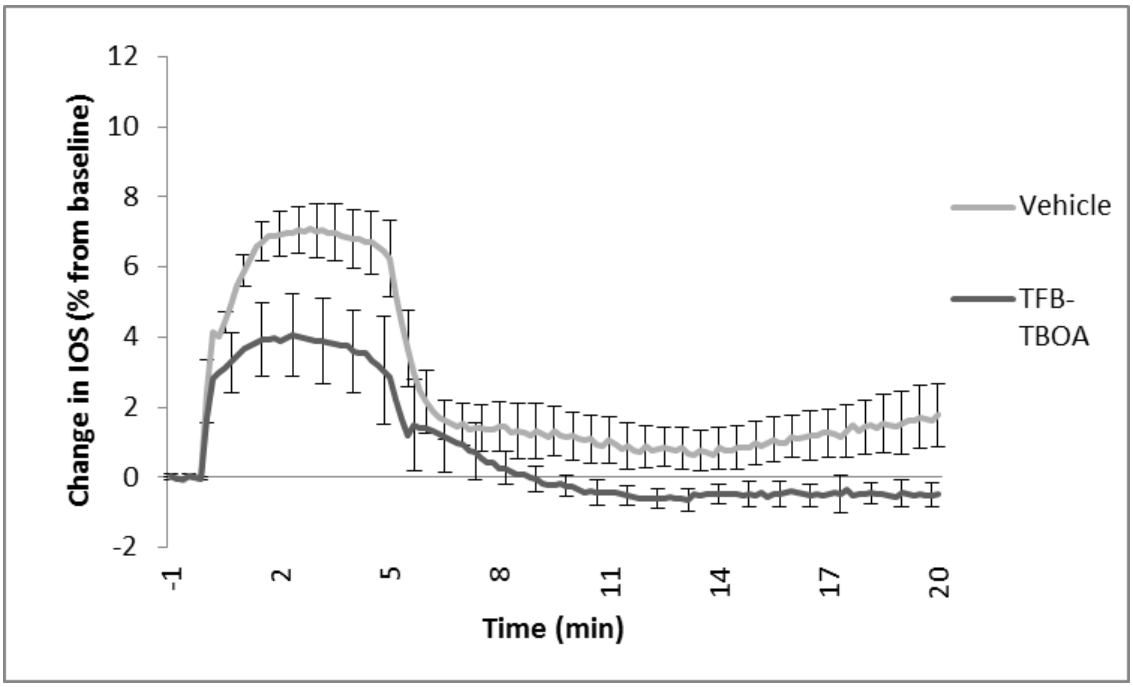
Change in IOS (% from baseline)
12
10
8
6
4
2
0
-2
-1
2
5
8
11
14
17
20
Time (min)
Vehicle
TFB-TBOA

Figure 26: Measured on-set slope and off-set slope with TFB-TBOA exposure. * Indicates values which are significantly different from those obtained from slices perfused with vehicle by a one-way ANOVA ($p<0.05$) and Dunnett's *post hoc* test.

Figure 26:

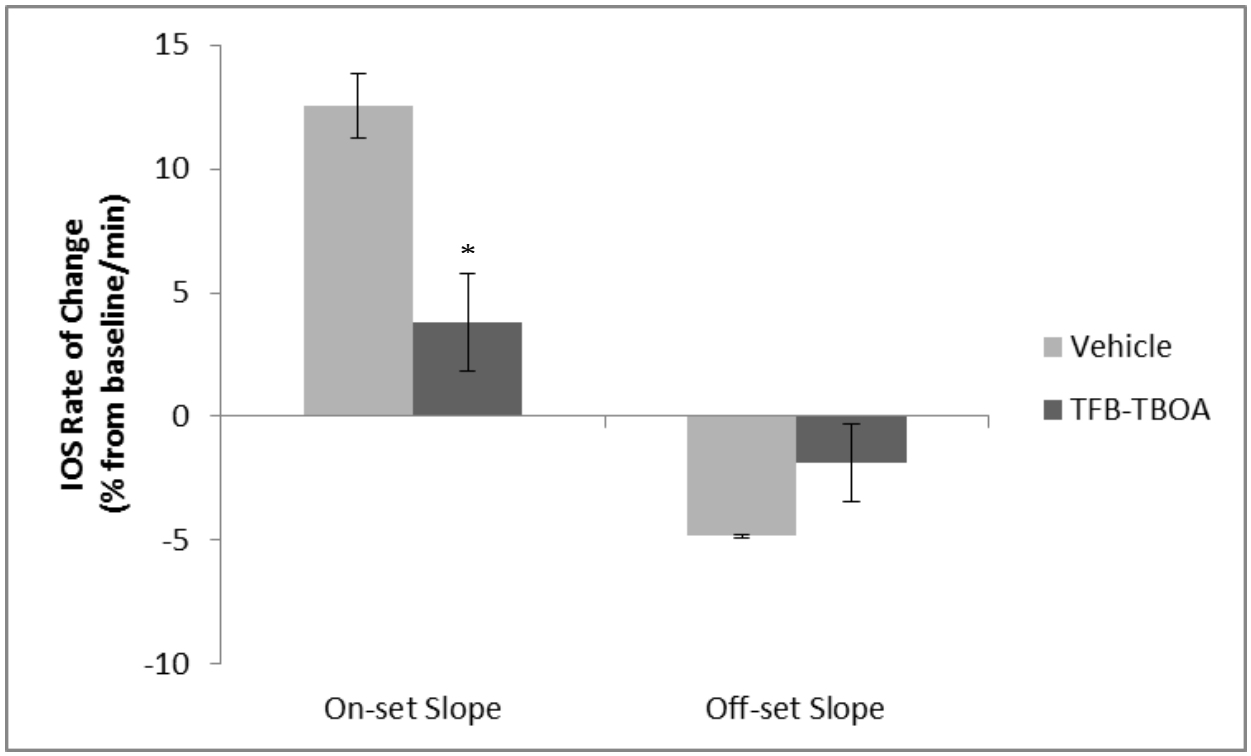
15
10
5
0
-5
-10
IOS Rate of Change
(% from baseline/min)
*
On-set Slope
Off-set Slope
Vehicle
TFB-TBOA

VRAC inhibition does not affect stimulation-induced changes in IOS

Population field potentials

Three drugs were used to inhibit of VRAC during high frequency stimulation. In the presence of niflumic acid or NPPB, the field potentials and population spike amplitude did not significantly change (Figures 27 and 28). In the presence of DCPIB, the population spike amplitude was increased following 20 min of perfusion (Figure 29). For all of these drugs, the population spike amplitude decreased during high frequency stimulation but showed at least partial recovery after the stimulation train was terminated (Table 5) possibly due to an exhausted supply of glutamate. Table 5 shows the mean population spike amplitudes prior to drug exposure, at the end of drug loading, at the end of the high frequency stimulation, and at the end of the experiment.

Stimulation-induced changes in IOS

Due to the differences in drug vehicle used, each VRAC inhibitor had different control series of slices for comparison. IOS responses of slices perfused with niflumic acid were similar to the control (Figure 30). Slices perfused with NPPB showed an elevated IOS response compared with their respective control slices (Figure 31); however, inhibition of VRACs with DCPIB significantly decreased the overall IOS response (Figure 32). The on-set slope and off-set slope for slices perfused with niflumic were similar to those measured in relevant control slices (Figure 33). The on-set slope of NPPB was similar to that measured in slices perfused with vehicle only but the off-set slope was significantly different (Figure 34). DCPIB perfusion significantly decreased both on-set and off-set slopes (Figure 35). Table 6 shows the effects of VRAC inhibition with the three drugs on the maximum IOS and the time at which the maximum IOS

occurred relative to the start of high frequency stimulation. IOS recovery measured 15 min after the end of high frequency stimulation was significantly reduced only for slices perfused with DCPIB ($p<0.01$). Niflumic acid and NPPB did not influence the maximum IOS but instead significantly delayed the time when the maximum occurred during high frequency stimulation ($p<0.05$ and $p<0.01$ respectively). The recovery IOS was reduced in niflumic acid to 1.18±0.49% above baseline compared to the control at 3.47±1.43% above baseline. Recovery IOS in the presence of NPPB was elevated to 3.33±1.23% above baseline compared to the ethanol vehicle at 0.24±0.75% above baseline. Exposure to DCPIB significantly reduced the recovery IOS ($p<0.05$) to 1.41±0.72% above baseline.

Figure 27: Effects of niflumic acid on stimulation-induced field potentials. Individual field potentials were taken at several periods during the experiment A) Baseline field potential taken prior to niflumic acid exposure B) Field potential after 15 min of drug loading C) Field potential at the end of 10 Hz stimulation. D) Field potential 15 min after the end of the 10 Hz stimulation train. The sampling interval of the individual field potential recordings was reduced by a factor of 10. The graphed field potentials were expanded to show the first 20 ms of the recording data for clarity purposes.

Figure 27:
A)

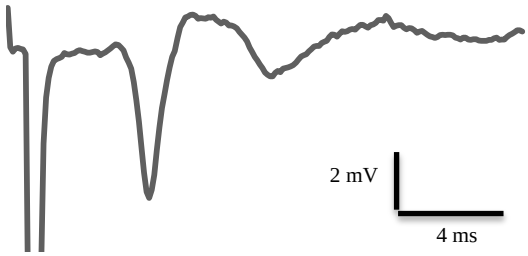

B)

C)

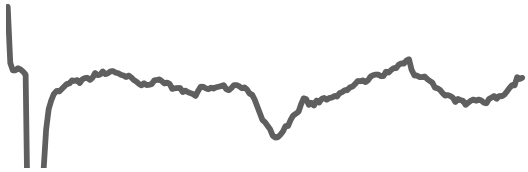

D)

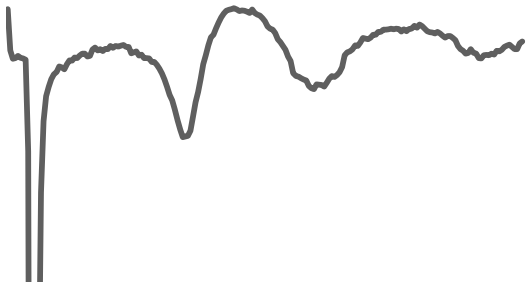

Figure 28: Effects of NPPB on stimulation-induced field potentials. Individual field potentials were taken at several periods during the experiment A) Baseline field potential taken prior to NPPB exposure B) Field potential after 15 min of drug loading C) Field potential at the end of 10 Hz stimulation. D) Field potential 15 min after the end of the 10 Hz stimulation train. The sampling interval of the individual field potential recordings was reduced by a factor of 10. The graphed field potentials were expanded to show the first 20 ms of the recording data for clarity purposes.

Figure 28:
A)

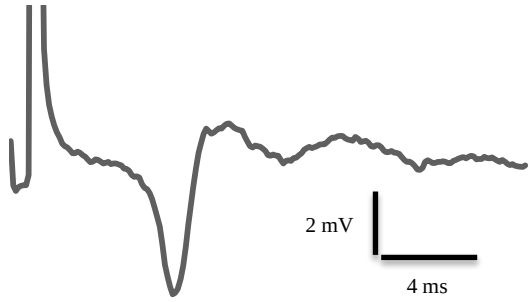

B)

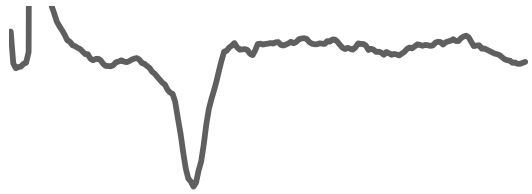

C)

D)

Figure 29: Effects of DCPIB on stimulation-induced field potentials. Individual field potentials were taken at several periods during the experiment A) Baseline field potential taken prior to DCPIB exposure B) Field potential after 15 min of drug loading C) Field potential at the end of 10 Hz stimulation. D) Field potential 15 min after the end of the 10 Hz stimulation train. The sampling interval of the individual field potential recordings was reduced by a factor of 10. The graphed field potentials were expanded to show the first 20 ms of the recording data for clarity purposes.

Figure 29:
A)

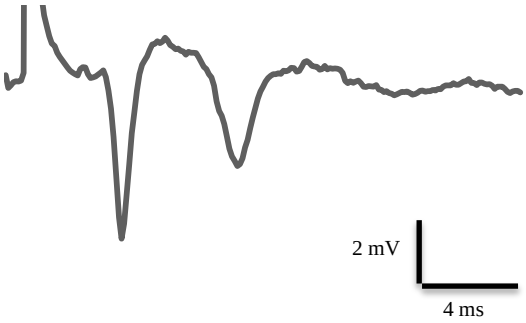

B)

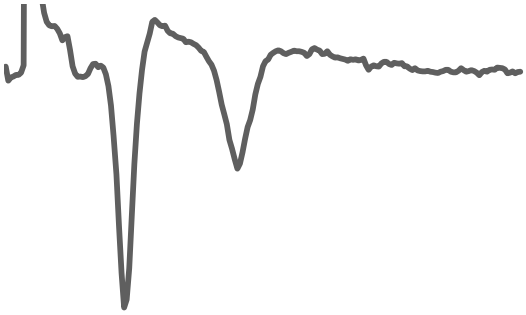

C)

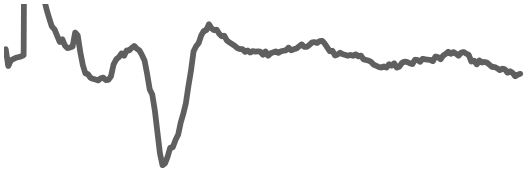

D)

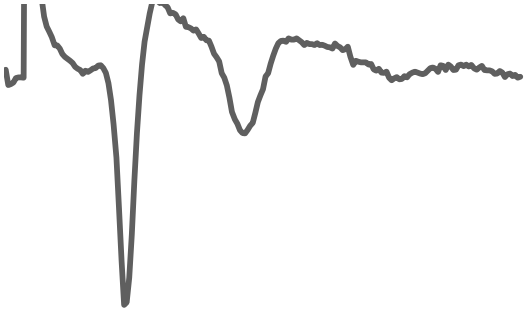

Table 5: Effects of VRAC inhibition on population spike amplitude. * Indicates values which are significantly different from the baseline amplitude by a one-way ANOVA ($p<0.05$) and Dunnett's *post hoc* test or a Mann-Whitney U test.

Table 5:

Group	Baseline amplitude (mV)	End of drug loading amplitude (mV)	End of 10 Hz train amplitude (mV)	End of experiment amplitude (mV)
Niflumic acid	2.77 ± 0.62	2.91 ± 0.61	1.39 ± 0.21	2.50 ± 0.50
NPPB	3.23 ± 0.49	3.37 ± 0.34	1.02 ± 0.10 *	2.55 ± 0.29
DCPIB	4.51 ± 0.72	5.87 ± 1.06	2.44 ± 0.41	6.74 ± 0.70*

Figure 30: Effects of niflumic acid on stimulation-induced changes in IOS. The vehicle slices were taurine-treated and perfused with aCSF. Values are the mean ± SEM of 6-7 independent observations. Some error bars for individual time points are removed for clarity.

Figure 30:

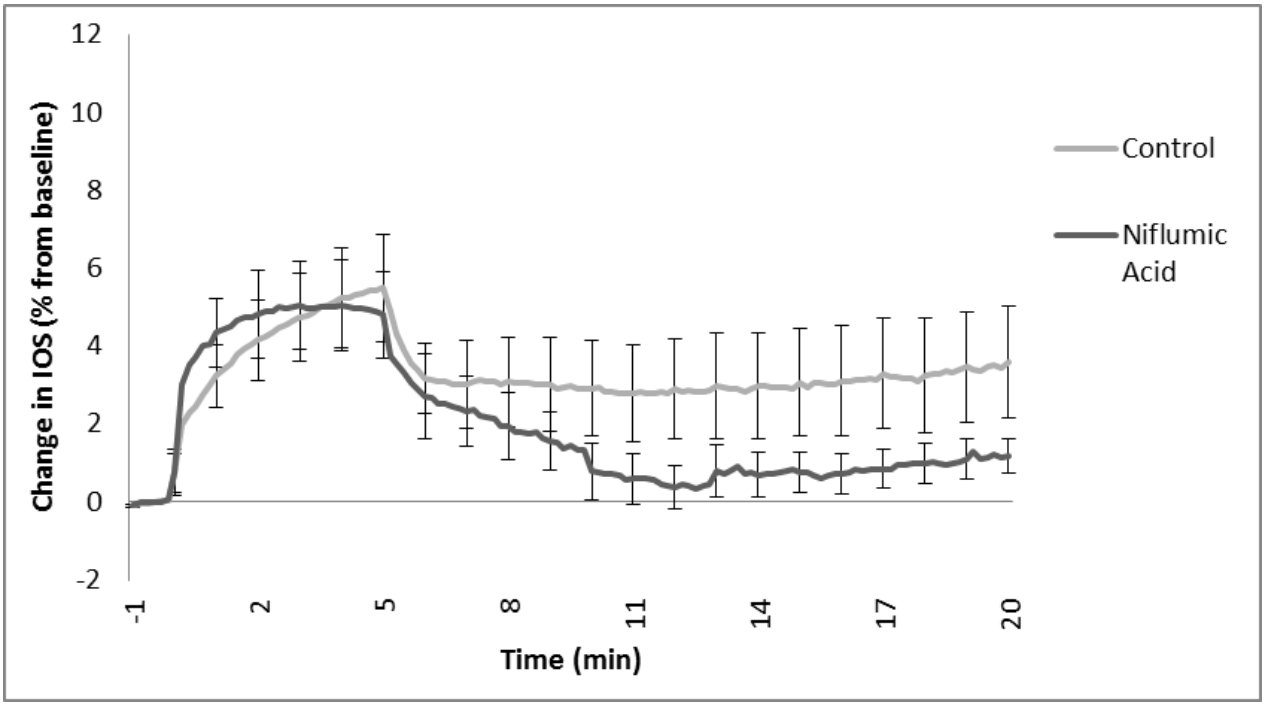
12
10
8
6
4
2
0
-2
Change in IOS (% from baseline)
-1
2
5
8
11
14
17
20
Time (min)
Control
Niflumic Acid

Figure 31: Effects of NPPB on stimulation-induced changes in IOS. The vehicle slices were taurine-treated and perfused with ethanol + aCSF. Values are the mean ± SEM of 4-5 independent observations. Some error bars for individual time points are removed for clarity.

Figure 31:

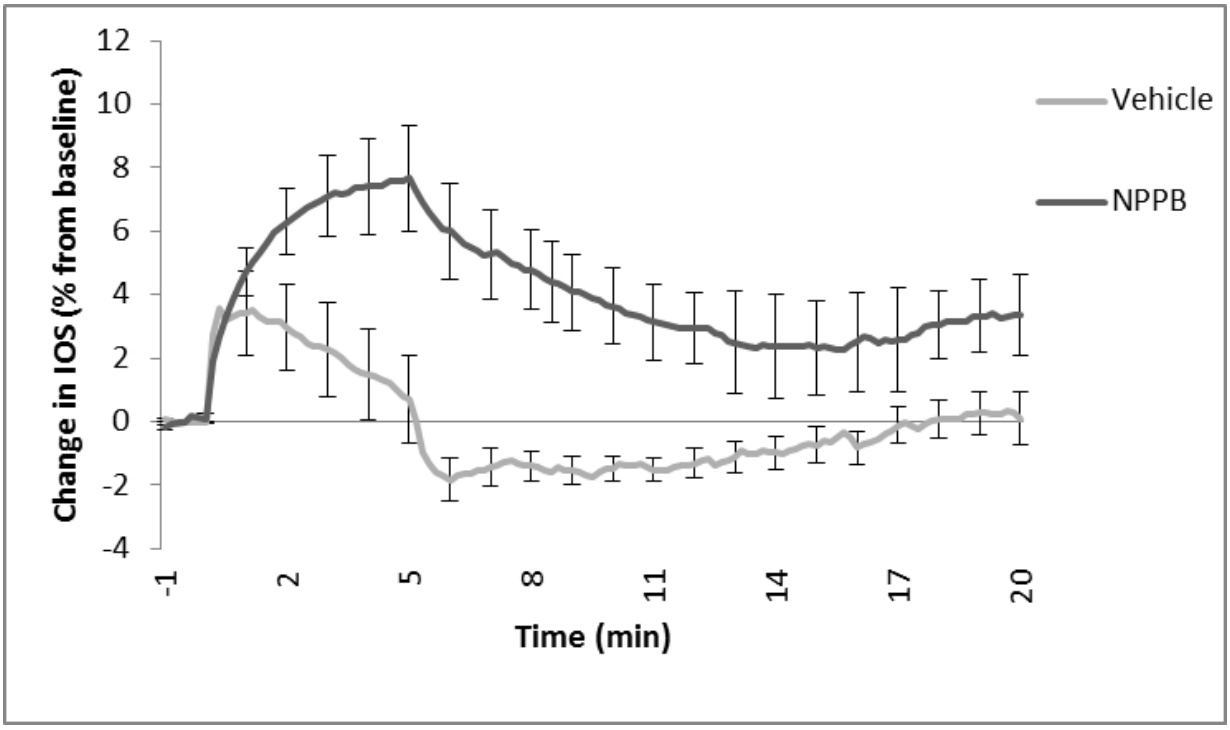
Change in IOS (% from baseline)
12
10
8
6
4
2
0
-2
-4
-1
2
5
8
11
14
17
20
Time (min)
Vehicle
NPPB

Figure 32: Effects of DCPIB on stimulation-induced changes in IOS. The vehicle slices were taurine-treated and perfused with DMSO + aCSF. Values are the mean ± SEM of 4-7 independent observations. Some error bars for individual time points are removed for clarity.

Figure 32:

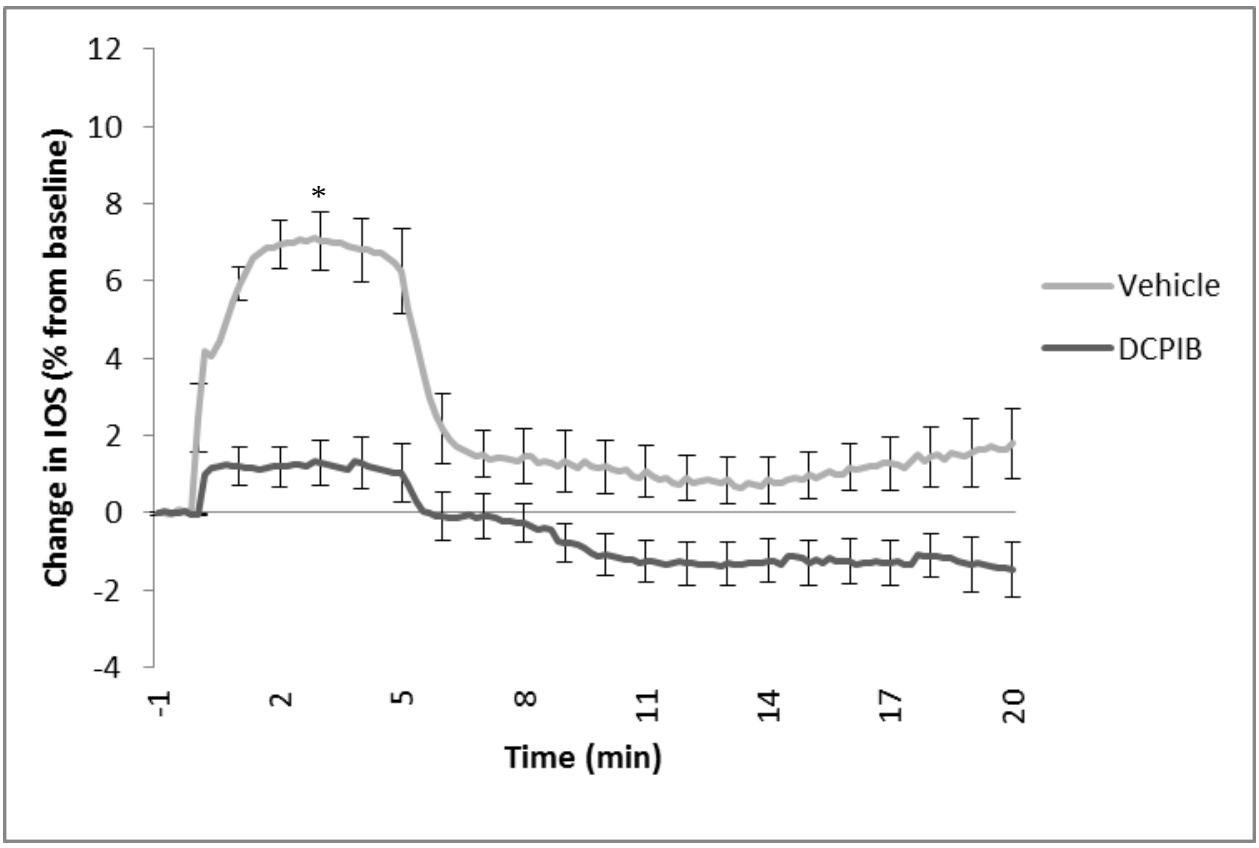
12
10
8
6
4
2
0
-2
-4
Change in IOS (% from baseline)
*
-1
2
5
8
11
14
17
20
Time (min)
Vehicle
DCPIB

Figure 33: Measured on-set slope and off-set slope with niflumic acid exposure. * Indicates values which are significantly different from the vehicle by a one-way ANOVA ($p<0.05$) and Dunnett's *post hoc* test.

Figure 33:

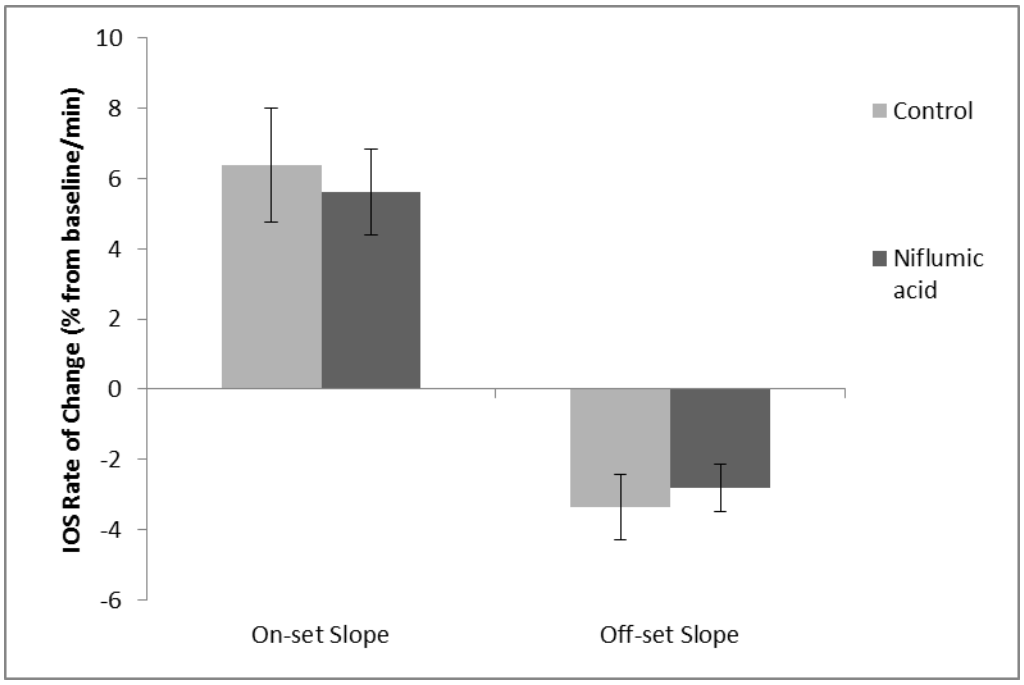
10
8
6
4
2
0
-2
-4
-6
IOS Rate of Change (% from baseline/min)
Control
Niflumic acid
On-set Slope
Off-set Slope

Figure 34: Measured on-set slope and off-set slope with NPPB exposure. * Indicates values which are significantly different from the ethanol vehicle by a one-way ANOVA ($p<0.05$) and Dunnett's *post hoc* test.

Figure 34:

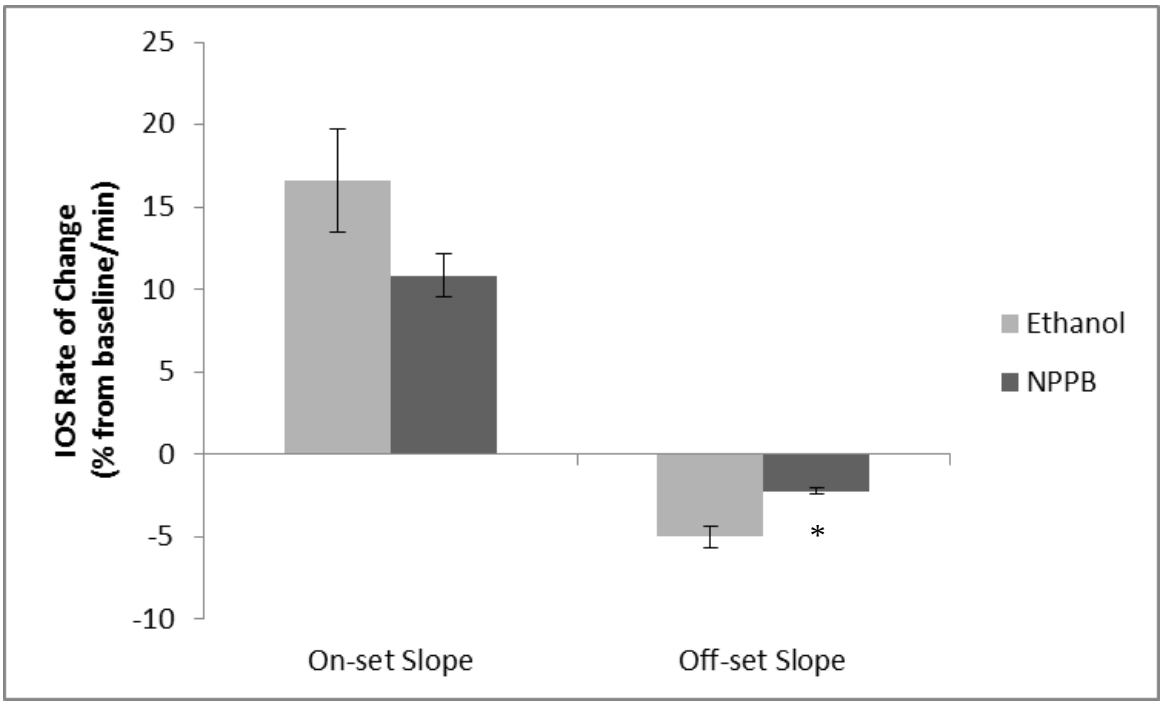
25
20
15
10
5
0
-5
-10
IOS Rate of Change
(% from baseline/min)
On-set Slope
Off-set Slope
*
Ethanol
NPPB

Figure 35: Measured on-set slope and off-set slope with DCPIB exposure. Data values represent mean ± SEM for 4-7 independent experiments. * Indicates values which are significantly different from the vehicle by a one-way ANOVA ($p<0.05$) and Dunnett's *post hoc* test.

Figure 35:

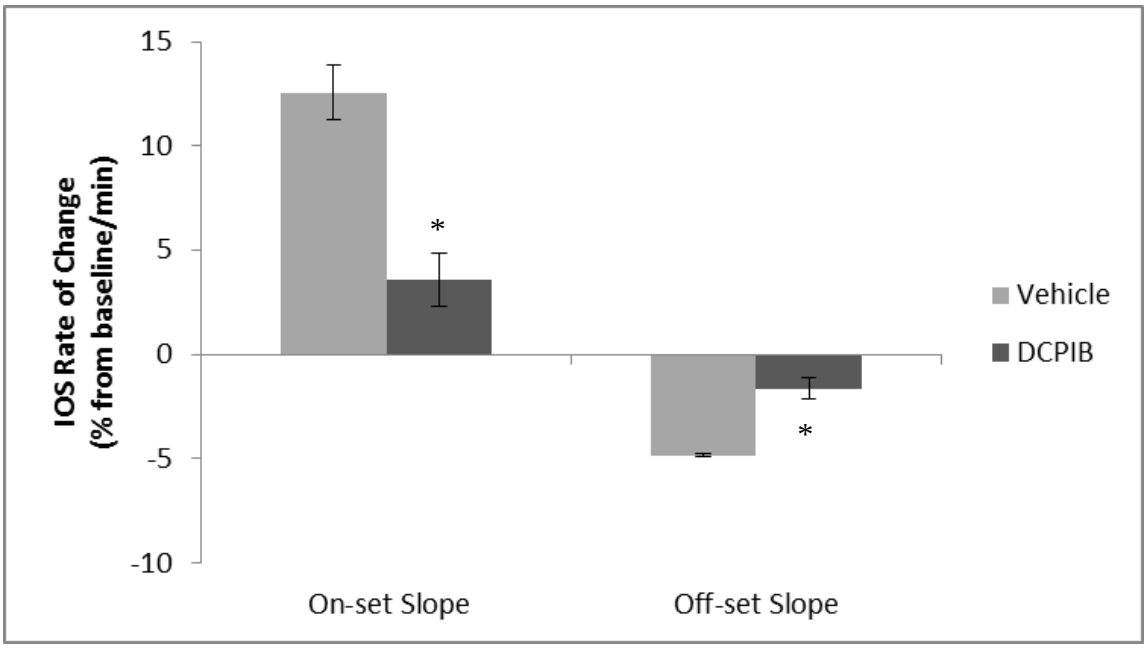
15
10
5
0
-5
-10
IOS Rate of Change
(% from baseline/min)
*
*
On-set Slope
Off-set Slope
Vehicle
DCPIB

Table 6: Effect of VRAC antagonists on maximum IOS, time at the maximal IOS, and IOS value measured at the last min of the experiment. Due to differences in solubility among the VRAC antagonists, each drug had a different control for comparison. Niflumic acid, NPPB, and DCPB were dissolved in aCSF, ethanol, and DMSO respectively. ◊ Indicates values which are significantly different from control by a one-way ANOVA ($p<0.05$) and Dunnett's *post hoc* test. † Indicates values which are significantly different from ethanol vehicle by a one-way ANOVA ($p<0.05$) and Dunnett's *post hoc* test.* Indicates values which are significantly different from the vehicle by a one-way ANOVA ($p<0.05$) and Dunnett's *post hoc* test.

Table 6:

Groups	Maximum IOS (% from baseline)	Time at Maximum IOS (min)	Last min of IOS (% from baseline)
Vehicle	7.34 ± 0.79	3.00 ± 0.52	1.68 ± 0.87
Control	6.22 ± 1.61	4.69 ± 0.19	3.47 ± 1.43
Ethanol	4.39 ± 1.19	0.70 ± 0.35	0.24 ± 0.79
Niflumic acid	5.63 ± 1.01	3.17 ± 0.65 ◊	1.18 ± 0.49
NPPB	7.77 ± 1.66	4.54 ± 0.31 †	3.33 ± 1.23
DCPIB	2.08 ± 0.36 *	2.55 ± 0.81	-1.41 ± 0.72 *

VI. DISCUSSION

The results of these studies elucidate mechanisms underlying stimulation-induced swelling of neurons and glia at the glutamatergic synapse and potential sources of volume regulation. The physiological consequence of synaptic activity results in cellular swelling to stimulation that is largely due to NMDA activation and glutamate uptake. These studies suggest glutamate receptor activation is a significant factor for volume regulation. Finally, volume regulation via VRACs is minimal at most during stimulation-induced swelling.

Volume response to stimulation is frequency dependent

During neuronal activity, axonal studies in crab leg nerves revealed light scattering changes that were suggested to represent axon swelling resulting from the ionic exchanges that occur during the action potential (Cohen and Keynes, 1971). Following these studies, several investigators have observed similar changes in light transmission during stimulation. Stimulation of rat hippocampal slices with photodiodes to detect transmitted light also showed an association of optical signals with synaptic activity (Grinvald et al., 1982; MacVicar and Hochman, 1991). These changes in light scattering and transmission during electrical activity were found to be associated with cell-volume changes (Andrew and MacVicar, 1994; Witte et al., 2001; Fayuk et al., 2002).

In this present study, stimulation of the SC pathway in most slices exhibited a frequency related trend for the on-set slope, off-set slope, and maximum change in IOS. These results together confirm previous findings (MacVicar and Hochman, 1991) and demonstrate that stimulation-induced changes in IOS are related to stimulation frequency.

Previous studies in the mouse optic nerve have found that increases in extracellular K^+ are proportional to stimulation frequency (Bay and Butt, 2012). Likewise, research in the rat cerebral cortex has revealed glutamate release is proportional to neuronal activity (Moroni et al., 1981). Glutamate release may in turn lead to cell swelling during its re-uptake into glial cells or by activating GluRs which cause cation influx into neurons and glia. Taken together, this suggests that stimulation-induced changes of IOS are related to stimulation frequency because uptake of extracellular K^+, activation of glutamate receptors, and glutamate uptake are proportional to stimulation frequency. Astrocytes are predominately involved in glutamate and K^+ uptake following neuronal discharge and have been shown to swell due to this influx of osmolytes (Schneider et al., 1992; Macaulay and Zeuthen, 2012). A previous study measuring IOS changes in the CA1 str. rad. found that IOS changes were proportional to the level of hypo-osmolality (Andrew and MacVicar, 1994) which would indicate that cellular influx of water is proportional to intracellular osmolytes which drive water influx. Overall, these findings support the notion that changes in IOS indicate cellular swelling proportional to the influx of K^+, glutamate, and cation influx via GluR which is dictated by the level of synaptic activity.

Interestingly, slices stimulated at 1 Hz exhibited an initial decrease in IOS. This finding might indicate initiation of regulatory volume mechanisms during stimulation that can over compensate during low levels of activity. A study in the optic nerve revealed that stimulation of nerves at 1 Hz did not evoke a change of extracellular K^+, indicating K^+ efflux and uptake were in balance at low levels of activity (Ransom et al., 2000; Bay and Butt, 2012) and thus, would not result in water influx and cellular swelling. During low levels of activity, the movement of K^+ and glutamate between the intracellular and

extracellular compartments causes negligible water movement therefore no cellular swelling. Glutamate-mediated regulatory volume mechanisms initiated during low-levels of synaptic activity would reduce cellular volume of non-swollen cells. These events could explain the reduced IOS during stimulation at 1Hz in the present study.

Synaptic blockage inhibits stimulation-induced swelling

Orthodromic stimulation of the SC pathway evokes action potentials of CA3 pyramidal cell axons resulting in an influx of Na^{+}, Ca^{+2}, and efflux of K^{+}. Elevated intracellular Ca^{+2} via voltage-gated Ca^{+2} channels facilitates synaptic vesicle release which can be blocked by polyvalent cations such as Mn^{+2}, Co^{+2}, and Mg^{+2} (Taft and DeLorenzo, 1987). In the present study, low extracellular Ca^{+2} and high extracellular Mg^{+2} were used to block voltage-gated Ca^{+2} channels and thus block intracellular Ca^{+2} influx and glutamate release. Synaptic blockage was confirmed by measuring field potentials that indicated the presence of only presynaptic activation of the SC pathway and no postsynaptic response in synaptic block conditions (Figure 14).

During synaptic blockage, action potentials cause K^{+} accumulation in the extracellular and periaxonal space (Kiernan et al., 1997) which is predominantly cleared by astrocytes and results in a cellular influx of water (Kofuji and Newman, 2004). Additionally, neurons experience an influx of Na^{+} resulting in neuronal swelling (Churchwell et al., 1996). In this study, synaptic blockage of the SC pathway significantly reduced stimulation-induced changes in IOS. Similar results were reported with Ca^{+2}-free EGTA perfusate of hippocampal slices (MacVicar and Hochman, 1991). Antidromic stimulation, which initiates action potentials in the axon without synaptic activity also showed reduced changes in IOS in hippocampal slices (Andrew and

MacVicar, 1994). In the presence of tetrodotoxin, a potent neurotoxin that blocks voltage-gated sodium channels, there is no change in IOS present in hippocampal slices indicating that generation of action potentials is necessary for the observed cellular swelling (Pal et al., 2013). These findings together imply that while there is some K^+ and Na^+ induced swelling during SC activation, the majority of cellular swelling is a consequence of Ca^{+2} influx and/or glutamate release.

Under perfusion with normal aCSF, glutamate release may in turn lead to cell swelling during its re-uptake into glial cells or by activating post-synaptic glutamate receptors. Glutamate mediated swelling via GluR activation is well known and associated with multiple pathophysiological conditions (Andrew et al., 1996; Arundine and Tymianski, 2004; Kimelberg, 2004a; Liang et al., 2007; Ho et al., 2012). For example, Ca^{+2} accumulations by GluR activation is involved in hippocampal cell damage associated with ischemia (Benveniste et al., 1988; Lobner and Lipton, 1993) which results in cellular swelling (Zhang et al., 2011).

Synaptic blocked slices exhibited a lack of recovery following stimulation-induced changes in IOS. These findings indicate that intracellular Ca^{+2}, glutamate release, and/or GluR activation might be involved in volume regulatory mechanisms during neuronal activity. Ca^{+2} signaling activates Ca^{+2}-sensitive protein kinases (Bender et al., 1992; Crepel et al., 1998), Ca^{+2} dependent ion channels (Scemes and Giaume, 2006), and gliotransmitters (Zorec et al., 2012), each of which can potentially mediate RVD. In most cell types, including neurons and astrocytes, influx of Ca^{2+} precedes RVD suggesting that it serves as a second messenger for effector proteins (Hua et al., 2010). Increases in intracellular Ca^{+2} are required for activation of neuronal volume-regulatory

pathways following swelling caused by Na^{+} influx (Churchwell et al., 1996). Likewise, RVD mechanisms are Ca^{+} dependent in cultured astrocytes (Olson et al., 2004; Benfenati et al., 2011). There also is evidence of Ca^{+2} signaling of NMDA-induced taurine efflux during volume regulation in hippocampal slices (Menendez et al., 1993).

Synaptically released glutamate also may be an important signal that initiates volume regulatory mechanisms. Glutamate activation of all three iGluRs has been found to commence taurine efflux (Oja and Saransaari, 2013b). In synaptically blocked slices, none of the glutamate receptors would be able to initiate taurine efflux and this could explain the lack of recovery IOS. Glutamate mediated volume regulation through purinergic signaling has also been shown in numerous studies during osmotic challenges of retinal glial cells (Kalisch et al., 2006; Wurm et al., 2008; Wurm et al., 2010; Linnertz et al., 2011). These studies showed glutamate activation of mGluR , which causes Ca^{+2} influx, resulted in ATP release that initiated purinergic signaling pathways to facilitate ion and taurine effluxes. Synaptically blocked slices would be unable to activate mGluR and start purinergic signaling cascades for volume regulation. Taken together, previous research supports the notion that Ca^{+2} and glutamate can potentially mediate regulation of cellular volume during stimulation-induced swelling.

Results in conjunction with past research suggests stimulation-induced swelling is mainly an outcome of synaptic glutamate release which leads to glutamate uptake from the extracellular space into astrocytes as well as an influx of cations into neurons and astrocytes via glutamate receptors. Subsequently, glutamate mediates a volume regulatory mechanism likely associated to taurine efflux, Ca^{+2} –dependent processes, or purinergic signaling.

iGluR inhibition affects stimulation-induced changes in IOS

The activation of iGLuRs causes an influx of Na^{+}, K^{+}, and Ca^{+2} into neurons and glia (Mano and Teichberg, 1998; Pinheiro and Mulle, 2006; Kalia et al., 2008; Langer and Rose, 2009). This influx of osmolytes would be expected to cause cellular swelling. Various studies have demonstrated activity dependent swelling in hippocampus slices during stimulation. Orthodromic stimulation and kainate application increase IOS in hippocampus revealing cellular swelling associated with excitatory synaptic input (Andrew and MacVicar, 1994). Additionally, application of the glutamate agonist NMDA increases IOS in the rat hippocampal slices, particularly in the CA1 region (Jarvis et al., 1999). Further studies showed that blockade of iGluRs with kynurenic acid inhibited hippocampal changes in IOS (MacVicar and Hochman, 1991).

Inhibition of AMPARs and NMDARs were examined with the application of CNQX and MK-801, a competitive antagonist at non-NMDA glutamate receptors (Honore et al., 1988; Andreasen et al., 1989) and non-competitive antagonist that blocks the channel pore of NMDARs (Lau and Tymianski, 2010), respectively. The inhibition of AMPAs was confirmed by field potential recordings that displayed reduced population spike amplitude.

AMPAR inhibition did not the affect the maximum change in stimulation-induced IOS while NMDAR inhibition significantly reduced the maximum change in IOS (Table 4). These results suggest that the NMDARs contribute to hippocampal swelling induced by synaptic activation while AMPARs have little to no effect. Similarly, AMPA inhibition with NBQX did not block glutamate-induced swelling in astrocyte cultures (Hansson et al., 1994). Reduced IOS with complete iGluR inhibition was likely due to

NMDAR inhibition. Stimulation-induced swelling via NMDARs might be associated with increased Ca^{+2} permeability of the postsynaptic membranes. Mouse cortical neuron cultures treated with NMDA demonstrated Ca^{+2} influx via NMDARs. This leads to the activation of kinases, which in turn phosphorylates NOX_2, increases superoxide production and induces cellular swelling from oxidative stress (Brennan-Minnella et al., 2013). Cellular swelling from oxidative stress has also been demonstrated in hippocampal slices (Tucker and Olson, 2010).

AMPAR and NMDAR inhibition hindered recovery of IOS at the termination of stimulation while complete iGluR inhibition with both drugs present resulted in an additive effect on cellular volume regulation (Figure 23). This inhibition of recovery with the application of iGluRs implies that glutamate-mediated volume regulation involves activation of iGluR during electrical activity. Overall, these findings suggest that only NMDARs contribute to stimulation-induced swelling of the hippocampus while both iGLuRs mediate cellular volume recovery mechanisms during neuronal activity. NMDAR activation has been linked to volume regulation by facilitating taurine efflux during oxidative stress (Tucker and Olson, 2010; Oja and Saransaari, 2013b). It is possible that Ca^{+2} influx via NMDARs could signal volume regulatory mechanisms via kinases and Ca^{+2} activated ion channels. The involvement of Ca^{+2} in RVD responses following cell swelling has been found in many cell systems, particularly those of epithelial origin but not as of yet in neuronal cells (Hoffmann et al., 2009)

Glutamate uptake inhibition reduced IOS response

Although GluTs are expressed by all CNS cell types, astrocytes are the cell type primarily responsible for glutamate uptake (Bergles and Jahr, 1998; Anderson and

Swanson, 2000). Absence of GluTs results in excessive activation of GluRs, abnormal neuronal activity, and eventual excitotoxic degeneration (Rothstein et al., 1996; Tanaka et al., 1997). Several studies have shown TFB-TBOA to potently inhibit glutamate uptake. This drug can be used to selectively target different glial GluTs at nanomolar concentration levels (Shimamoto et al., 2004; Tsukada et al., 2005; Bozzo and Chatton, 2010; Torres et al., 2013). In this present study, 1 µM of TFB-TBOA was used to effective block all GluTs.

During stimulation-induced volume changes, inhibition of GluTs with TFB-TBOA increased the population spike amplitude suggesting glutamate persistence in the synaptic space was influencing neuronal excitability (Figure 24). Increased changes in IOS would indicate that neuronal activity contributes to cellular volume changes more than glutamate uptake. However, glutamate inhibition reduced changes in IOS indicating cellular volume changes due to neuronal activity have minimal effect compared to glutamate uptake. These results indicating glutamate uptake induced swelling are similar to results from a previous study that showed EAAT2 inhibition, the most prominent GluTs in the str. rad of CA1 (Lehre and Danbolt, 1998), reduced IOS amplitude (Pal et al., 2013). GluTs uptake of one glutamate molecule is thermodynamically coupled with the influx of three Na^+, one H^+, and the efflux of one K^+ (Lopez-Bayghen and Ortega, 2011; Stone et al., 2012) thus cation influx should be impaired with GluT inhibition. Na^+ is an important osmolyte that can drive water influx. The majority of Na^+ infux in astrocytes is mediated by GluT activation (Langer and Rose, 2009). These results joined with other studies suggest that glutamate and Na^+ influx via GluTs contribute to glial swelling during neuronal activity.

VRAC inhibition does not affect stimulation-induced changes in IOS

Efflux of intracellular Cl^- coupled with K^+ is one of the main contributors to RVD (Hoffmann et al., 2009). It is accepted that many cells regulate their volume through cell swelling-activated VRAC that generates RVD through efflux of Cl^- and small organic osmolytes (Kimelberg et al., 2006). VRACs are also permeable to water in addition to various organic anions such as taurine (Nilius, 2004; Tucker and Olson, 2010). During excitotoxic conditions, VRACs are responsible for the persistence of dendritic beadings and neuronal swelling in cultured cortical neurons (Inoue and Okada, 2007). In hypoxic-ischemic conditions, inhibition of VRACs is neuroprotective by blocking glutamate and taurine efflux (Feustel et al., 2004; Kimelberg et al., 2004; Zhang et al., 2008; Alibrahim et al., 2013).

There is wide source of pharmacological inhibitors for VRACs including NPPB, niflumic acid, and DCPIB. These pharmacological agents were used separately in this present study to examine the effects of VRAC on stimulation-induced changes in IOS. VRAC inhibition during stimulation produced inconsistent results with these various drugs. Inhibition of VRACs with NPPB increased the maximum IOS response and delayed IOS recovery suggesting that VRACs are vital for volume regulation during stimulation induced swelling (Figure 31). In contrast, VRAC inhibition with niflumic acid produced IOS changes similar to the control suggesting the absence of VRAC involvement during synaptic activity (Figure 30). Finally, VRAC inhibition with DCPIB significantly decreased initial, maximum, and recovery IOS responses suggesting VRACs contribute to stimulation induced volume changes (Figure 32). The conflicting results

imply that various effects of these vehicles and drugs on cellular components other than VRAC could have affected the changes in IOS during stimulation.

NPPB is a potent but non-selective Cl^- channel blocker that has been extensively studied (Alibrahim et al., 2013) and shown to inhibit RVD during osmotic challenges (Kreisman and Olson, 2003). A previous study found NPPB, at the same concentration level of this present study, can dramatically reduce cellular ATP content in hippocampal neuron cultures (Olson and Martinho, 2006). In the hippocampus, reduced intracellular ATP would disrupt numerous mechanisms such as K^+ clearance via Na^+/K^+ATPase , glutamate uptake, and glutamate-glutamine. ATP is an important component of glutamatergic-purinergic signaling which has been shown to regulate cellular volume in retinal glial cells (Wurm et al., 2008). Together these findings suggest that reduced ATP would jeopardize cellular energy demands and affect changes in IOS.

Niflumic acid also blocks or modulates a wide spectrum of ion channels including: Ca^{2+}-activated K^+ channels (Ottolia and Toro, 1994), Ca^{+2}-activated Cl^- channels (White and Aylwin, 1990; Korn et al., 1991), and a voltage-gated potassium channels (Wang et al., 1997; Lee and Wang, 1999). Since niflumic acid is a weak acid, it can lower intracellular pH and induce necrosis in cultured hippocampal neurons (Ding et al., 2000), which can result in necrotic volume increase (Okada et al., 2001). However, the dilated weak acid in this project would not have been able to induce necrosis. Recently niflumic acid was found to only partially inhibit of swelling-activated Cl^- currents and had little effect on EAA release (Abdullaev et al., 2006). These findings indicate that niflumic acid is not ideal for studying effects of VRAC inhibition.

DCPIB, once considered a specific VRAC inhibitor (Abdullaev et al., 2006; Zhang et al., 2008) has been shown to inhibit several glutamate transport pathways (Bowens et al., 2013). DCPIB exposure significantly reduced the maximum IOS and the rates of changes for swelling and recovery. In addition, population spike amplitudes were increased with DCPIB exposure similar to TFB-TBOA exposure. These results support the recent evidence that DCPIB inhibits glutamate transport. Since DCPIB exposure inhibited both VRACs and glutamate transport it is difficult to interrupt VRACs role in stimulation-induced swelling.

VRACs contribution during stimulation-induced volume changes remains inconclusive. Results from this study could not support or refute volume changes associated with VRACs. It is possible that the effects of VRAC were minimized by the various other effects the drugs had on IOS. Thus, current pharmacological agents used in this study were insufficient for evaluating the role of VRACs during stimulation-induced volume changes.

Conclusion

This study illuminates several mechanisms involved in swelling and volume regulation in the hippocampus exposed to high frequency stimulation. We confirmed that neuronal activity increases cellular volume proportional to stimulation frequency. The cellular volume increases during stimulation are a result of both action potentials and synaptic glutamate release. Most cellular swelling is due to glutamate uptake and activation of NMDARs. Our experiments indicate that glutamate also plays a significant role in volume regulation during neuronal stimulation. Although VRACs support volume

regulation during osmotic challenges, volume recovery from stimulation-induced swelling may not be dependent on VRACs.

Limitations and future directions

There are a number of limitations and future directions in this study. One of the major limitations concerns IOS, which indirectly measures cellular volume by changes in light transmission through tissue. IOS can be compromised as an indicator of cellular volume changes by several factors including dendritic beading, cellular membrane configuration, and mitochondrial swelling (Jarvis et al., 1999; Johnson et al., 2000). Additionally, IOS measurements cannot distinguish among volume changes in glial cells, neurons, or myelin. Although this study focused on neurons and glia, myelin also can swell during stimulation. K^+ accumulates in the periaxonal space that can cause Schwann cell swelling and myelin restructuring (Kiernan et al., 1997). There also are a couple of pharmacological limitations in this study concerning VRACs and iGluRs. The effects of VRACs could not be thoroughly addressed with the use of different vehicles and pharmacological agents. This limitation might be resolved in the future once the molecular nature of VRACs has been identified (Abdullaev et al., 2006) There also is a current absence of drugs to selective target presynaptic and postsynaptic iGluRs. It is likely that iGluRs on neurons have different functions based on presynaptic or post-synaptic location (Pinheiro and Mulle, 2008).

Several factors were not evaluated in this study and potentially could contribute to stimulation-induced swelling. Previous studies have shown that K^+ plays a role in glutamate-induced swelling both in cultured astrocytes (Hansson et al., 1994) and hippocampal slices (Andrew and MacVicar, 1994; Pal et al., 2013). mGLuR, present on

neurons and glia, exert a variety of effects on second messenger systems and ion channels (D'Antoni et al., 2008). These receptors have been shown to activate mitogen-activated protein kinase (Peavy and Conn, 1998) which has been shown to facilitate RVD (Crepel et al., 1998). A study with astrocyte cultures has demonstrated that mGluRs are involved in glutamate-induced swelling (Hansson et al., 1994). There is evidence that mGluRs enhance glutamate uptake (Yao et al., 2005) which would contribute to stimulation-induced swelling. Some studies have suggested mGluRs influence the release of gliotransmitters such as ATP which has been shown to regulate cellular volume (Wurm et al., 2008). This suggests further research should examine the role of mGluRs, gliotransmission, and purinergic signaling in stimulation-induced volume changes.

Finally, since this study demonstrated that neuronal activity affects volume changes, modulation of that activity will regulate volume changes. The effect of inhibitory signaling on stimulation-induced volume changes should be addressed in future studies. A previous study in hippocampal slices demonstrated that inhibition of GABA receptors increased IOS thus suggesting that inhibitory signals also can modulate volume (Pal et al., 2013). Recent evidence shows that glycine and glutamate co-exist in the hippocampus at the glutamatergic presynaptic terminals and are thought to modulate NMDARs and decrease neuronal excitability (Muller et al., 2013). This also could control stimulation-induced swelling.

VII. BIBLIOGRAPHY

Abdullaev IF, Rudkouskaya A, Schools GP, Kimelberg HK, Mongin AA (2006) Pharmacological comparison of swelling-activated excitatory amino acid release and Cl- currents in cultured rat astrocytes. The Journal of physiology 572:677-689.

Aitken PG, Fayuk D, Somjen GG, Turner DA (1999) Use of intrinsic optical signals to monitor physiological changes in brain tissue slices. Methods 18:91-103.

Albrecht J, Sidoryk-Wegrzynowicz M, Zielinska M, Aschner M (2010) Roles of glutamine in neurotransmission. Neuron glia biology 6:263-276.

Alibrahim A, Zhao LY, Bae CY, Barszczyk A, Sun CL, Wang GL, Sun HS (2013) Neuroprotective effects of volume-regulated anion channel blocker DCPIB on neonatal hypoxic-ischemic injury. Acta pharmacologica Sinica 34:113-118.

Altman J, Bayer SA (2012) Postnatal neurogensis in the developing hippocampus. In.

Amaral DG, Witter MP (1989) The three-dimensional organization of the hippocampal formation: a review of anatomical data. Neuroscience 31:571-591.

Andersen P, Bliss TV, Skrede KK (1971) Lamellar organization of hippocampal pathways. Experimental brain research Experimentelle Hirnforschung Experimentation cerebrale 13:222-238.

Anderson CM, Swanson RA (2000) Astrocyte glutamate transport: review of properties, regulation, and physiological functions. Glia 32:1-14.

Andreasen M, Lambert JD, Jensen MS (1989) Effects of new non-N-methyl-D-aspartate antagonists on synaptic transmission in the in vitro rat hippocampus. The Journal of physiology 414:317-336.

Andrew RD, MacVicar BA (1994) Imaging cell volume changes and neuronal excitation in the hippocampal slice. Neuroscience 62:371-383.

Andrew RD, Adams JR, Polischuk TM (1996) Imaging NMDA- and kainate-induced intrinsic optical signals from the hippocampal slice. Journal of neurophysiology 76:2707-2717.

Andrew RD, Jarvis CR, Obeidat AS (1999) Potential sources of intrinsic optical signals imaged in live brain slices. Methods 18:185-196, 179.

Arundine M, Tymianski M (2004) Molecular mechanisms of glutamate-dependent neurodegeneration in ischemia and traumatic brain injury. Cellular and molecular life sciences : CMLS 61:657-668.

Assentoft M, Kaptan S, Fenton RA, Hua SZ, de Groot BL, Macaulay N (2013) Phosphorylation of rat aquaporin-4 at Ser is not required for channel gating. Glia.

Bahar S, Fayuk D, Somjen GG, Aitken PG, Turner DA (2000) Mitochondrial and intrinsic optical signals imaged during hypoxia and spreading depression in rat hippocampal slices. Journal of neurophysiology 84:311-324.

Bay V, Butt AM (2012) Relationship between glial potassium regulation and axon excitability: a role for glial Kir4.1 channels. Glia 60:651-660.

Bender AS, Neary JT, Blicharska J, Norenberg LO, Norenberg MD (1992) Role of calmodulin and protein kinase C in astrocytic cell volume regulation. Journal of neurochemistry 58:1874-1882.

Benfenati V, Caprini M, Dovizio M, Mylonakou MN, Ferroni S, Ottersen OP, Amiry-Moghaddam M (2011) An aquaporin-4/transient receptor potential vanilloid 4 (AQP4/TRPV4) complex is essential for cell-volume control in astrocytes. Proceedings of the National Academy of Sciences of the United States of America 108:2563-2568.

Benveniste H, Jorgensen MB, Diemer NH, Hansen AJ (1988) Calcium accumulation by glutamate receptor activation is involved in hippocampal cell damage after ischemia. Acta neurologica Scandinavica 78:529-536.

Berger ML, Pohler T, Schadt O, Stanger M, Rebernik P, Scholze P, Noe CR (2013) Exploring the polyamine regulatory site of the NMDA receptor: a parallel synthesis approach. ChemMedChem 8:82-94.

Bergles DE, Jahr CE (1998) Glial contribution to glutamate uptake at Schaffer collateral-commissural synapses in the hippocampus. The Journal of neuroscience : the official journal of the Society for Neuroscience 18:7709-7716.

Bowens NH, Dohare P, Kuo YH, Mongin AA (2013) DCPIB, the proposed selective blocker of volume-regulated anion channels, inhibits several glutamate transport pathways in glial cells. Molecular pharmacology 83:22-32.

Bozzo L, Chatton JY (2010) Inhibitory effects of (2S, 3S)-3-[3-[4-(trifluoromethyl)benzoylamino]benzyloxy]aspartate (TFB-TBOA) on the astrocytic sodium responses to glutamate. Brain research 1316:27-34.

Brennan-Minnella AM, Shen Y, El-Benna J, Swanson RA (2013) Phosphoinositide 3-kinase couples NMDA receptors to superoxide release in excitotoxic neuronal death. Cell death & disease 4:e624.

Cai X, Kallarackal AJ, Kvarta MD, Goluskin S, Gaylor K, Bailey AM, Lee HK, Huganir RL, Thompson SM (2013) Local potentiation of excitatory synapses by serotonin and its alteration in rodent models of depression. Nature neuroscience 16:464-472.

Canto CB, Wouterlood FG, Witter MP (2008) What does the anatomical organization of the entorhinal cortex tell us? Neural plasticity 2008:381243.

Cenquizca LA, Swanson LW (2007) Spatial organization of direct hippocampal field CA1 axonal projections to the rest of the cerebral cortex. Brain research reviews 56:1-26.

Chaudhry FA, Schmitz D, Reimer RJ, Larsson P, Gray AT, Nicoll R, Kavanaugh M, Edwards RH (2002) Glutamine uptake by neurons: interaction of protons with system a transporters. The Journal of neuroscience : the official journal of the Society for Neuroscience 22:62-72.

Churchwell KB, Wright SH, Emma F, Rosenberg PA, Strange K (1996) NMDA receptor activation inhibits neuronal volume regulation after swelling induced by veratridine-stimulated Na+ influx in rat cortical cultures. The Journal of neuroscience : the official journal of the Society for Neuroscience 16:7447-7457.

Cohen LB, Keynes RD (1971) Changes in light scattering associated with the action potential in crab nerves. The Journal of physiology 212:259-275.

Collingridge GL, Olsen RW, Peters J, Spedding M (2009) A nomenclature for ligand-gated ion channels. Neuropharmacology 56:2-5.

Conti F, DeBiasi S, Minelli A, Melone M (1996) Expression of NR1 and NR2A/B subunits of the NMDA receptor in cortical astrocytes. Glia 17:254-258.

Contractor A, Mulle C, Swanson GT (2011) Kainate receptors coming of age: milestones of two decades of research. Trends in neurosciences 34:154-163.

Copits BA, Swanson GT (2012) Dancing partners at the synapse: auxiliary subunits that shape kainate receptor function. Nature reviews Neuroscience 13:675-686.

Cox DJ, Racca C (2013) Differential dendritic targeting of AMPA receptor subunit mRNAs in adult rat hippocampal principal neurons and interneurons. The Journal of comparative neurology 521:Spc1.

Crepel V, Panenka W, Kelly ME, MacVicar BA (1998) Mitogen-activated protein and tyrosine kinases in the activation of astrocyte volume-activated chloride current. The Journal of neuroscience : the official journal of the Society for Neuroscience 18:1196-1206.

D'Antoni S, Berretta A, Bonaccorso CM, Bruno V, Aronica E, Nicoletti F, Catania MV (2008) Metabotropic glutamate receptors in glial cells. Neurochemical research 33:2436-2443.

Danbolt NC (1994) The high affinity uptake system for excitatory amino acids in the brain. Progress in neurobiology 44:377-396.

Danbolt NC (2001) Glutamate uptake. Progress in neurobiology 65:1-105.

Darby M, Kuzmiski JB, Panenka W, Feighan D, MacVicar BA (2003) ATP released from astrocytes during swelling activates chloride channels. Journal of neurophysiology 89:1870-1877.

DeFelipe J, Fernandez-Gil MA, Kastanauskaite A, Bote RP, Presmanes YG, Ruiz MT (2007) Macroanatomy and microanatomy of the temporal lobe. Seminars in ultrasound, CT, and MR 28:404-415.

Deng W, Aimone JB, Gage FH (2010) New neurons and new memories: how does adult hippocampal neurogenesis affect learning and memory? Nature reviews Neuroscience 11:339-350.

Dietzel I, Heinemann U, Hofmeier G, Lux HD (1982) Stimulus-induced changes in extracellular Na+ and Cl- concentration in relation to changes in the size of the extracellular space. Experimental brain research Experimentelle Hirnforschung Experimentation cerebrale 46:73-84.

Ding D, Moskowitz SI, Li R, Lee SB, Esteban M, Tomaselli K, Chan J, Bergold PJ (2000) Acidosis induces necrosis and apoptosis of cultured hippocampal neurons. Experimental neurology 162:1-12.

Dingledine R, Borges K, Bowie D, Traynelis SF (1999) The glutamate receptor ion channels. Pharmacological reviews 51:7-61.

Duan D, Winter C, Cowley S, Hume JR, Horowitz B (1997) Molecular identification of a volume-regulated chloride channel. Nature 390:417-421.

Duffy AM, Schaner MJ, Chin J, Scharfman HE (2013) Expression of c-fos in hilar mossy cells of the dentate gyrus in vivo. Hippocampus.

Fayuk D, Aitken PG, Somjen GG, Turner DA (2002) Two different mechanisms underlie reversible, intrinsic optical signals in rat hippocampal slices. Journal of neurophysiology 87:1924-1937.

Feustel PJ, Jin Y, Kimelberg HK (2004) Volume-regulated anion channels are the predominant contributors to release of excitatory amino acids in the ischemic cortical penumbra. Stroke; a journal of cerebral circulation 35:1164-1168.

Filosa JA, Bonev AD, Straub SV, Meredith AL, Wilkerson MK, Aldrich RW, Nelson MT (2006) Local potassium signaling couples neuronal activity to vasodilation in the brain. Nature neuroscience 9:1397-1403.

Freeman WD, Dawson SB, Flemming KD (2010) The ABC's of stroke complications. Seminars in neurology 30:501-510.

Gameiro A, Braams S, Rauen T, Grewer C (2011) The discovery of slowness: low-capacity transport and slow anion channel gating by the glutamate transporter EAAT5. Biophysical journal 100:2623-2632.

Garcia Dopico J, Perdomo Diaz J, Alonso TJ, Gonzalez Hernandez T, Castro Fuentes R, Rodriguez Diaz M (2004) Extracellular taurine in the substantia nigra: taurine-glutamate interaction. Journal of neuroscience research 76:528-538.

Ghasemi M, Dehpour AR (2011) The NMDA receptor/nitric oxide pathway: a target for the therapeutic and toxic effects of lithium. Trends in pharmacological sciences 32:420-434.

Grinvald A, Manker A, Segal M (1982) Visualization of the spread of electrical activity in rat hippocampal slices by voltage-sensitive optical probes. The Journal of physiology 333:269-291.

Hansson E, Johansson BB, Westergren I, Ronnback L (1994) Glutamate-induced swelling of single astroglial cells in primary culture. Neuroscience 63:1057-1066.

He K, Song L, Cummings LW, Goldman J, Huganir RL, Lee HK (2009) Stabilization of Ca2+-permeable AMPA receptors at perisynaptic sites by GluR1-S845 phosphorylation. Proceedings of the National Academy of Sciences of the United States of America 106:20033-20038.

Ho ML, Rojas R, Eisenberg RL (2012) Cerebral edema. AJR American journal of roentgenology 199:W258-273.

Hoffmann EK, Lambert IH, Pedersen SF (2009) Physiology of cell volume regulation in vertebrates. Physiological reviews 89:193-277.

Hollmann M, Heinemann S (1994) Cloned glutamate receptors. Annual review of neuroscience 17:31-108.

Honore T, Davies SN, Drejer J, Fletcher EJ, Jacobsen P, Lodge D, Nielsen FE (1988) Quinoxalinediones: potent competitive non-NMDA glutamate receptor antagonists. Science 241:701-703.

Horio Y (2001) Potassium channels of glial cells: distribution and function. Japanese journal of pharmacology 87:1-6.

Hua SZ, Gottlieb PA, Heo J, Sachs F (2010) A mechanosensitive ion channel regulating cell volume. American journal of physiology Cell physiology 298:C1424-1430.

Huang YH, Bergles DE (2004) Glutamate transporters bring competition to the synapse. Current opinion in neurobiology 14:346-352.

Inoue H, Okada Y (2007) Roles of volume-sensitive chloride channel in excitotoxic neuronal injury. The Journal of neuroscience : the official journal of the Society for Neuroscience 27:1445-1455.

Jackson TC, Foster TC (2009) Regional Health and Function in the hippocampus: Evolutionary compromises for a critical brain region. Bioscience hypotheses 2:245-251.

Jane DE, Lodge D, Collingridge GL (2009) Kainate receptors: pharmacology, function and therapeutic potential. Neuropharmacology 56:90-113.

Jarvis CR, Lilge L, Vipond GJ, Andrew RD (1999) Interpretation of intrinsic optical signals and calcein fluorescence during acute excitotoxic insult in the hippocampal slice. NeuroImage 10:357-372.

Jinde S, Zsiros V, Nakazawa K (2013) Hilar mossy cell circuitry controlling dentate granule cell excitability. Frontiers in neural circuits 7:14.

Johnson LJ, Hanley DF, Thakor NV (2000) Optical light scatter imaging of cellular and sub-cellular morphology changes in stressed rat hippocampal slices. Journal of neuroscience methods 98:21-31.

Kajiwara R, Wouterlood FG, Sah A, Boekel AJ, Baks-te Bulte LT, Witter MP (2008) Convergence of entorhinal and CA3 inputs onto pyramidal neurons and interneurons in hippocampal area CA1--an anatomical study in the rat. Hippocampus 18:266-280.

Kalia LV, Kalia SK, Salter MW (2008) NMDA receptors in clinical neurology: excitatory times ahead. Lancet neurology 7:742-755.

Kalisch F, Wurm A, Iandiev I, Uckermann O, Dilsiz N, Reichenbach A, Wiedemann P, Bringmann A (2006) Atrial natriuretic peptide inhibits osmotical glial cell swelling in the ischemic rat retina: dependence on glutamatergic-purinergic signaling. Experimental eye research 83:962-971.

Kiernan MC, Mogyoros I, Hales JP, Gracies JM, Burke D (1997) Excitability changes in human cutaneous afferents induced by prolonged repetitive axonal activity. The Journal of physiology 500 (Pt 1):255-264.

Kimelberg HK (2004a) Water homeostasis in the brain: basic concepts. Neuroscience 129:851-860.

Kimelberg HK (2004b) Increased release of excitatory amino acids by the actions of ATP and peroxynitrite on volume-regulated anion channels (VRACs) in astrocytes. Neurochemistry international 45:511-519.

Kimelberg HK, Nestor NB, Feustel PJ (2004) Inhibition of release of taurine and excitatory amino acids in ischemia and neuroprotection. Neurochemical research 29:267-274.

Kimelberg HK, Macvicar BA, Sontheimer H (2006) Anion channels in astrocytes: biophysics, pharmacology, and function. Glia 54:747-757.

Kimelberg HK, Goderie SK, Higman S, Pang S, Waniewski RA (1990) Swelling-induced release of glutamate, aspartate, and taurine from astrocyte cultures. The Journal of neuroscience : the official journal of the Society for Neuroscience 10:1583-1591.

Kofuji P, Newman EA (2004) Potassium buffering in the central nervous system. Neuroscience 129:1045-1056.

Korn SJ, Bolden A, Horn R (1991) Control of action potentials and Ca2+ influx by the Ca(2+)-dependent chloride current in mouse pituitary cells. The Journal of physiology 439:423-437.

Kreisman NR, Olson JE (2003) Taurine enhances volume regulation in hippocampal slices swollen osmotically. Neuroscience 120:635-642.

Kvamme E, Roberg B, Torgner IA (2000) Phosphate-activated glutaminase and mitochondrial glutamine transport in the brain. Neurochemical research 25:1407-1419.

Lalo U, Pankratov Y, Parpura V, Verkhratsky A (2011) Ionotropic receptors in neuronal-astroglial signalling: what is the role of "excitable" molecules in non-excitable cells. Biochimica et biophysica acta 1813:992-1002.

Lalo U, Pankratov Y, Kirchhoff F, North RA, Verkhratsky A (2006) NMDA receptors mediate neuron-to-glia signaling in mouse cortical astrocytes. The Journal of neuroscience : the official journal of the Society for Neuroscience 26:2673-2683.

Langer J, Rose CR (2009) Synaptically induced sodium signals in hippocampal astrocytes in situ. The Journal of physiology 587:5859-5877.

Lau A, Tymianski M (2010) Glutamate receptors, neurotoxicity and neurodegeneration. Pflugers Archiv : European journal of physiology 460:525-542.

Leao RN, Mikulovic S, Leao KE, Munguba H, Gezelius H, Enjin A, Patra K, Eriksson A, Loew LM, Tort AB, Kullander K (2012) OLM interneurons differentially modulate CA3 and entorhinal inputs to hippocampal CA1 neurons. Nature neuroscience 15:1524-1530.

Lee YT, Wang Q (1999) Inhibition of hKv2.1, a major human neuronal voltage-gated K+ channel, by meclofenamic acid. European journal of pharmacology 378:349-356.

Lehre KP, Danbolt NC (1998) The number of glutamate transporter subtype molecules at glutamatergic synapses: chemical and stereological quantification in young adult rat brain. The Journal of neuroscience : the official journal of the Society for Neuroscience 18:8751-8757.

Lein PJ, Barnhart CD, Pessah IN (2011) Acute hippocampal slice preparation and hippocampal slice cultures. Methods in molecular biology 758:115-134.

Liang D, Bhatta S, Gerzanich V, Simard JM (2007) Cytotoxic edema: mechanisms of pathological cell swelling. Neurosurgical focus 22:E2.

Linnertz R, Wurm A, Pannicke T, Krugel K, Hollborn M, Hartig W, Iandiev I, Wiedemann P, Reichenbach A, Bringmann A (2011) Activation of voltage-gated Na(+) and Ca(2)(+) channels is required for glutamate release from retinal glial cells implicated in cell volume regulation. Neuroscience 188:23-34.

Liotta A, Rosner J, Huchzermeyer C, Wojtowicz A, Kann O, Schmitz D, Heinemann U, Kovacs R (2012) Energy demand of synaptic transmission at the hippocampal Schaffer-collateral synapse. Journal of cerebral blood flow and metabolism : official journal of the International Society of Cerebral Blood Flow and Metabolism 32:2076-2083.

Liu SJ, Zukin RS (2007) Ca2+-permeable AMPA receptors in synaptic plasticity and neuronal death. Trends in neurosciences 30:126-134.

Lobner D, Lipton P (1993) Intracellular calcium levels and calcium fluxes in the CA1 region of the rat hippocampal slice during in vitro ischemia: relationship to

electrophysiological cell damage. The Journal of neuroscience : the official journal of the Society for Neuroscience 13:4861-4871.

Lopez-Bayghen E, Ortega A (2011) Glial glutamate transporters: New actors in brain signaling. IUBMB life 63:816-823.

MacAulay N, Zeuthen T (2010) Water transport between CNS compartments: contributions of aquaporins and cotransporters. Neuroscience 168:941-956.

Macaulay N, Zeuthen T (2012) Glial K(+) clearance and cell swelling: key roles for cotransporters and pumps. Neurochemical research 37:2299-2309.

MacVicar BA, Hochman D (1991) Imaging of synaptically evoked intrinsic optical signals in hippocampal slices. The Journal of neuroscience : the official journal of the Society for Neuroscience 11:1458-1469.

Mano I, Teichberg VI (1998) A tetrameric subunit stoichiometry for a glutamate receptor-channel complex. Neuroreport 9:327-331.

Meeks JP, Mennerick S (2007) Astrocyte membrane responses and potassium accumulation during neuronal activity. Hippocampus 17:1100-1108.

Menendez N, Solis JM, Herreras O, Galarreta M, Conejero C, Martin del Rio R (1993) Taurine release evoked by NMDA receptor activation is largely dependent on calcium mobilization from intracellular stores. The European journal of neuroscience 5:1273-1279.

Mizuseki K, Royer S, Diba K, Buzsaki G (2012) Activity dynamics and behavioral correlates of CA3 and CA1 hippocampal pyramidal neurons. Hippocampus 22:1659-1680.

Mongin AA, Kimelberg HK (2005) ATP regulates anion channel-mediated organic osmolyte release from cultured rat astrocytes via multiple Ca2+-sensitive mechanisms. American journal of physiology Cell physiology 288:C204-213.

Morales I, Fuentes A, Gonzalez-Hernandez T, Rodriguez M (2009) Osmosensitive response of glutamate in the substantia nigra. Experimental neurology 220:335-340.

Morales I, Dopico JG, Sabate M, Gonzalez-Hernandez T, Rodriguez M (2007) Substantia nigra osmoregulation: taurine and ATP involvement. American journal of physiology Cell physiology 292:C1934-1941.

Moroni F, Corradetti R, Casamenti F, Moneti G, Pepeu G (1981) The release of endogenous GABA and glutamate from the cerebral cortex in the rat. Naunyn-Schmiedeberg's archives of pharmacology 316:235-239.

Muller E, Bakkar W, Martina M, Sokolovski A, Wong AY, Legendre P, Bergeron R (2013) Vesicular storage of glycine in glutamatergic terminals in mouse hippocampus. Neuroscience 242:110-127.

Muller M, Somjen GG (1999) Intrinsic optical signals in rat hippocampal slices during hypoxia-induced spreading depression-like depolarization. Journal of neurophysiology 82:1818-1831.

Mulligan SJ, MacVicar BA (2006) VRACs CARVe a path for novel mechanisms of communication in the CNS. Science's STKE : signal transduction knowledge environment 2006:pe42.

Nilius B (2004) Is the volume-regulated anion channel VRAC a "water-permeable" channel? Neurochemical research 29:3-8.

Oja SS, Saransaari P (2013a) Modulation of taurine release in glucose-free media by glutamate receptors in hippocampal slices from developing and adult mice. Amino acids 44:533-542.

Oja SS, Saransaari P (2013b) Regulation of taurine release in the hippocampus of developing and adult mice. Advances in experimental medicine and biology 775:135-143.

Okada Y (2004) Ion channels and transporters involved in cell volume regulation and sensor mechanisms. Cell biochemistry and biophysics 41:233-258.

Okada Y, Sato K, Numata T (2009) Pathophysiology and puzzles of the volume-sensitive outwardly rectifying anion channel. The Journal of physiology 587:2141-2149.

Okada Y, Maeno E, Shimizu T, Dezaki K, Wang J, Morishima S (2001) Receptor-mediated control of regulatory volume decrease (RVD) and apoptotic volume decrease (AVD). The Journal of physiology 532:3-16.

Olson JE, Martinho E, Jr. (2006) Regulation of taurine transport in rat hippocampal neurons by hypo-osmotic swelling. Journal of neurochemistry 96:1375-1389.

Olson JE, Li GZ, Wang L, Lu L (2004) Volume-regulated anion conductance in cultured rat cerebral astrocytes requires calmodulin activity. Glia 46:391-401.

Ottolia M, Toro L (1994) Potentiation of large conductance KCa channels by niflumic, flufenamic, and mefenamic acids. Biophysical journal 67:2272-2279.

Pal I, Nyitrai G, Kardos J, Heja L (2013) Neuronal and astroglial correlates underlying spatiotemporal intrinsic optical signal in the rat hippocampal slice. PloS one 8:e57694.

Palygin O, Lalo U, Verkhratsky A, Pankratov Y (2010) Ionotropic NMDA and P2X1/5 receptors mediate synaptically induced Ca2+ signalling in cortical astrocytes. Cell calcium 48:225-231.

Paoletti P, Neyton J (2007) NMDA receptor subunits: function and pharmacology. Current opinion in pharmacology 7:39-47.

Papadopoulos MC, Verkman AS (2013) Aquaporin water channels in the nervous system. Nature reviews Neuroscience 14:265-277.

Pasantes-Morales H (1996) Volume regulation in brain cells: cellular and molecular mechanisms. Metabolic brain disease 11:187-204.

Peavy RD, Conn PJ (1998) Phosphorylation of mitogen-activated protein kinase in cultured rat cortical glia by stimulation of metabotropic glutamate receptors. Journal of neurochemistry 71:603-612.

Pinheiro P, Mulle C (2006) Kainate receptors. Cell and tissue research 326:457-482.

Pinheiro PS, Mulle C (2008) Presynaptic glutamate receptors: physiological functions and mechanisms of action. Nature reviews Neuroscience 9:423-436.

Poolos NP, Mauk MD, Kocsis JD (1987) Activity-evoked increases in extracellular potassium modulate presynaptic excitability in the CA1 region of the hippocampus. Journal of neurophysiology 58:404-416.

Ransom CB, Ransom BR, Sontheimer H (2000) Activity-dependent extracellular K+ accumulation in rat optic nerve: the role of glial and axonal Na+ pumps. The Journal of physiology 522 Pt 3:427-442.

Rodriguez-Moreno A, Herreras O, Lerma J (1997) Kainate receptors presynaptically downregulate GABAergic inhibition in the rat hippocampus. Neuron 19:893-901.

Rothstein JD, Dykes-Hoberg M, Pardo CA, Bristol LA, Jin L, Kuncl RW, Kanai Y, Hediger MA, Wang Y, Schielke JP, Welty DF (1996) Knockout of glutamate transporters reveals a major role for astroglial transport in excitotoxicity and clearance of glutamate. Neuron 16:675-686.

Rutledge EM, Aschner M, Kimelberg HK (1998) Pharmacological characterization of swelling-induced D-[3H]aspartate release from primary astrocyte cultures. The American journal of physiology 274:C1511-1520.

Ryu JH, Walcott BP, Kahle KT, Sheth SA, Peterson RT, Nahed BV, Coumans JV, Simard JM (2013) Induced and Sustained Hypernatremia for the Prevention and Treatment of Cerebral Edema Following Brain Injury. Neurocritical care.

Salter MG, Fern R (2005) NMDA receptors are expressed in developing oligodendrocyte processes and mediate injury. Nature 438:1167-1171.

Sans N, Vissel B, Petralia RS, Wang YX, Chang K, Royle GA, Wang CY, O'Gorman S, Heinemann SF, Wenthold RJ (2003) Aberrant formation of glutamate receptor complexes in hippocampal neurons of mice lacking the GluR2 AMPA receptor subunit. The Journal of neuroscience : the official journal of the Society for Neuroscience 23:9367-9373.

Scemes E, Giaume C (2006) Astrocyte calcium waves: what they are and what they do. Glia 54:716-725.

Scharfman HE, Myers CE (2012) Hilar mossy cells of the dentate gyrus: a historical perspective. Frontiers in neural circuits 6:106.

Schneider GH, Baethmann A, Kempski O (1992) Mechanisms of glial swelling induced by glutamate. Canadian journal of physiology and pharmacology 70 Suppl:S334-343.

Seifert G, Schilling K, Steinhauser C (2006) Astrocyte dysfunction in neurological disorders: a molecular perspective. Nature reviews Neuroscience 7:194-206.

Shimamoto K, Sakai R, Takaoka K, Yumoto N, Nakajima T, Amara SG, Shigeri Y (2004) Characterization of novel L-threo-beta-benzyloxyaspartate derivatives, potent blockers of the glutamate transporters. Molecular pharmacology 65:1008-1015.

Simard M, Nedergaard M (2004) The neurobiology of glia in the context of water and ion homeostasis. Neuroscience 129:877-896.

Simard M, Arcuino G, Takano T, Liu QS, Nedergaard M (2003) Signaling at the gliovascular interface. The Journal of neuroscience : the official journal of the Society for Neuroscience 23:9254-9262.

Small SA, Schobel SA, Buxton RB, Witter MP, Barnes CA (2011) A pathophysiological framework of hippocampal dysfunction in ageing and disease. Nature reviews Neuroscience 12:585-601.

Sprengel R (2006) Role of AMPA receptors in synaptic plasticity. Cell and tissue research 326:447-455.

Stobart JL, Anderson CM (2013) Multifunctional role of astrocytes as gatekeepers of neuronal energy supply. Frontiers in cellular neuroscience 7:38.

Stone E, Hoffman K, Kavanaugh M (2012) Identifying neurotransmitter spill-over in hippocampal field recordings. Mathematical biosciences 240:169-186.

Sudhof TC, Rizo J (2011) Synaptic vesicle exocytosis. Cold Spring Harbor perspectives in biology 3.

Swanson CJ, Bures M, Johnson MP, Linden AM, Monn JA, Schoepp DD (2005) Metabotropic glutamate receptors as novel targets for anxiety and stress disorders. Nature reviews Drug discovery 4:131-144.

Swanson GT, Heinemann SF (1998) Heterogeneity of homomeric GluR5 kainate receptor desensitization expressed in HEK293 cells. The Journal of physiology 513 (Pt 3):639-646.

Sykova E, Vargova L, Kubinova S, Jendelova P, Chvatal A (2003) The relationship between changes in intrinsic optical signals and cell swelling in rat spinal cord slices. NeuroImage 18:214-230.

Szilagyi T, Orban-Kis K, Horvath E, Metz J, Pap Z, Pavai Z (2011) Morphological identification of neuron types in the rat hippocampus. Romanian journal of morphology and embryology = Revue roumaine de morphologie et embryologie 52:15-20.

Taft WC, DeLorenzo RJ (1987) Regulation of calcium channels in brain: implications for the clinical neurosciences. The Yale journal of biology and medicine 60:99-106.

Takahashi M, Billups B, Rossi D, Sarantis M, Hamann M, Attwell D (1997) The role of glutamate transporters in glutamate homeostasis in the brain. The Journal of experimental biology 200:401-409.

Tanaka K, Watase K, Manabe T, Yamada K, Watanabe M, Takahashi K, Iwama H, Nishikawa T, Ichihara N, Kikuchi T, Okuyama S, Kawashima N, Hori S,

Takimoto M, Wada K (1997) Epilepsy and exacerbation of brain injury in mice lacking the glutamate transporter GLT-1. Science 276:1699-1702.

Teyler TJ (1980) Brain slice preparation: hippocampus. Brain research bulletin 5:391-403.

Thompson EM, Pishko GL, Muldoon LL, Neuwelt EA (2013) Inhibition of SUR1 Decreases the Vascular Permeability of Cerebral Metastases. Neoplasia 15:535-543.

Torres FV, Hansen F, Doridio Locks-Coelho L (2013) Increase of extracellular glutamate concentration increases its oxidation and diminishes glucose oxidation in isolated mouse hippocampus: Reversible by TFB-TBOA. Journal of neuroscience research.

Tsukada S, Iino M, Takayasu Y, Shimamoto K, Ozawa S (2005) Effects of a novel glutamate transporter blocker, (2S, 3S)-3-[3-[4-(trifluoromethyl)benzoylamino]benzyloxy]aspartate (TFB-TBOA), on activities of hippocampal neurons. Neuropharmacology 48:479-491.

Tucker B, Olson JE (2010) Glutamate receptor-mediated taurine release from the hippocampus during oxidative stress. Journal of biomedical science 17 Suppl 1:S10.

Tyzio R, Minlebaev M, Rheims S, Ivanov A, Jorquera I, Holmes GL, Zilberter Y, Ben-Ari Y, Khazipov R (2008) Postnatal changes in somatic gamma-aminobutyric acid signalling in the rat hippocampus. The European journal of neuroscience 27:2515-2528.

Uckermann O, Wolf A, Kutzera F, Kalisch F, Beck-Sickinger AG, Wiedemann P, Reichenbach A, Bringmann A (2006) Glutamate release by neurons evokes a purinergic inhibitory mechanism of osmotic glial cell swelling in the rat retina: activation by neuropeptide Y. Journal of neuroscience research 83:538-550.

Unterberg AW, Stover J, Kress B, Kiening KL (2004) Edema and brain trauma. Neuroscience 129:1021-1029.

van Groen T, Kadish I, Wyss JM (2002) Species differences in the projections from the entorhinal cortex to the hippocampus. Brain research bulletin 57:553-556.

van Vliet EA, da Costa Araujo S, Redeker S, van Schaik R, Aronica E, Gorter JA (2007) Blood-brain barrier leakage may lead to progression of temporal lobe epilepsy. Brain : a journal of neurology 130:521-534.

Ventura R, Harris KM (1999) Three-dimensional relationships between hippocampal synapses and astrocytes. The Journal of neuroscience : the official journal of the Society for Neuroscience 19:6897-6906.

Verkhratsky A, Kirchhoff F (2007) Glutamate-mediated neuronal-glial transmission. Journal of anatomy 210:651-660.

Wallraff A, Kohling R, Heinemann U, Theis M, Willecke K, Steinhauser C (2006) The impact of astrocytic gap junctional coupling on potassium buffering in the hippocampus. The Journal of neuroscience : the official journal of the Society for Neuroscience 26:5438-5447.

Walz W, Hertz L (1983) Functional interactions between neurons and astrocytes. II. Potassium homeostasis at the cellular level. Progress in neurobiology 20:133-183.

Wang F, Smith NA, Xu Q, Fujita T, Baba A, Matsuda T, Takano T, Bekar L, Nedergaard M (2012) Astrocytes modulate neural network activity by Ca(2)+-dependent uptake of extracellular K+. Science signaling 5:ra26.

Wang HS, Dixon JE, McKinnon D (1997) Unexpected and differential effects of Cl-channel blockers on the Kv4.3 and Kv4.2 K+ channels. Implications for the study of the I(to2) current. Circulation research 81:711-718.

White MM, Aylwin M (1990) Niflumic and flufenamic acids are potent reversible blockers of Ca2(+)-activated Cl- channels in Xenopus oocytes. Molecular pharmacology 37:720-724.

Witte OW, Niermann H, Holthoff K (2001) Cell swelling and ion redistribution assessed with intrinsic optical signals. Anais da Academia Brasileira de Ciencias 73:337-350.

Witter MP (2006) Connections of the subiculum of the rat: topography in relation to columnar and laminar organization. Behavioural brain research 174:251-264.

Wollmuth LP, Kuner T, Sakmann B (1998a) Adjacent asparagines in the NR2-subunit of the NMDA receptor channel control the voltage-dependent block by extracellular Mg2+. The Journal of physiology 506 (Pt 1):13-32.

Wollmuth LP, Kuner T, Sakmann B (1998b) Intracellular Mg2+ interacts with structural determinants of the narrow constriction contributed by the NR1-subunit in the NMDA receptor channel. The Journal of physiology 506 (Pt 1):33-52.

Wright WL (2012) Sodium and fluid management in acute brain injury. Current neurology and neuroscience reports 12:466-473.

Wurm A, Pannicke T, Wiedemann P, Reichenbach A, Bringmann A (2008) Glial cell-derived glutamate mediates autocrine cell volume regulation in the retina: activation by VEGF. Journal of neurochemistry 104:386-399.

Wurm A, Lipp S, Pannicke T, Linnertz R, Krugel U, Schulz A, Farber K, Zahn D, Grosse J, Wiedemann P, Chen J, Schoneberg T, Illes P, Reichenbach A, Bringmann A (2010) Endogenous purinergic signaling is required for osmotic volume regulation of retinal glial cells. Journal of neurochemistry 112:1261-1272.

Yao HH, Ding JH, Zhou F, Wang F, Hu LF, Sun T, Hu G (2005) Enhancement of glutamate uptake mediates the neuroprotection exerted by activating group II or III metabotropic glutamate receptors on astrocytes. Journal of neurochemistry 92:948-961.

Zhang H, Cao HJ, Kimelberg HK, Zhou M (2011) Volume regulated anion channel currents of rat hippocampal neurons and their contribution to oxygen-and-glucose deprivation induced neuronal death. PloS one 6:e16803.

Zhang Y, Zhang H, Feustel PJ, Kimelberg HK (2008) DCPIB, a specific inhibitor of volume regulated anion channels (VRACs), reduces infarct size in MCAo and the release of glutamate in the ischemic cortical penumbra. Experimental neurology 210:514-520.

Zorec R, Araque A, Carmignoto G, Haydon PG, Verkhratsky A, Parpura V (2012) Astroglial excitability and gliotransmission: an appraisal of Ca2+ as a signalling route. ASN neuro 4.